Synthesis and Photophysical Properties of Chiral Cu(I) Complexes

M.Sc. Research Thesis

By
PRACHI SINGH
(2303131015)



DEPARTMENT OF CHEMISTRY INDIAN INSTITUTE OF TECHNOLOGY INDORE MAY, 2025

Synthesis and Photophysical Properties of Chiral Cu(I) Complexes

A THESIS

Submitted in partial fulfillment of the requirements for the award of the degree of

Master of Science

by **Prachi Singh**(2303131015)



DEPARTMENT OF CHEMISTRY INDIAN INSTITUTE OF TECHNOLOGY INDORE MAY, 2025



CANDIDATE'S DECLARATION

I hereby certify that the work being presented in the thesis entitled "Synthesis and Photophysical Properties of Chiral Cu(I) Complexes" in the partial fulfilment of the requirements for the award of the degree of MASTER OF SCIENCE and submitted to the **Department of Chemistry, Indian Institute of Technology Indore**, is an authentic record of my work carried out during the period from July 2024 to May 2025 under the supervision of **Dr. Abhinav Raghuvanshi**, Assistant Professor, Department of Chemistry, IIT Indore. The matter presented in this thesis has not been submitted by me for the award of any other degree of this or any other institute.

Prachi Singh

This is to certify that the above statement made by the candidate is

correct to the best of my/our knowledge.

t made by the candidate is

Dr. Abhinav Raghuvanshi

Prachi Singh has successfully given her M.Sc. Oral Examination held on 14/05/2025.

Signature of Supervisor of M.Sc. thesis

Signature of Supervisor of M.Sc. thesis Dr. Abhinav Raghuvanshi Date 15/05/2025

ACKNOWLEDGEMENTS

First, I would like to express my deepest gratitude to my thesis supervisor, **Dr. Abhinav Raghuvanshi**, for giving me such guidance, supervision and advice and for constantly directing and instructing me on the right path to concluding my thesis. I am obliged to thank my mentor and all the seniors, **Mr Laxman Kharabe**, **Mr Dilip Pandey**, **Mr Anurudh Mishra** and **Mr Sarvesh Maurya**, **Ms Jyoti**; you all have constantly guided me and helped me during my lab work despite having their own projects then have also given me suggestions that made this work possible. I would also like to thank my friends and family, who have constantly supported me, even during my times of failure.

Prachi Singh

M.Sc. Second Year

2303131015

Department of Chemistry

DEDICATE TO MY FAMILY.....

ABSTRACT

Recently, researchers are focusing on to fabricate optoelectronic devices using cost effective and environment friendly materials. Cu(I) complexes are promising candidate and used as emitters in optoelectronic devices (OLEDs, LEECs etc), photocatalyst for organic transformations, sensing of gases and organic volatiles. Chiral emissive complexes are important due to their potential in various fields, including nonlinear optics, anti-counterfeiting, and 3D displays. This project aims to synthesize and characterize oxazoline-derived chiral ligands and their Cu(I) complexes.

The present study includes the synthesis of chiral (R and S) oxazoline-based ligands (L1–L4) and characterization. L1 and L2 were prepared from 2-cyanopyridine, L3 and L4 ligands were prepared from 4-cyanopyridine. Furthermore, various complexes were formed using these ligands. These complexes were successfully characterized by NMR and SCXRD. Additionally, the photophysical and chiroptical properties of some complexes were studied using UV-Vis, photoluminescence, and circular dichroism.

TABLE OF CONTENTS

LIST OF FIGURES XII-X1V
LIST OF SCHEMES XV
ACRONYMS XVI
NOMENCLATURE XVII

CHAPTER 1: INTRODUCTION

- 1.1 Copper(I) complexes
- 1.2 Chiral Copper complexes
- 1.3 Chiral N^N or phosphine donor ligands
- 1.4 Chiral terminologies

CHAPTER 2: EXPERIMENTAL SECTION

- 2.1 Material and Instrumentation
- 2.2 Synthesis of oxazoline ring- based ligands (L1-L4)
- 2.2.1 Synthesis of (R)-4-phenyl-2-(pyridin-2-yl)-4,5-dihydrooxazole (L1)
- 2.2.2 Synthesis of (S)-4-phenyl-2-(pyridin-4-yl)-4,5-dihydrooxazole (L2)
- 2.2.3 Synthesis of (R)-4-phenyl-2-(pyridin-2-yl)-4,5-dihydrooxazole (L3)
- 2.2.4 Synthesis of (S)-4-phenyl-2-(pyridin-4-yl)-4,5-dihydrooxazole (L4)
- 2.3 Synthesis of complexes
- 2.3.1 Synthesis of C1
- 2.3.2 Synthesis of C2
- 2.3.3 Synthesis of C3
- 2.3.4 Synthesis of C4
- 2.3.5 Synthesis of C5
- 2.3.6 Synthesis of C6
- 2.3.7 Synthesis of C7
- 2.3.8 Synthesis of C8
- 2.3.9 Synthesis of C9
- 2.3.10 Synthesis of C10
- 2.3.11 Synthesis of C11
- 2.3.12 Synthesis of C12
- 2.3.13 Synthesis of C13
- 2.3.14 Synthesis of C14

CHAPTER 3: RESULTS AND DISCUSSION

- 3.1 Characterization
- 3.1.1 Characterization of ligands
- 3.1.1.1 Characterization of L1
- 3.1.1.2 Characterization of L2
- 3.1.1.3 Characterization of L3
- 3.1.1.4 Characterization of L4
- 3.1.2 Characterization of complexes
- 3.1.2.1 Characterization of C1
- 3.1.2.2 Characterization of C2
- 3.1.2.3 Characterization of C3
- 3.1.2.4 Characterization of C4
- 3.1.2.5 Characterization of C5
- 3.1.2.6 Characterization of C6
- 3.1.2.7 Characterization of C7
- 3.1.2.8 Characterization of C8
- 3.1.2.9 Characterization of C9
- 3.1.2.10 Characterization of C10
- 3.1.2.11 Characterization of C11
- 3.1.2.12 Characterization of C12
- 3.1.2.13 Characterization of C13
- 3.1.2.14 Characterization of C14
- 3.2 Photoluminescent Studies
- 3.2.1 Photoluminescent properties of Cu(I) Complexes
- 3.2.1.1 UV-Vis and PL spectra of C1
- 3.2.1.2 UV-Vis and PL spectra of C2
- 3.2.1.3 UV-Vis and PL spectra of C3
- 3.2.1.4 UV-Vis and PL spectra of C4
- 3.2.1.5 UV-Vis and PL spectra of C5
- 3.2.1.6 UV-Vis and PL spectra of C6
- 3.2.1.7 UV-Vis and PL spectra of C7
- 3.2.1.8 UV-Vis and PL spectra of C8
- 3.2.1.9 UV-Vis and PL spectra of C9
- 3.2.1.10 UV-Vis and PL spectra of C10
- 3.2.1.11 UV-Vis and PL spectra of C13
- 3.2.1.12 UV-Vis and PL spectra of C14
- 3.3 Chiroptical Studies

- 3.3.1 Chiroptical properties of Cu(I) Complexes
- 3.3.1.1 CD spectra of C1-C2
- 3.3.1.2 CD spectra of C3-C4
- 3.3.1.3 CD spectra of C7-C8

CHAPTER 4: CONCLUSION

REFERENCES

LIST OF FIGURES

Fig. 1: Applications of Cu(I) complexes

- **Fig. 2:** Strategy to design chiral Cu(I) complexes
- **Fig. 3:** Chiral Cu(I) complexes using P donor ligand
- Fig. 4: Mass spectrogram of L1
- Fig. 5: ¹H NMR spectra of L1
- Fig. 6: ${}^{13}C{}^{1}H}$ NMR spectra of L1
- Fig. 7: Mass spectrogram of L2
- Fig. 8: ¹H NMR spectra of L2
- Fig. 9: ${}^{13}C{}^{1}H}$ NMR spectra of L2
- Fig. 10: ¹H NMR spectra of L3
- Fig. 11: ${}^{13}C{}^{1}H}$ NMR spectra of L3
- Fig. 12: ¹H NMR spectra of L4
- Fig. 13: ${}^{13}C{}^{1}H}$ NMR spectra of L4
- Fig. 14: Mass spectrogram of C1
- Fig. 15: ¹H NMR spectra of C1
- Fig. 16: ${}^{13}C{}^{1}H}$ NMR spectra of C1
- **Fig. 17:** ³¹P{¹H} NMR spectra of **C1**
- Fig. 18: SCXRD of C1
- Fig. 19: Mass spectrogram of C2
- Fig. 20: ¹H NMR spectra of C2
- **Fig. 21:** ¹³C{ ¹H} NMR spectra of **C2**
- **Fig. 22:** ³¹P{¹H} NMR spectra of **C2**
- Fig. 23: Mass spectrogram of C3
- Fig. 24: ¹H NMR spectra of L4
- **Fig. 25:** ¹³C{¹H} NMR spectra of **C3**
- **Fig. 26:** ³¹P{¹H} NMR spectra of **C3**
- Fig. 27: SCXRD of C3
- Fig. 28: Mass spectrogram of C4
- Fig. 29: ¹H NMR spectra of C4

- Fig. 30: ${}^{13}C{}^{1}H}$ NMR spectra of C4
- **Fig. 31:** ³¹P{ ¹H} NMR spectra of **C4**
- Fig. 32: SCXRD of C4
- Fig. 33:Mass spectrogram of C5
- Fig. 34: ¹H NMR spectra of C5
- **Fig. 35:** ¹³C{¹H} NMR spectra of **C5**
- **Fig. 36:** ³¹P{ ¹H} NMR spectra of **C5**
- Fig. 37: Mass spectrogram of C6
- Fig. 38: ¹H NMR spectra of C6
- **Fig. 39:** ³¹P{¹H} NMR spectra of **C6**
- Fig. 40: Mass spectrogram of C7
- Fig. 41: ¹H NMR spectra of C7
- **Fig. 42:** ¹³C{¹H} NMR spectra of **C7**
- Fig. 43: SCXRD of C7
- Fig. 44: Mass spectrogram of C8
- Fig. 45: ¹H NMR spectra of C8
- **Fig. 46:** ¹³C{ ¹H} NMR spectra of **C8**
- Fig. 47: ¹H NMR spectra of C9
- **Fig. 48:** ${}^{13}C{}^{1}H{}^{1}$ NMR spectra of **C9**
- **Fig. 49:** ³¹P{ ¹H} NMR spectra of **C9**
- Fig. 50: ¹H NMR spectra of C10
- **Fig. 51:** ${}^{13}C{}^{1}H}$ NMR spectra of **C10**
- **Fig. 52:** ³¹P{¹H} NMR spectra of **C10**
 - Fig. 53: ¹H NMR spectra of C11
 - **Fig. 54:** ¹³C{¹H} NMR spectra of **C11**
 - **Fig. 55:** ³¹P{ ¹H} NMR spectra of **C11**
 - Fig. 56: SCXRD of C11
 - Fig. 57: ¹H NMR spectra of C12
 - **Fig. 58:** ${}^{13}C{}^{1}H}$ NMR spectra of **C12**

- **Fig. 59:** ³¹P{¹H} NMR spectra of **C12**
- Fig. 60: ¹H NMR spectra of C13
- **Fig. 61:** ${}^{13}C{}^{1}H}$ NMR spectra of **C13**
- **Fig. 62:** ³¹P{¹H} NMR spectra of **C13**
- Fig. 63: ¹H NMR spectra of C14
- **Fig. 64:** ¹³C{¹H} NMR spectra of **C14**
- **Fig. 65:** ³¹P{¹H} NMR spectra of **C14**
- Fig. 66: UV-Vis and PL spectra of C1
- Fig. 67: UV-Vis and PL spectra of C2
- Fig. 68: UV-Vis and PL spectra of C3
- Fig. 69: UV-Vis and PL spectra of C4
- Fig. 70: UV-Vis and PL spectra of C5
- Fig. 71: UV-Vis and PL spectra of C6
- Fig. 72: UV-Vis and PL spectra of C7
- Fig. 73: UV-Vis and PL spectra of C8
- Fig. 74: UV-Vis and PL spectra of C9
- Fig. 75: UV-Vis and PL spectra of C10
- Fig. 76: UV-Vis and PL spectra of C13
- Fig. 77: UV-Vis and PL spectra of C14
- Fig. 78: CD spectra of C1 and C2
- Fig. 79: CD spectra of C3 and C4
- Fig. 80: CD spectra of C7 and C8

LIST OF SCHEMES

Scheme 1: Synthesis of **L1**

Scheme 2: Synthesis of L2

Scheme 3: Synthesis of L3

Scheme 4: Synthesis of L4

Scheme 5: Synthesis of C1

Scheme 6: Synthesis of C2

Scheme 7: Synthesis of **C3**

Scheme 8: Synthesis of C4

Scheme 9: Synthesis of C5

Scheme 10: Synthesis of C6

Scheme 11: Synthesis of C7

Scheme 12: Synthesis of C8

Scheme 13: Synthesis of C9

Scheme 14: Synthesis of C10

Scheme 15: Synthesis of C11

Scheme 16: Synthesis of C12

Scheme 17: Synthesis of C13

Scheme 18: Synthesis of C14

NOMENCLATURE

 π pi

δ Chemical shift

cm Centimetre

nm Nanometre

K Kelvin

mmol Millimole

mL Millilitre

rt Room temperature

ACRONYMS

CDCl₃ Chloroform-D

ACN Acetonitrile

MeOH Methanol

EA Ethyl acetate

LCMS Liquid Chromatography Mass Spectrometry

NMR Nuclear Magnetic Resonance

UV-Vis Ultraviolet-Visible

M Molar

Ppm Parts per million

CD Circular dichoism

PL Photoluminescence

Chapter 1: INTRODUCTION

1.1 Copper(I) complexes

Copper(I) complexes have become a central focus in current science and technology due to their remarkable adaptability and potential for innovation. One particularly fascinating characteristic that certain molecules exhibit is luminescence via fluorescence, phosphorescence, and thermally activated delayed fluorescence (TADF). These properties enable the emission of visible light, making them highly valuable in diverse fields, particularly in bio- imaging and the development of optoelectronic materials. Specifically, Cu(I), with its preferred d¹⁰ configuration over Cu(II), reduces non-radioactive decay and does not show metal-centered d-d transitions; therefore, it exhibits a high photoluminescence quantum efficiency of up to 100%.² These complexes are especially significant in the context of innovations such as dye-sensitized solar cells, catalysts for organic transformations, CO₂ reduction, organic light-emitting diodes (OLEDs), light-emitting electrochemical cells (LEECs), electrochromic devices, and various sensor technologies.³ The remarkable properties of these complexes can be finely tuned by slight alterations in external stimuli, leading to changes in the electronic structure, such as the band gap (HOMO-LUMO), which directly impacts the molecular properties and behavior. Recently, our laboratory reported on the Cu(I) complex [Xantphos-Cudieng] PF₆, which exhibits notable electrochromic activity.⁴ This discovery led to the development of a device (ITO/P3HT/Cu complex/ITO), allowing for a thorough investigation into its electrochromic properties. Cu(I) complexes display fascinating redox and optical characteristics that can be easily manipulated by varying the ligands used in their coordination. This tunability opens up exciting possibilities for designing electrochromic materials with a wide range of colors and response times, offering great potential for advanced applications in optoelectronics. Additionally, this particular heteroleptic

Cu(I) complex has been shown to exhibit exceptional vapochromic behavior when exposed to π - π stacking solvents, resulting in a distinct blue shift in emission. Such dynamic responsiveness to environmental changes makes Cu(I) complexes highly promising for applications requiring rapid and reversible changes in optical properties.⁵

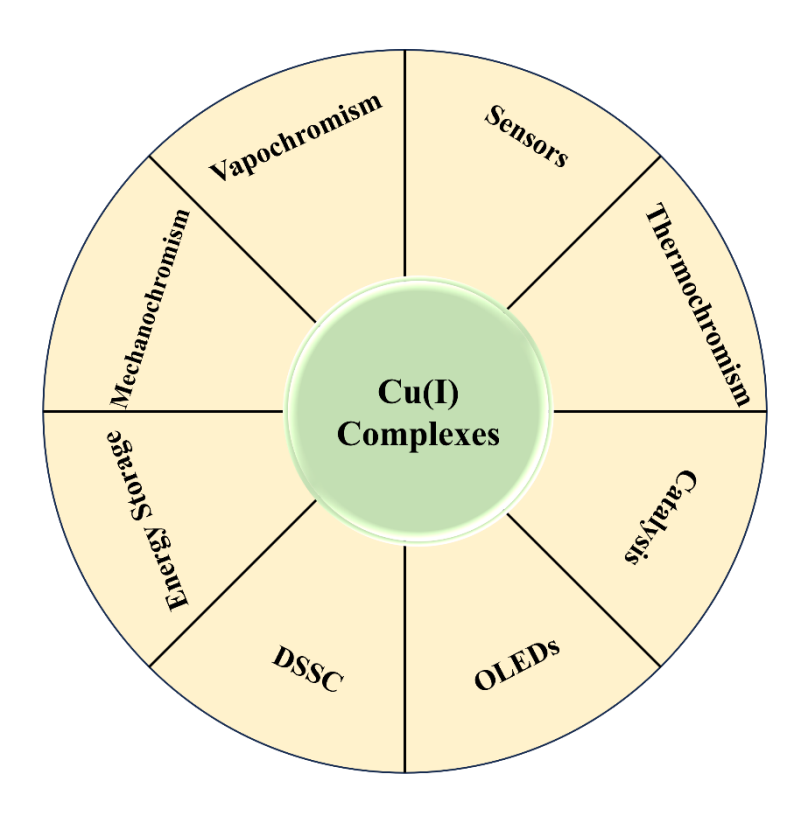


Figure 1: Properties and applications of Cu(I) complexes

1.2 Chiral Copper Complexes

Recently, a different class of Cu(I) complexes—specifically, chiral Cu(I) complexes emerged as promising candidates for circularly polarized luminescence (CPL) applications. These exhibits emissions via either thermally activated delayed fluorescence (TADF) or phosphorescence, both of which are desirable for achieving efficient light emission from triplet excited states. In addition to their favorable photophysical behavior, chiral Cu(I) complexes offer several intrinsic advantages, including structural tunability of emission properties, straightforward synthetic routes, cost-effectiveness, and the

environmentally benign nature of copper compared to noble metal alternatives Moreover, chiral copper(I) complexes have emerged as an important class of catalysts with wide-ranging applications, particularly in asymmetric synthesis and other catalytic processes.⁶ As a result, they present a highly attractive alternative for use in various chemical transformations, including those that require fine control over stereochemistry. However, despite these promising benefits, challenges remain in terms of improving the stability and selectivity of these catalysts. Addressing these challenges is essential to fully exploit the potential of chiral copper(I) complexes in diverse catalytic processes and further advance their applications in green chemistry and other sustainable practices.⁷

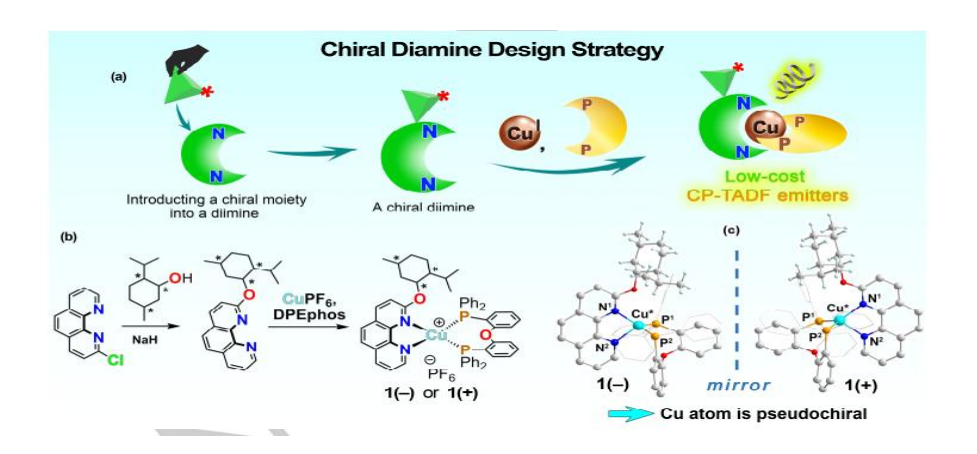


Figure 2: Strategy to design chiral Cu(I) complexes

1.3 Chiral N^N donor or Phosphine ligands

These are a class of ligands commonly used in coordination chemistry. These ligands have two nitrogen atoms that coordinate to a metal center (**Figure 2**). Nitrogen atoms are strong donor sites because of their lone pairs, making them ideal for binding with metal ions.

Oxazoline compounds are five-membered oxygen and nitrogen containing heterocycles that are of great interest to organic chemistry. Present in some biologically active natural products, optically active oxazolines have been proven to be useful as effective auxiliaries and ligands for selected asymmetric syntheses.⁸ To elucidate the coordination chemistry of copper supported by pyridine-oxazoline (Pyox) ligands. Pyox ligands have been successfully employed as chiral supporting ligands for a range of catalytically active complexes.

Chiral phosphorus atom or phosphine ligand provides chirality to central metal atom (**Figure 1**). In these systems, the phosphorus atom functions as a Lewis base, donating its lone pair of electrons to the vacant orbitals of the metal center. The resulting metal—ligand complex may exhibit chirality originating from the ligand, the coordination geometry, or a combination of both, thereby enabling applications in stereoselective processes and asymmetric catalysis. One class includes backbone chirality ligands that possess their stereogenic centers on the linking carbon chain. Most of the hitherto reported chiral phosphine ligands belong to this class, and some of them are used as benchmark ligands not only for the synthesis of various chiral compounds but also for the development of new catalytic asymmetric reactions. ¹⁰

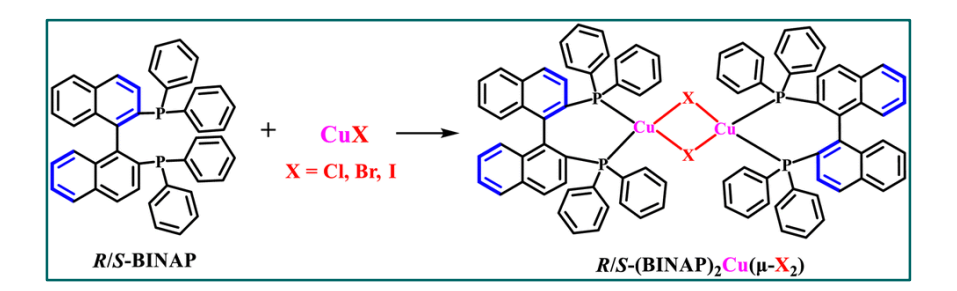


Figure 2: Chiral Cu(I) complexes using P donor ligand

1.4 Chiral terminologies

Chiral complexes, another fascinating subset of these materials, have a broad array of applications across various scientific and industrial fields, largely due to their ability to induce or interact with chirality. Certain systems have been observed to selectively absorb one specific

handedness of circularly polarized light, a phenomenon known as circular dichroism (CD).¹¹ When these chiral luminescent systems are capable of emitting light with a preference for left or right-handed circular polarization, often at varying intensities, this process is referred to as circularly polarized luminescence (CPL). CPL can be further categorized into two subtypes: circularly polarized photoluminescence (CPPL) and circularly polarized electroluminescence (CPEL), depending on the method of excitation. CPL is a particularly intriguing chiroptical phenomenon, characterized by the emission of light that shows a distinct preference for one circular polarization over the other. 12 This property is often observed in chiral luminescent systems and is a key indicator of chirality-induced luminescence. The "polarization" itself refers to the asymmetry observed in the vibration direction of the light wave relative to its propagation direction. While natural white light contains a mixture of wavelengths and does not exhibit polarization, polarized light can be classified into several types, including linear, elliptical, circular, and partially polarized light. 13 In particular, circularly polarized light is defined by the circular trajectory of the electric field vector as the light wave propagates. For circularly polarized light, the magnitude of the electric field remains constant, but its direction continuously changes over time, providing a unique and identifiable property for certain materials.¹⁴

Chapter 2: EXPERIMENTAL SECTION

2.1 Material and Instrumentation

Unless otherwise specified, chemicals were used exactly as received. TLC was used to monitor reaction progress using a Merck 60 F254 precoated silica gel plate (0.25 mm thickness), and the products were judged in a UV chamber. All ¹H{¹H} and ¹³C{¹H} and ³¹P{¹H} NMR spectra were collected using a Bruker 400/500 spectrometer in CDCl₃ and DMSO-d₆ at 400/500 MHz for ¹H and ¹³C{¹H} NMR. Data for proton NMR chemical shifts are shown in ppm downfield from tetramethyl silane and are mentioned in delta (δ) units. CDCl₃ is used as an internal standard, which shows a peak at 7.26 ppm. The ¹H NMR splitting patterns are singlet (s), doublet (d), triplet (t), and multiplet (m), and the NMR data was processed by Mestre Nova.

2.2 Synthesis of oxazoline ring- based ligands (L1-L4)

2.2.1 Synthesis of (R)-4-phenyl-2-(pyridin-2-yl)-4,5-dihydrooxazole (L1)

In a two-neck r.b. 2-cyanopyridine (100 mg, 0.96 mmol) and R-phenylglycinol (197.5 mg, 1.44 mmol) was added and dissolved in dry MeOH under N₂ atmosphere. After this, Na₂CO₃ (102 mg, 0.96 mmol) was added under reflux conditions at 80 °C. The reaction was monitored using TLC. The mixture was extracted by DCM. The combined organic phase was washed with brine, dried over Na₂SO₄, and filtered. The filtrate was concentrated under vacuum the product was purified by column chromatography using 20% EtOAc-Hexane and the product (L1) was obtained of a yellow liquid with 70% yield. LCMS (ESI) m/z calculated for C₁₄H₁₃N₂O[M+H]⁺: 225.0973, found: 225.1022. ¹H NMR (500 MHz, CDCl₃) δ 8.73 (d, J = 5.2 Hz, 1H), 8.16 (d, J = 7.9 Hz,

1H), 7.79 (td, J = 7.8, 2.0 Hz,1H), 7.42 (dd, J = 7.6, 4.8 Hz, 2H), 7.38 – 7.27 (m, 5H), 5.46 (t, J = 9.4 Hz, 1H), 4.93 – 4.85 (m, 1H), 4.38 (t, J = 8.5 Hz, 1H). ¹³C{¹H} (126 MHz, CDCl₃) 164.09, 149.85, 148.24, 141.87, 137.51, 128.91, 127.87, 126.90, 126.46, 122.48, 66.82, 56.35.

Scheme 1: Synthesis of L1

2.2.2 Synthesis of (S)-4-phenyl-2-(pyridin-2-yl)-4,5-dihydrooxazole (L2)

In a two-neck r.b. 2-cyanopyridine (100 mg, 0.96 mmol) and S-phenylglycinol (197.5 mg, 1.44 mmol) was added and dissolved in dry MeOH under N_2 atmosphere. After this, Na_2CO_3 (102 mg, 0.96 mmol) was added under reflux conditions at 80 °C. The reaction was monitored using TLC. The mixture was extracted by DCM. The combined organic phase was washed with brine, dried over Na_2SO_4 , and filtered. The filtrate was concentrated under vacuum the product was purified by column chromatography using 20% EtOAc-Hexane, the product (L2) was obtained of a yellow liquid with 86% yield. LCMS (ESI) m/z calculated for $C_{14}H_{13}N_2O[M+H]+225.1023$, found: 225.1022. 1H NMR (500 MHz, CDCl₃) δ 8.68 (s, 1H), 8.13 (s, 1H), 7.74 (s, 1H), 7.35 (s, 1H), 7.33 – 7.28 (m, 3H), 7.25 – 7.21 (m, 1H), 5.38 (s, 1H), 4.82 (s, 1H), 4.33 (s, 1H). $^{13}C\{^1H\}$ (126 MHz, CDCl₃) δ 149.87, 146.76, 141.89, 136.82, 128.91, 126.92, 124.37, 70.44.

Scheme 2: Synthesis of L2

2.2.3 Synthesis of (R)-4-phenyl-2-(pyridine-4-yl)-4,5-dihydrooxazole (L3)

In a two-neck r.b. 4-cyanopyridine (2000 mg, 0.019 mmol) and R-phenylglycinol (3980 mg, 0.029 mmol) was added and dissolved in dry MeOH under N₂ atmosphere. After this, Na₂CO₃ (2014 mg, 0.019 mmol) was added under reflux conditions at 80 °C. The reaction was monitored using TLC. The mixture was extracted by DCM. The combined organic phase was washed with brine, dried over Na₂SO₄, and filtered. The filtrate was concentrated under vacuum the product was purified by column chromatography using 20% EtOAc-Hexane and the product (L3) was obtained of a yellow liquid with 41% yield. ¹H NMR (500 MHz, CDCl₃) δ 8.74 (d, J = 5.2 Hz, 2H), 7.86 (d, J = 6.0 Hz, 2H), 7.41 – 7.27 (m, 5H), 5.48 – 5.38 (m, 1H), 4.87 – 4.79 (m, 1H), 4.31 (t, J = 8.5 Hz, 1H). ¹³C{¹H} (126 MHz, CDCl₃) δ 163.12, 150.44, 141.68, 135.02, 128.98, 127.99, 126.80, 122.26, 75.24, 70.39.

Scheme 3: Synthesis of L3

2.2.4 Synthesis of (S)-4-phenyl-2-(pyridine-4-yl)-4,5-dihydrooxazole (L4)

In a two-neck r.b. 4-cyanopyridine (2000 mg, 0.019 mmol) and S-phenylglycinol (3980 mg, 0.029 mmol) was added and dissolved in dry MeOH under N_2 atmosphere. After this, Na_2CO_3 (2014 mg, 0.019 mmol) was added under reflux conditions at 80 °C. The reaction was monitored using TLC. The mixture was extracted by DCM. The combined organic phase was washed with brine, dried over Na_2SO_4 , and filtered. The filtrate was concentrated under vacuum the product was purified by column chromatography using 20% EtOAc-Hexane and the product (**L4**) was obtained of a yellow liquid with 47% yield. ¹H NMR (500 MHz, CDCl₃) δ 8.73 (s, 2H), 7.85 (d, J = 5.5 Hz, 2H), 7.49 – 7.26 (m, 5H), 5.40 (t, J = 9.4 Hz, 1H), 4.81 (t, J = 9.4 Hz, 1H), 4.29 (t, J =

8.5 Hz, 1H). ¹³C{¹H} (**126 MHz, CDCl**₃) δ 163.01, 150.38, 141.63, 134.95, 128.90, 127.91, 126.72, 122.17, 75.16, 70.32.

Scheme 4: Synthesis of L4

2.3 Synthesis of complexes

2.3.1 Synthesis of C1

In a clean and dry Schlenk tube, Cu(CH₃CN)₄PF₆ (100 mg, 0.27 mmol) and DPEphos (145.2 mg, 0.27 mmol) were added. To this, 10 ml of DCM was added. L1 (60.5 mg, 0.27 mmol) was added to the reaction mixture, which was stirred for 15 hours at room temperature. On filtration, the filtrate was concentrated and hexane was added. A yellow solid product obtained in 88% yield. LCMS (ESI) m/z calculated for C₅₀H₄₀CuN₂O₂P₃F₆[M-PF₆] 825.1856, found: 825.160. ¹H NMR (500 **MHz, CDCl**₃) δ 8.23 – 8.13 (m, 2H), 7.99 (d, J = 5.0 Hz, 1H), 7.53 – 7.46 (m, 2H), 7.45 - 7.38 (m, 4H), 7.36 - 7.27 (m, 4H), 7.19 (q, J = 7.2Hz, 5H), 7.10 (d, J = 7.5 Hz, 3H), 7.02 (t, J = 7.7 Hz, 3H), 6.86 (dt, J =15.3, 7.3 Hz, 6H), 6.78 - 6.65 (m, 3H), 6.61 - 6.51 (m, 3H), 6.45 - 6.32(m, 3H), 5.07 (d, J = 3.5 Hz, 2H), 4.51 - 4.41 (m, 1H) ¹³C{¹H} NMR (126 MHz, CDCl₃) δ 165.68, 149.98, 142.53, 139.59, 138.66, 135.87, 134.17, 134.07, 133.33, 133.24, 133.14, 132.94, 132.82, 132.40, 132.32, 131.79, 130.82, 129.30, 129.09, 129.00, 128.84, 128.38, 127.64, 126.46, 125.03, 123.89, 123.77, 117.03, 69.27 ³¹P{¹H} NMR (**202** MHz, **CDCl₃**) δ -13.02, -144.32.

Scheme 5: Synthesis of C1

2.3.2 Synthesis of C2

In a clean and dry Schlenk tube, Cu(CH₃CN)₄PF₆ (100 mg, 0.27 mmol) and DPEphos (145.2 mg, 0.27 mmol) were added. To this, 10 ml of DCM was added. **L2** (60.5 mg, 0.27 mmol) was added to the reaction mixture, which was stirred for 15 hours. On filtration, the filtrate was concentrated and hexane was added. A yellow solid product obtained in 88% yield. **LCMS** (ESI) m/z calculated for C₅₀H₄₀CuN₂O₂P₃F₆[M-PF₆] 825.1856, found: 825.1656. ¹H NMR (500 MHz, CDCl₃) δ 8.18 (s, 2H), 7.99 (s, 1H), 7.49 (s, 2H), 7.42 (s, 5H), 7.28 (s, 4H), 7.19 (s, 6H), 7.09 (s, 3H), 7.02 (s, 3H), 6.88 (s, 6H), 6.68 (s, 2H), 6.56 (s, 3H), 6.39 (s, 3H), 5.08 (s, 2H), 4.47 (s, 1H) ¹³C{¹H} NMR (126 MHz, CDCl₃) δ 149.98, 142.52, 139.57, 135.86, 134.14, 133.33, 132.40, 131.78, 130.82, 130.39, 130.20, 130.06, 129.30, 129.16, 129.00, 128.90, 128.83, 128.43, 127.63, 126.44, 125.02, 123.90, 123.76, 117.04, 77.41, 76.91, 69.27. ³¹P{¹H} NMR (202 MHz, CDCl₃) δ -12.99, -144.29.



Scheme 6: Synthesis of C2

2.3.3 Synthesis of C3

In a clean and dry Schlenk tube, $Cu(CH_3CN)_4PF_6$ (100 mg, 0.27 mmol) and Xantphos (156.2 mg, 0.27 mmol) were added. To this, 10 ml of DCM was added. **L1** (60.5 mg, 0.27 mmol) was added to the reaction mixture, which was stirred for 15 hours. On filtration, the filtrate was

concentrated and hexane was added. A yellow solid product obtained in 83% yield. LCMS (ESI) m/z calculated for $C_{53}H_{44}CuN_2O_2P_3F_6[M-PF_6]$ 865.2169, found: 865.2088. ¹H NMR (500 MHz, CDCl₃) δ 8.18 (s, 1H), 7.67 – 7.31 (m, 3H), 7.28 – 6.72 (m, 10H), 6.72 – 6.21 (m, 4H), 5.36 – 4.39 (m, 2H), 2.05 – 0.59 (m, 14H) ¹³C{¹H} NMR (126 MHz, CDCl₃) δ 149.19, 139.66, 138.64, 133.17, 132.55, 131.99, 131.11, 130.06, 128.92, 127.27, 125.25, 68.72, 35.91, 31.47, 25.16, 22.53, 14.00, 11.31. ³¹P{¹H} NMR (202 MHz, CDCl₃) δ -12.35, -13.82, -144.28.

$$\begin{array}{c|c} & PPh_2 & PPh_2 \\ \hline O & & \\$$

Scheme 7: Synthesis of C3

2.3.4 Synthesis of C4

In a clean and dry Schlenk tube, Cu(CH₃CN)₄PF₆ (100 mg, 0.27 mmol) and Xantphos (156.2 mg, 0.27 mmol) were added. To this, 10 ml of DCM was added. **L2** (60.5 mg, 0.27 mmol) was added to the reaction mixture, which was stirred for 15 hours. On filtration, the filtrate was concentrated and hexane was added. A yellow solid product obtained in 64% yield. **LCMS** (ESI) m/z calculated for C₅₃H₄₄CuN₂O₂P₃F₆[M-PF₆] 865.2169, found: 865.1938. HNMR (500 MHz, CDCl₃) δ 8.17 (s, 1H), 7.61 (s, 1H), 7.48 (d, J = 48.8 Hz, 2H), 7.36 (s, 1H), 7.13 (s, 3H), 7.00 (s, 4H), 6.89 (s, 1H), 6.63 (s, 3H), 6.30 (s, 2H), 5.06 (s, 1H), 4.53 (s, 1H), 1.61 (s, 6H) 13 C{ 1 H} NMR (126 MHz, CDCl₃) δ 149.70, 140.18, 139.15, 133.18, 132.86, 132.50, 130.81, 129.37, 128.79, 127.58, 125.76, 125.47, 69.23, 31.98, 31.71, 25.19, 23.05, 14.52. 31 P{ 1 H} NMR (202 MHz, CDCl₃) δ -12.43,-13.02, -144.29

$$\begin{array}{c} PPh_2 & PPh_2 \\ \hline O & \\$$

Scheme 8: Synthesis of C4

2.3.5 Synthesis of C5

In a clean and dry Schlenk tube, Cu(CH₃CN)₄PF₆ (100 mg, 0.27 mmol) and Johnphos (77.58 mg, 0.27 mmol) were added. To this, 10 ml of DCM was added. L1 (58.24 mg, 0.27 mmol) was added to the reaction mixture, which was stirred for 15 hours. On filtration, the filtrate was concentrated and hexane was added. A yellow-green solid product obtained in 75% yield. **LCMS** (ESI) m/z calculated C₃₄H₃₉CuN₂OP₂F₆[M-PF₆] 585.2091, found: 585.2011. ¹H NMR (500 **MHz, CDCl₃**) δ 8.17 (s, 1H), 8.06 (d, J = 7.8 Hz, 1H), 7.85 (s, 2H), 7.46 (s, 3H), 7.32 (s, 4H), 7.17 (s, 1H), 6.89 (s, 1H), 6.54 (s, 1H), 5.30 (s, 1H), 1.63 (s, 2H), 1.47 (d, J = 17.5 Hz, 1H), 1.31 (d, J = 14.5 Hz, 9H), 0.81 (s, 4H).¹³C{¹H} NMR (126 MHz, CDCl₃δ 150.45, 140.49, 133.83, 132.62, 130.82, 129.51, 127.90, 127.62, 126.92, 124.97, 34.96, 34.84, 31.21, 30.03,28.41. ³¹P{ 1 H} NMR (202 MHz, CDCl₃) δ -32.02, -144.23.

$$+ \underbrace{ \frac{|Cu(CH_3CN)_4|PF_6}{DCM, r.t., 15h}}_{PCM}$$

Scheme 9: Synthesis of C5

2.3.6 Synthesis of C6

In a clean and dry Schlenk tube, $Cu(CH_3CN)_4PF_6$ (100 mg, 0.27 mmol) and Johnphos (77.58 mg, 0.27 mmol) were added. To this, 10 ml of DCM was added. **L2** (58.24 mg, 0.27 mmol) was added to the reaction mixture, which was stirred for 15 hours. On filtration, the filtrate was concentrated and hexane was added. A yellow-green solid product obtained in 73% yield. **LCMS** (ESI) m/z calculated for $C_{34}H_{39}CuN_2OP_2F_6[M-PF_6]$ 585.2091, found: 585.2011. ¹H NMR (500 MHz, CDCl₃) δ 8.17 (s, 1H), 8.08 (d, J = 7.6 Hz, 1H), 7.85 (s, 2H), 7.56 – 7.28 (m, 8H), 7.18 (s, 2H), 5.32 (s, 1H), 4.64 (s, 1H), 1.57 (s, 7H), 1.32 (d, J = 14.3 Hz, 11H). ³¹P{¹H} NMR (202 MHz, CDCl₃) δ -33.02, -144.29

Scheme 10: Synthesis of C6

2.3.7 Synthesis of C7

In a clean and dry Schlenk tube, CuI (100 mg, 0.53 mmol) and PPh₃ (138.86 mg, 0.53 mmol) were added. To this, 3 ml of Toluene was added. **L1** (118.72 mg, 0.53 mmol) was added to the reaction mixture, which was stirred for 15 hours. On filtration, the filtrate was concentrated and hexane was added. A red solid product obtained in 58% yield. **LCMS** (ESI) m/z calculated for $C_{32}H_{27}CuN_2OPI[M-I]$ 549.1151, found: 549.1064. The NMR (500 MHz, CDCl₃) δ 8.17 (s, 1H), 7.61 (s, 1H), 7.48 (d, J = 48.8 Hz, 2H), 7.36 (s, 1H), 7.13 (s, 3H), 7.00 (s, 4H), 6.89 (s, 1H), 6.63 (s, 3H), 6.30 (s, 2H), 5.06 (s, 1H), 4.53 (s, 1H), 1.61 (s, 6H) $^{13}C\{^{1}H\}$ NMR (126 MHz, CDCl₃) δ 149.70, 140.18, 139.15, 133.18, 132.86, 132.50, 130.81, 129.37, 128.79, 127.58, 125.76, 125.47, 69.23, 31.98, 31.71, 25.19, 23.05, 14.52.

$$CuI + PPh_3 + N$$

$$\frac{Toluene}{110 \, {}^{\circ}C, 15h}$$
 V

Scheme 11: Synthesis of C7

2.3.8 Synthesis of C8

In a clean and dry Schlenk tube, CuI (100 mg, 0.53 mmol) and PPh₃ (138.86 mg, 0.53 mmol) were added. To this, 3 ml of Toluene was added. **L2** (118.72 mg, 0.53 mmol) was added to the reaction mixture, which was stirred for 15 hours. On filtration, the filtrate was concentrated and hexane was added. A red solid product obtained in 88% yield. **LCMS** (ESI) m/z calculated for C₃₂H₂₇CuN₂OPI[M-I] 549.1151, found: 549.089..¹H NMR (500 MHz, CDCl₃ δ 8.50 (s, 1H), 7.95 (s, 1H), 7.90 (s, 1H), 7.45 (s, 2H), 7.34 (s, 3H), 7.28 (s, 4H), 7.24

(s, 5H), 7.16 (s, 1H), 7.09 (s, 2H), 5.60 (s, 1H), 5.08 (s, 1H), 4.52 (s, 1H). ¹³C{¹H} NMR (126 MHz, CDCl₃) δ 164.54, 150.34, 137.48, 133.92, 133.81, 129.52, 128.82, 128.50, 128.43, 128.11, 127.43, 127.23, 123.68, 68.17, 67.03.

Scheme 12: Synthesis of C8

2.3.9 Synthesis of C9

In a clean and dry Schlenk tube, Cu(CH₃CN)₄PF₆ (100 mg, 0.27 mmol) and Xantphos (156.2 mg, 0.27 mmol) were added. To this, 10 ml of DCM was added. **L3** (60.5 mg, 0.27 mmol) was added to the reaction mixture, which was stirred for 15 hours. On filtration, the filtrate was concentrated and hexane was added. A yellow solid product obtained in 83% yield. ¹H NMR (500 MHz, CDCl₃) δ 8.27 (s, 2H), 7.76 (d, J = 6.3 Hz, 2H), 7.61 (d, J = 7.6 Hz, 2H), 7.32 (dt, J = 19.8, 7.6 Hz, 4H), 7.21 (dt, J = 16.2, 7.6 Hz, 8H), 7.13 (dd, J = 15.6, 7.9 Hz, 6H), 7.01 (h, J = 5.9 Hz, 8H), 6.63 – 6.55 (m, 2H), 5.37 – 5.24 (m, 1H), 4.94 (t, J = 9.7 Hz, 1H), 4.43 (t, J = 9.2 Hz, 1H), 1.68 (s, 6H). ¹³C{¹H} NMR (126 MHz, CDCl₃) δ 164.02, 154.27, 150.49, 133.48, 133.29, 133.23, 133.17, 132.99, 132.93, 132.87, 131.65, 130.68, 130.54, 129.15, 128.61, 127.72, 127.08, 125.43, 123.64, 119.17, 70.49, 35.96, 31.71, 28.64. ³¹P{¹H} NMR (101 MHz, CDCl₃) δ -14.61, -144.28.



Scheme 13: Synthesis of C9

2.3.10 Synthesis of C10

In a clean and dry Schlenk tube, Cu(CH₃CN)₄PF₆ (100 mg, 0.27 mmol) and Xantphos (156.2 mg, 0.27 mmol) were added. To this, 10 ml of DCM was added. **L4** (60.5 mg, 0.27 mmol) was added to the reaction

mixture, which was stirred for 15 hours. On filtration, the filtrate was concentrated and hexane was added. A yellow solid product obtained in 83% yield. ¹H NMR (500 MHz, CDCl₃) δ 8.27 (s, 2H), 7.76 (d, J = 6.3 Hz, 2H), 7.61 (d, J = 7.6 Hz, 2H), 7.32 (dt, J = 19.8, 7.6 Hz, 4H), 7.21 (dt, J = 16.2, 7.6 Hz, 8H), 7.13 (dd, J = 15.6, 7.9 Hz, 6H), 7.01 (h, J = 5.9 Hz, 8H), 6.63 – 6.55 (m, 2H), 5.37 – 5.24 (m, 1H), 4.94 (t, J = 9.7 Hz, 1H), 4.43 (t, J = 9.2 Hz, 1H), 1.68 (s, 6H). ¹³C{¹H} NMR (126 MHz, CDCl₃) δ 164.02, 154.27, 150.49, 133.48, 133.29, 133.23, 133.17, 132.99, 132.93, 132.87, 131.65, 130.68, 130.54, 129.15, 128.61, 127.72, 127.08, 125.43, 123.64, 119.17, 70.49, 35.96, 31.71, 28.64..³¹P{¹H} NMR (101 MHz, CDCl₃) δ -14.61, -144.28

$$\begin{array}{c} PPh_2 \\ PPPh_2 \\ PPPH_2$$

Scheme 14: Synthesis of C10

2.3.11 Synthesis of C11

In a clean and dry Schlenk tube, $Cu(CH_3CN)_4PF_6$ (100 mg, 0.27 mmol) and Johnphos (77.58 mg, 0.27 mmol) were added. To this, 10 ml of DCM was added. **L3** (58.24 mg, 0.27 mmol) was added to the reaction mixture, which was stirred for 15 hours. On filtration, the filtrate was concentrated and hexane was added. A yellow solid product obtained in 76% yield. ¹H NMR (500 MHz, CDCl₃) δ 8.47 – 8.36 (m, 2H), 7.93 (d, J = 6.0 Hz, 2H), 7.81 (t, J = 7.6 Hz, 1H), 7.56 (t, J = 7.6 Hz, 1H), 7.49 (p, J = 6.4, 5.8 Hz, 2H), 7.36 (t, J = 7.5 Hz, 1H), 7.30 (h, J = 7.0, 6.3 Hz, 5H), 7.24 (s, 2H), 7.23 – 7.20 (m, 1H), 7.11 (t, J = 7.6 Hz, 1H), 5.35 (t, J = 9.4 Hz, 1H), 4.95 (t, J = 9.6 Hz, 1H), 4.37 (t, J = 8.6 Hz, 1H), 1.24 (d, J = 15.1 Hz, 9H), 1.14 (d, J = 15.1 Hz, 9H). ¹³C{¹H} NMR (126 MHz,

CDCl₃) δ 150.44, 133.45, 132.07, 131.17, 131.02, 129.34, 128.65, 127.99, 127.55, 127.21, 123.92, 70.40, 35.19, 35.05, 30.71, 30.64, 30.51, 30.45. ³¹P{¹H} NMR (101 MHz, CDCl₃) δ -33.09, -144.23.

$$+ \sqrt[]{\frac{O}{DCM, r.t., 15h}} + \sqrt[]{\frac{Cu(CH_3CN)_4|PF_6}{DCM, r.t., 15h}}$$

Scheme 15: Synthesis of C11

2.3.12 Synthesis of C12

In a clean and dry Schlenk tube, Cu(CH₃CN)₄PF₆ (100 mg, 0.27 mmol) and Johnphos (77.58 mg, 0.27 mmol) were added. To this, 10 ml of DCM was added. L3 (29.12 mg, 0.13 mmol) was added to the reaction mixture, which was stirred for 15 hours. On filtration, the filtrate was concentrated and hexane was added. A yellow solid product obtained in 70% yield. ¹H NMR (500 MHz, CDCl₃) δ 8.43 (d, J = 6.6 Hz, 2H), 7.99 (d, J = 6.6 Hz, 2H), 7.87 - 7.81 (m, 2H), 7.63 (t, J = 7.6 Hz, 2H), 7.52(q, J = 8.7, 7.2 Hz, 4H), 7.47 (t, J = 7.8 Hz, 2H), 7.37 (d, J = 8.2 Hz, 1H),7.35 (d, J = 4.1 Hz, 2H), 7.32 (s, 4H), 7.31 - 7.28 (m, 4H), 7.28 - 7.27(m, 1H), 7.26 - 7.23 (m, 1H), 5.32 (t, J = 9.3 Hz, 1H), 5.12 (t, J = 9.8)Hz, 1H), 4.52 (t, J = 8.7 Hz, 1H), 1.27 (d, J = 15.0 Hz, 18H), 1.15 (d, J= 15.0 Hz, 18H).¹³C $\{^{1}$ H $\}$ NMR (126 MHz, CDCl₃) δ 150.76, 149.38, 149.22, 142.37, 138.74, 135.43, 133.43, 132.10, 132.04, 131.22, 131.14, 131.08, 129.78, 129.45, 128.11, 127.88, 127.84, 127.72, 127.56, 127.47, 127.33, 124.71, 117.54, 70.36, 35.16, 31.72, 30.68, 30.38, 25.41, 22.79, 14.25. ${}^{31}P{}^{1}H}$ NMR (101 MHz, CDCl₃) δ -32.33, -144.29

$$+ N \longrightarrow \frac{|Cu(CH_3CN)_4|PF_6}{DCM, r.t., 15h}$$

Scheme 16: Synthesis of C12

2.3.13 Synthesis of C13

In a clean and dry Schlenk tube, Cu(CH₃CN)₄PF₆ (100 mg, 0.27 mmol) and Johnphos (77.58 mg, 0.27 mmol) were added. To this, 10 ml of DCM was added. **L3** (116.48 mg, 0.52 mmol) was added to the reaction mixture, which was stirred for 15 hours. On filtration, the filtrate was concentrated and hexane was added. A yellow solid product obtained in 68% yield. ¹H NMR (500 MHz, CDCl₃) δ 8.53 – 8.38 (m, 2H), 7.92 (d, J = 5.0 Hz, 2H), 7.82 (td, J = 6.3, 2.2 Hz, 1H), 7.55 (t, J = 7.6 Hz, 1H), 7.49 (t, J = 6.3 Hz, 2H), 7.34 (td, J = 13.2, 11.7, 5.9 Hz, 5H), 7.28 (d, J = 4.3 Hz, 1H), 7.27 – 7.23 (m, 3H), 7.08 (t, J = 7.6 Hz, 1H), 5.37 (t, J = 9.4 Hz, 1H), 4.91 (t, J = 9.5 Hz, 1H), 4.35 (t, J = 8.5 Hz, 1H), 1.26 (d, J = 15.1 Hz, 9H), 1.17 (d, J = 15.1 Hz, 9H). ¹³C{¹H} NMR (126 MHz, CDCl₃) δ 150.40, 149.36, 149.20, 142.44, 140.72, 133.47, 132.08, 132.03, 131.19, 131.03, 129.24, 128.47, 127.99, 127.94, 127.91, 127.54, 127.09, 123.64, 70.42, 35.21, 35.01, 31.70, 30.73, 30.66, 30.49, 25.40.³¹P{¹H} NMR (101 MHz, CDCl₃) δ -33.02, -144.19.

$$+ N \longrightarrow \frac{|Cu(CH_3CN)_4|PF_6}{DCM, r.t., 15h}$$

Scheme 17: Synthesis of C13

2.3.14 Synthesis of C14

In a clean and dry Schlenk tube, $Cu(CH_3CN)_4PF_6$ (100 mg, 0.27 mmol) and Johnphos (77.58 mg, 0.27 mmol) were added. To this, 10 ml of DCM was added. **L4** (58.24 mg, 0.27 mmol) was added to the reaction mixture, which was stirred for 15 hours. On filtration, the filtrate was concentrated and hexane was added. A yellow solid product obtained in 77% yield. ¹H NMR (500 MHz, CDCl₃) δ 8.37 (s, 2H), 7.90 (s, 2H), 7.80 (s, 1H), 7.46 (d, J = 31.0 Hz, 4H), 7.29 (d, J = 20.4 Hz, 4H), 7.21 (d, J = 7.6 Hz, 3H), 7.15 (s, 1H), 7.09 (s, 1H), 5.31 (t, J = 9.5 Hz, 1H), 4.90 (t, J = 9.7 Hz, 1H), 4.30 (t, J = 8.8 Hz, 1H), 1.19 (d, J = 15.0 Hz,

9H), 1.10 (d, J = 15.0 Hz, 9H). ¹³C{¹H} NMR (126 MHz, CDCl₃) δ 150.32, 149.19, 149.03, 142.51, 140.31, 136.13, 133.48, 131.91, 131.01, 130.76, 129.21, 128.47, 127.86, 127.78, 127.30, 127.09, 70.27, 35.07, 31.59, 30.53, 25.30, 22.66, 14.16. ³¹P{¹H} NMR (101 MHz, CDCl₃) δ -32.15, -144.19.

$$+ \sum_{N} \left(\frac{Cu(CH_3CN)_4|PF_6}{DCM, r.t., 15h} \right) \left(\frac{PF_6}{DCM} \right$$

Scheme 18: Synthesis of C14

Chapter 3: RESULT AND DISCUSSION

3.1 Characterization

3.1.1 Characterization of ligands

3.1.1.1 Characterization of L1

L1 was synthesised according to scheme 1. In the reaction, dry MeOH used as a solvent. The final product was pale yellow liquid compound with an 70 % yield. The obtained product was characterised by Mass spectrometry (Figure 4) and ¹H and ¹³C{¹H} NMR spectroscopy (Figures 5 and 6). Peaks of most deshielded hydrogen were observed near nine ppm, thereby confirming that ligand is formed.

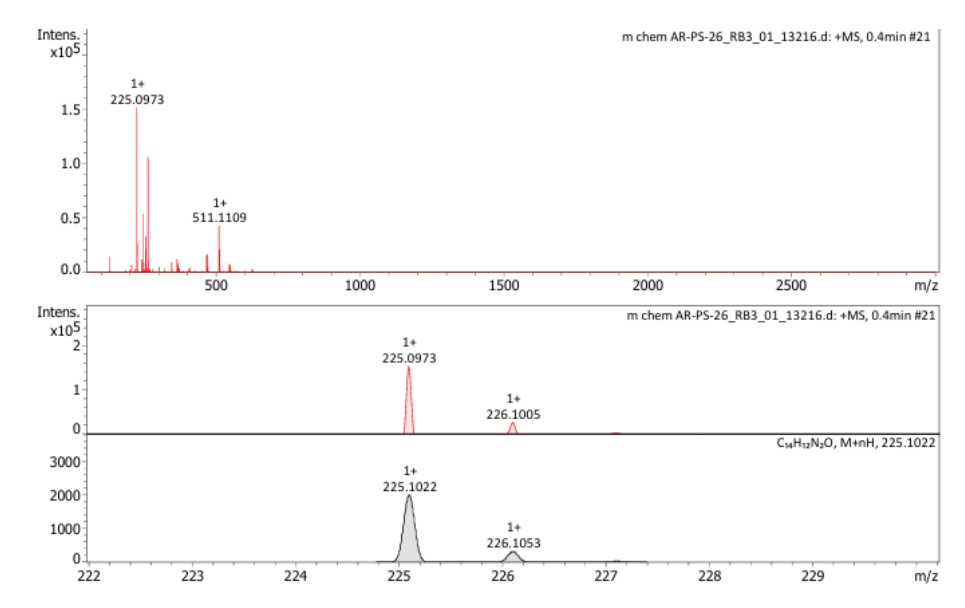


Figure 4: Mass spectrogram of L1

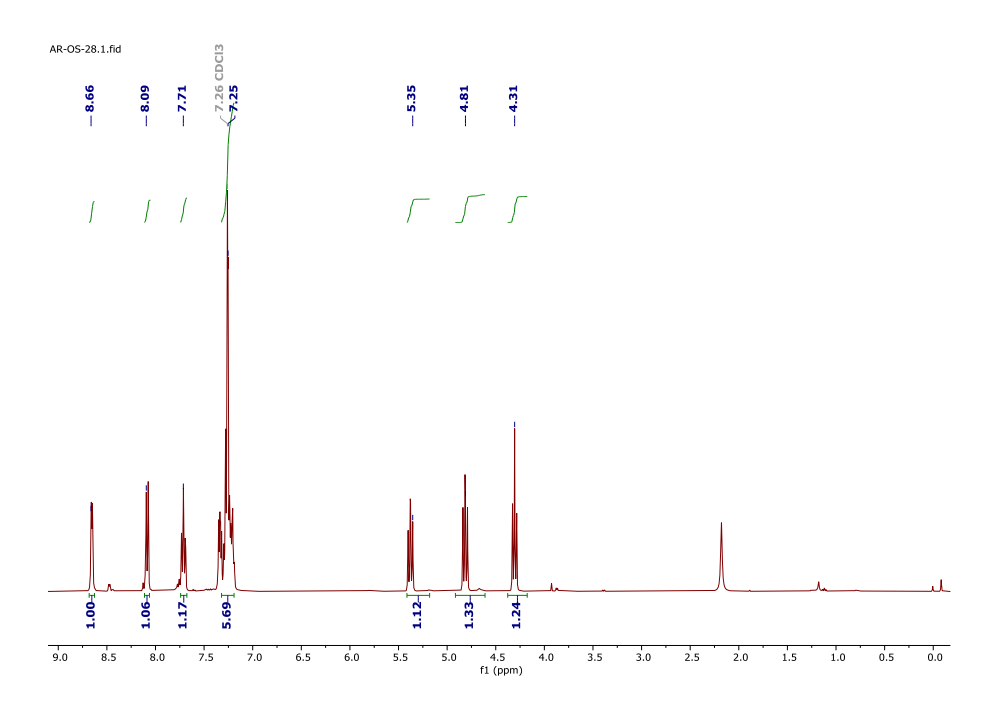


Figure 5: ¹H NMR spectra of L1

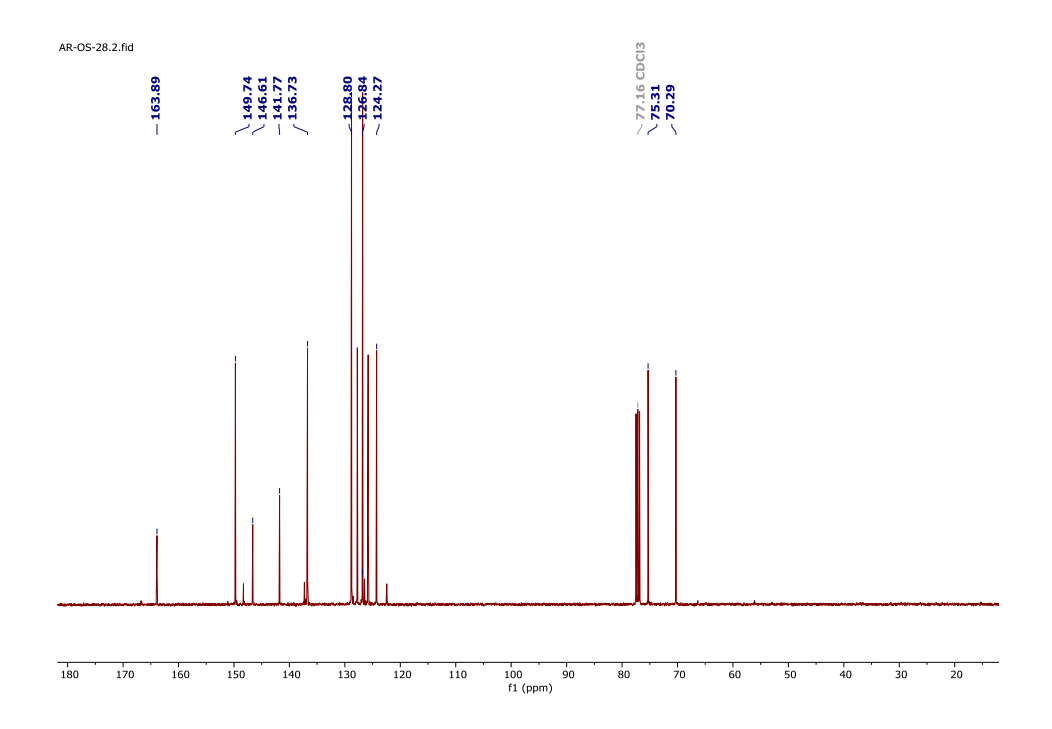


Figure 6: ¹³C{¹H} NMR spectra of L1

3.1.1.2 Characterization of L2

L2 was synthesised according to scheme 2. In the reaction, dry MeOH used as a solvent. The final product was pale yellow liquid compound with an 86 % yield. The obtained product was characterised by Mass spectrometry (Figure 7) and ¹H and ¹³C{¹H} NMR spectroscopy (Figures 8 and 9). Peaks of most deshielded hydrogen were observed near nine ppm, thereby confirming that ligand is formed.

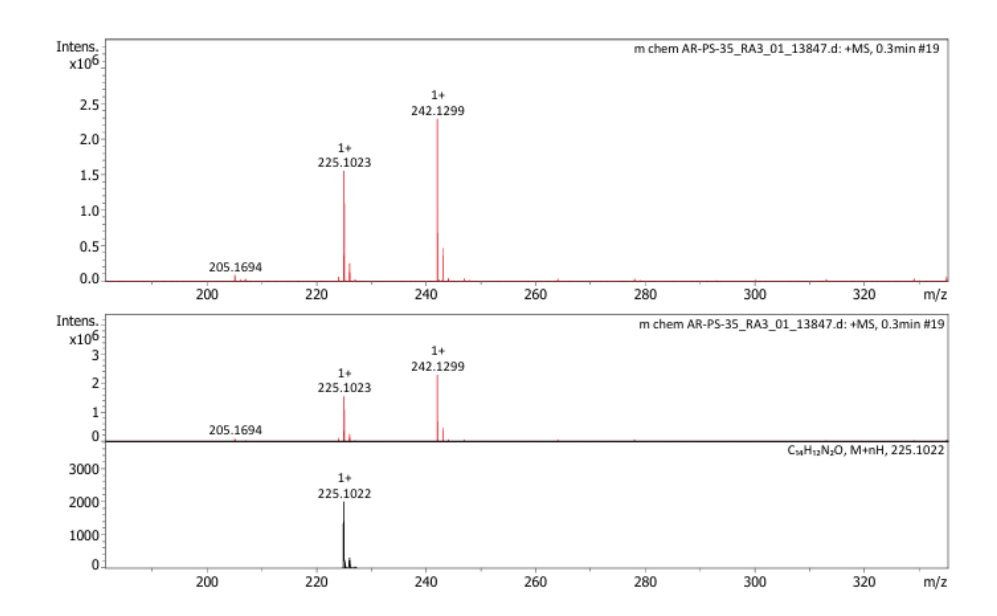


Figure 7: Mass spectrogram of L2

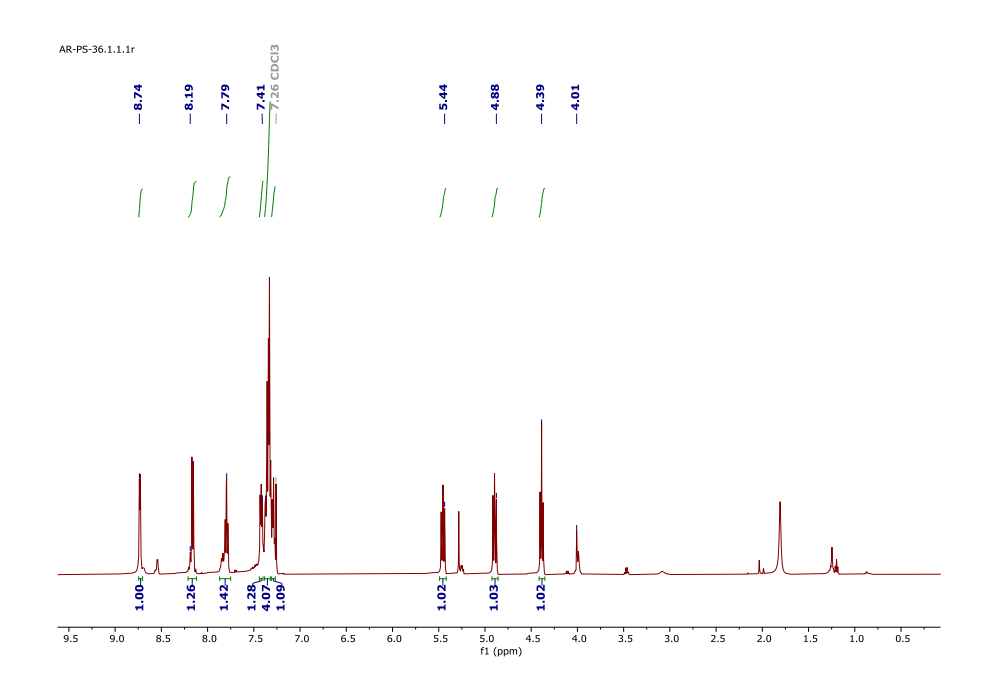


Figure 8: ¹H NMR spectra of L2

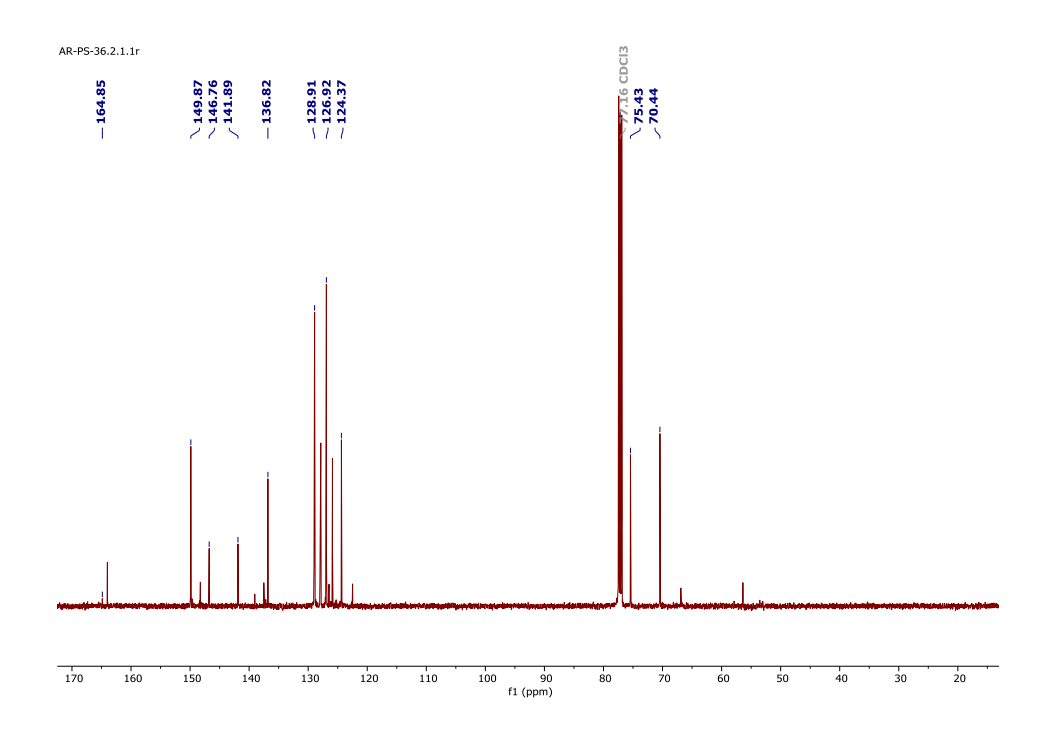
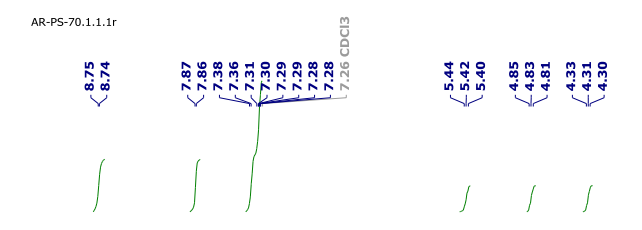


Figure 9: ¹³C{¹H} NMR spectra of **L2**

3.1.1.3 Characterization of L3

L3 was synthesised according to scheme 3. In the reaction, dry MeOH used as a solvent. The final product was pale white solid compound with an 41 % yield. The obtained product was characterised by ¹H and ¹³C{¹H} NMR spectroscopy (Figures 10 and 11). Peaks of most deshielded hydrogen were observed near nine ppm, thereby confirming that ligand is formed.



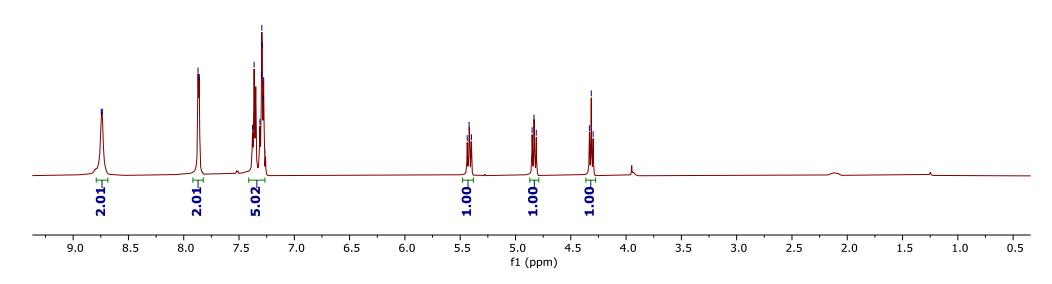


Figure 10: ¹H NMR spectra of L3

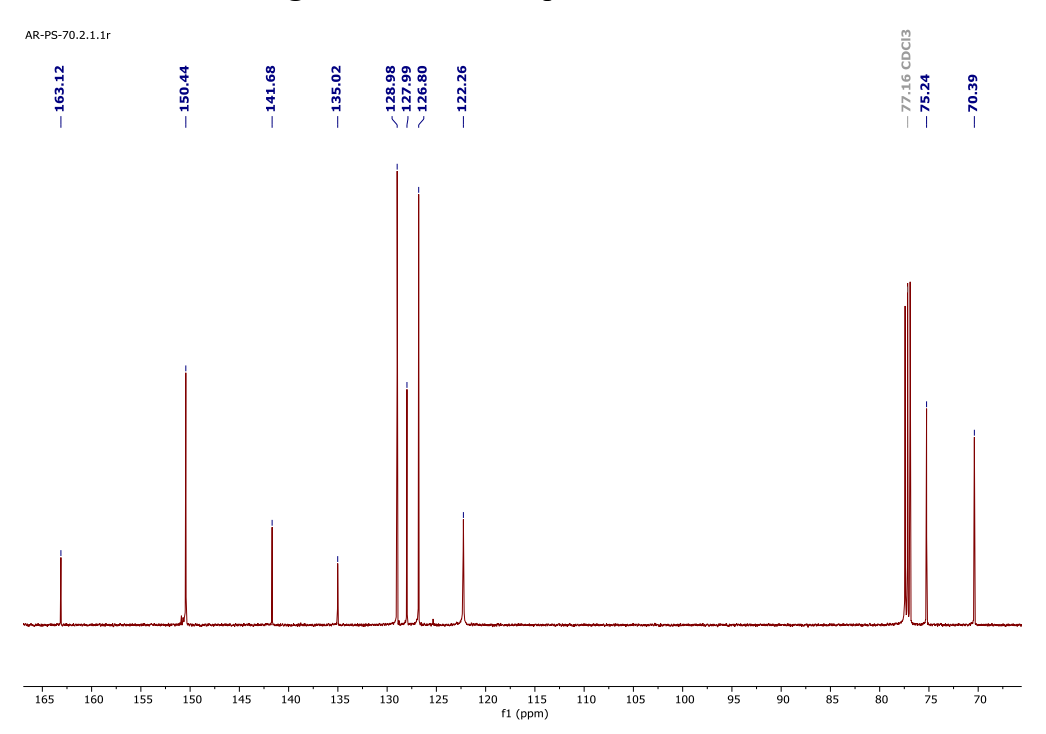


Figure 11: ${}^{13}C\{{}^{1}H\}$ NMR spectra of L3

3.1.1.4 Characterization of L4

L4 was synthesised according to scheme 4. In the reaction, dry MeOH used as a solvent. The final product was pale white solid compound with a 47 % yield. The obtained product was characterised by ¹H and ¹³C{¹H}

NMR spectroscopy (Figures 12 and 13). Peaks of most deshielded hydrogen were observed near nine ppm, thereby confirming that ligand is formed.

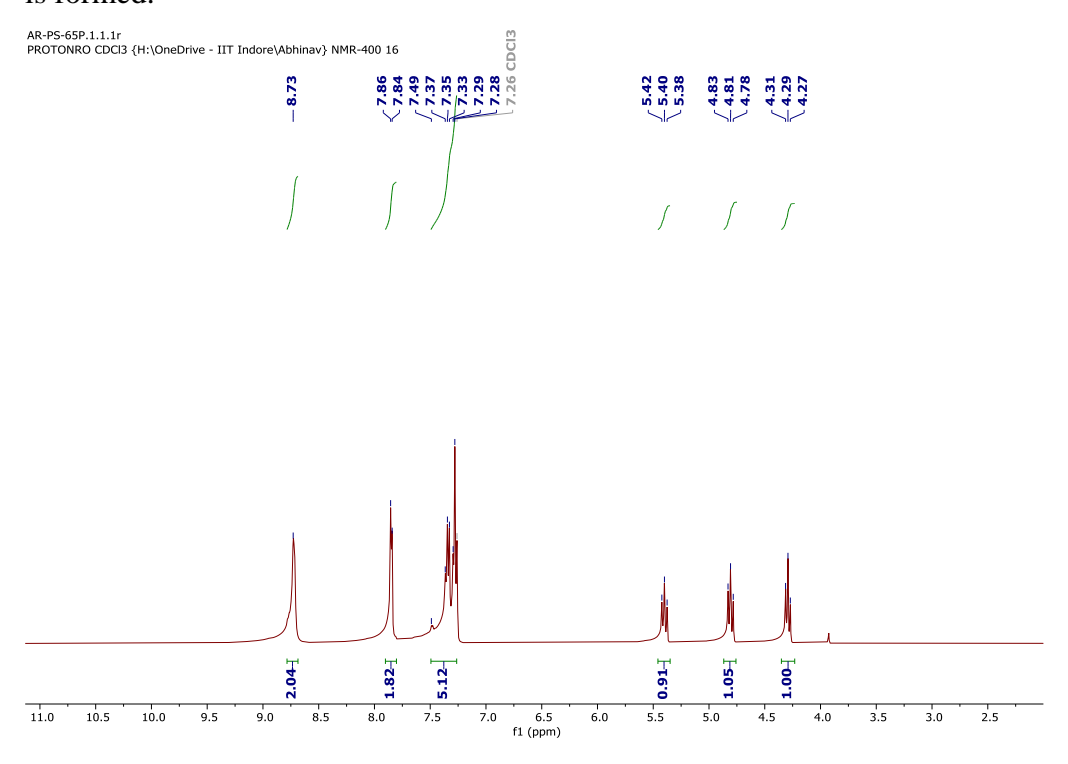


Figure 12: ¹H NMR spectra of L4

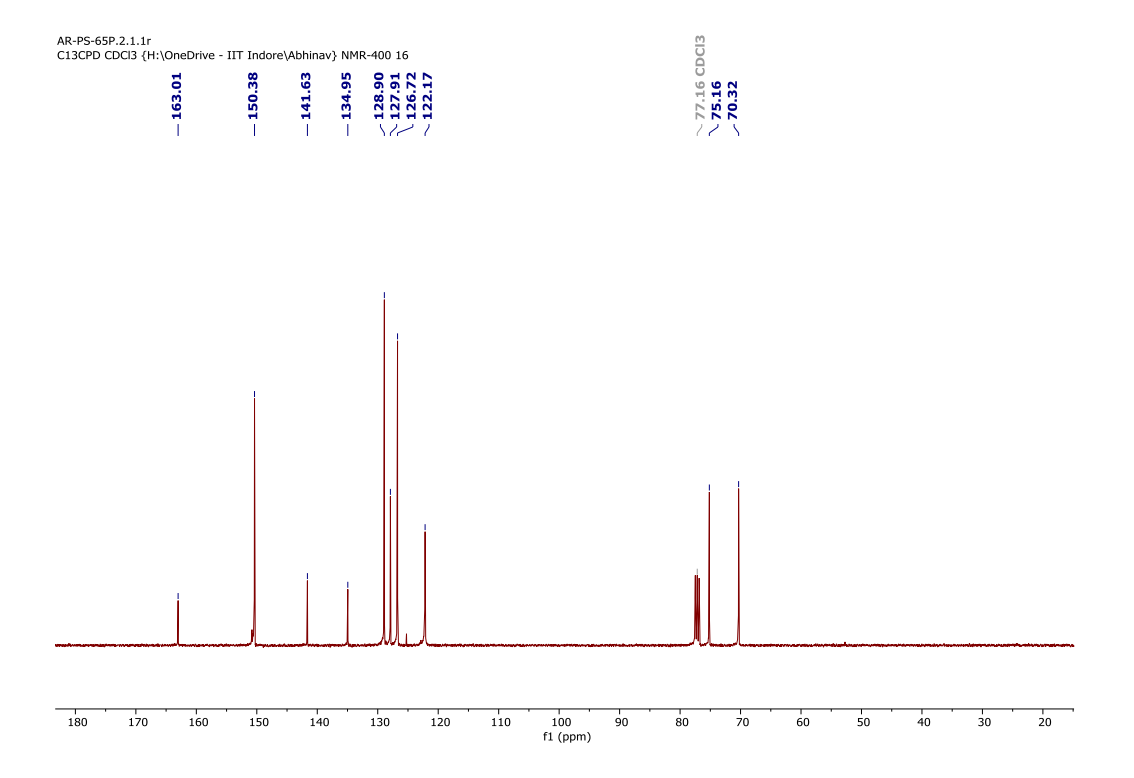


Figure 13: ¹³C{¹H} NMR spectra of L4

3.1.2 Characterization of complexes

3.1.2.1 Characterization of C1

The complex formation of **C1** was confirmed by LCMS (Figure. 14). The complex was yellow in colour when synthesised in the solid state with an yield of 88%. **C1** had good solubility in most of the solvents. It was further characterized by different nuclei NMR ¹H (Figure 15), ¹³C{¹H} (Figure 16), ³¹P{¹H} (Figure 17).

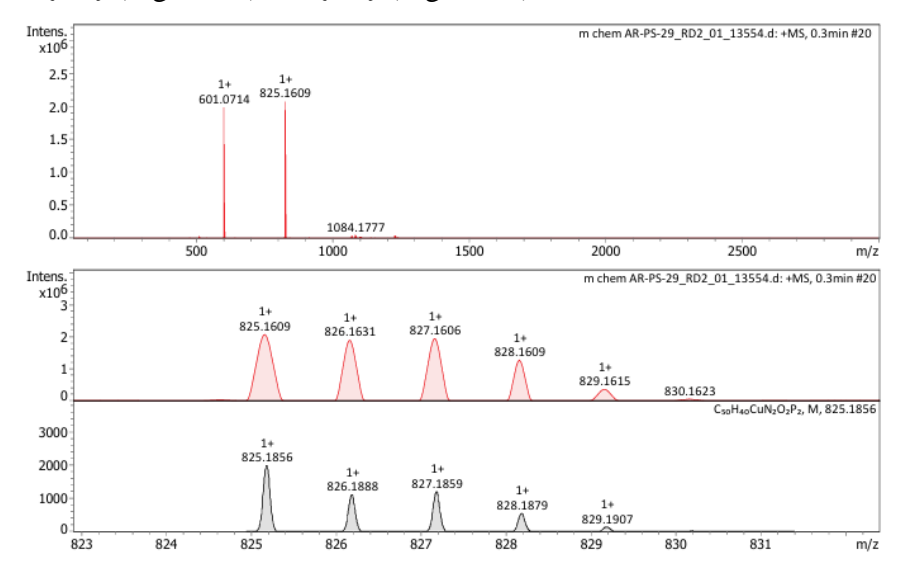


Figure 14: Mass spectrogram of C1

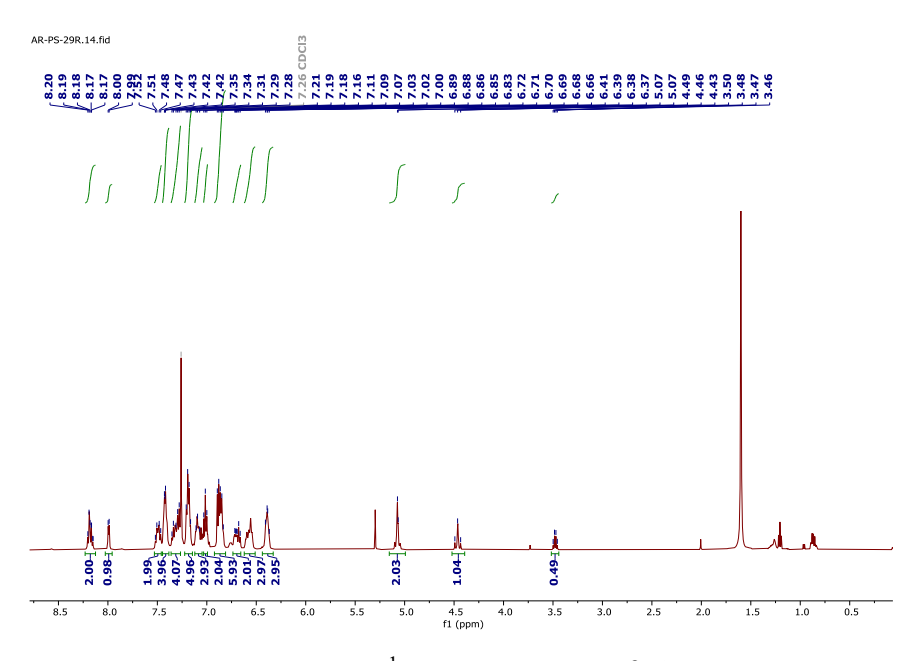


Figure 15: ¹H NMR spectra of C1

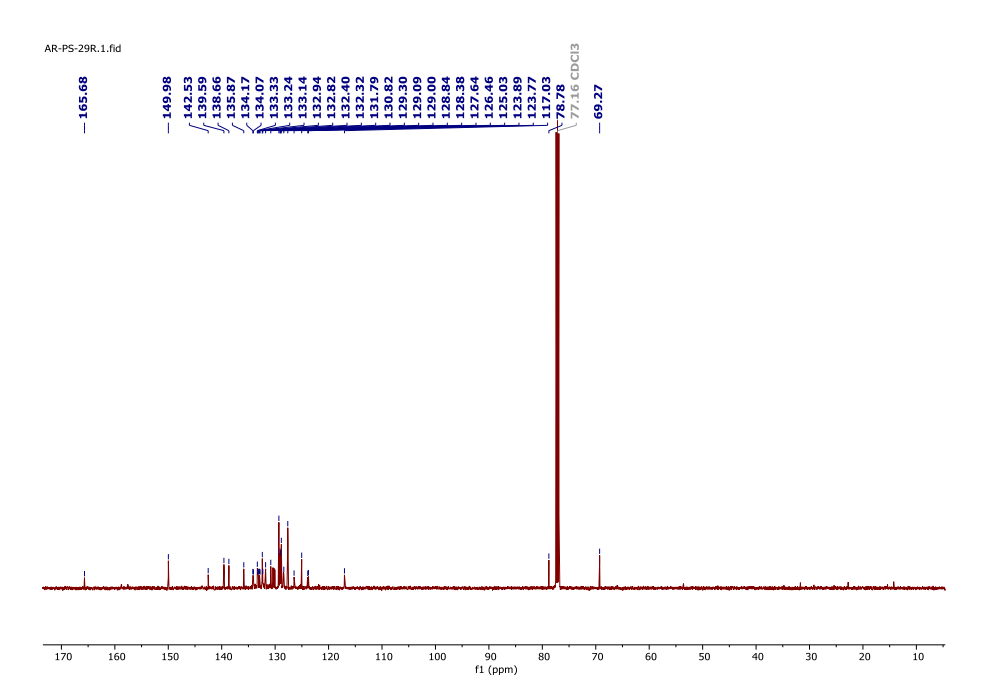


Figure 16: ${}^{13}C\{{}^{1}H\}$ NMR spectra of C1

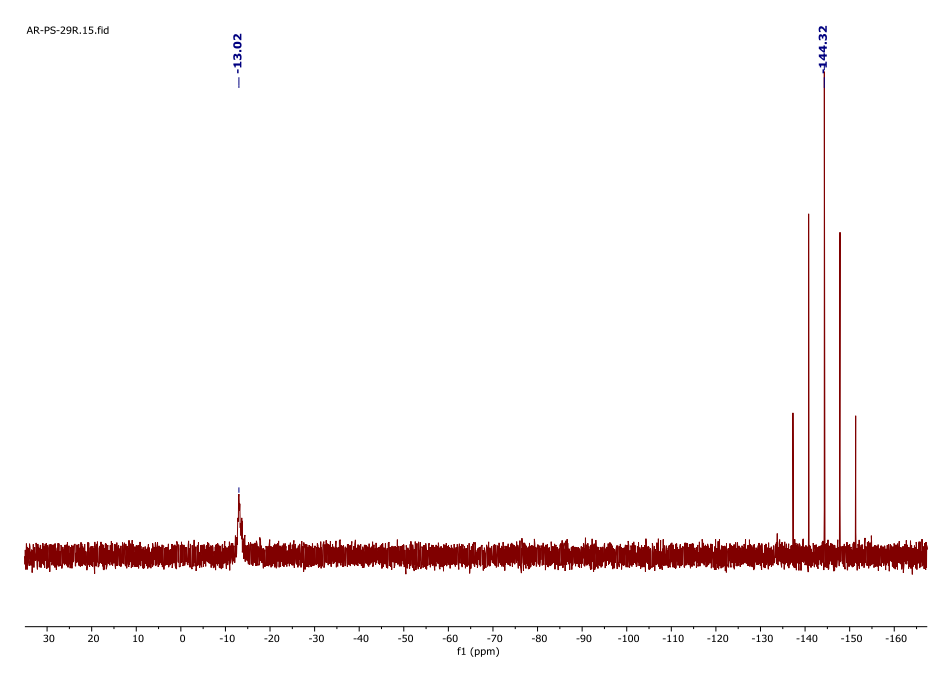


Figure 17: $^{31}P\{^{1}H\}$ NMR spectra of C1

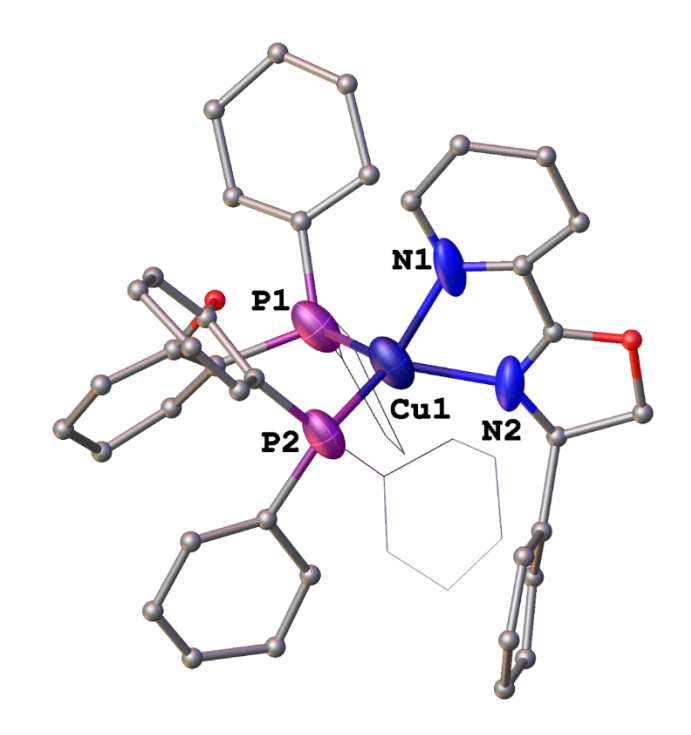


Figure 18: SCXRD of C1

3.1.2.2 Characterization of C2

The complex formation of **C2** was confirmed by LCMS (Figure. 19). The complex was yellow in colour when synthesised in the solid state with an yield of 83%. **C2** had good solubility in most of the solvents. It was further characterized by different nuclei NMR ¹H (Figure 20), ¹³C{¹H} (Figure 21), ³¹P{¹H} (Figure 22).

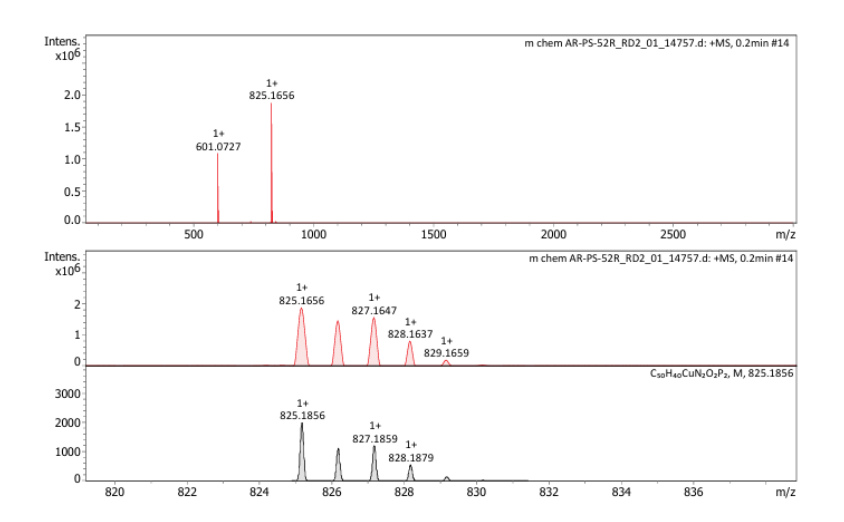
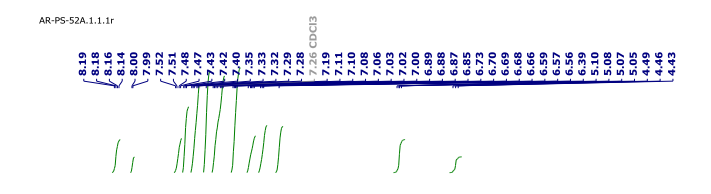


Figure 19: Mass spectrogram of C2



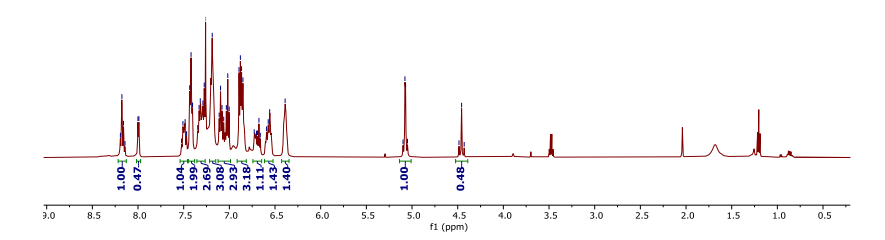


Figure 20: ¹H NMR spectra of C2

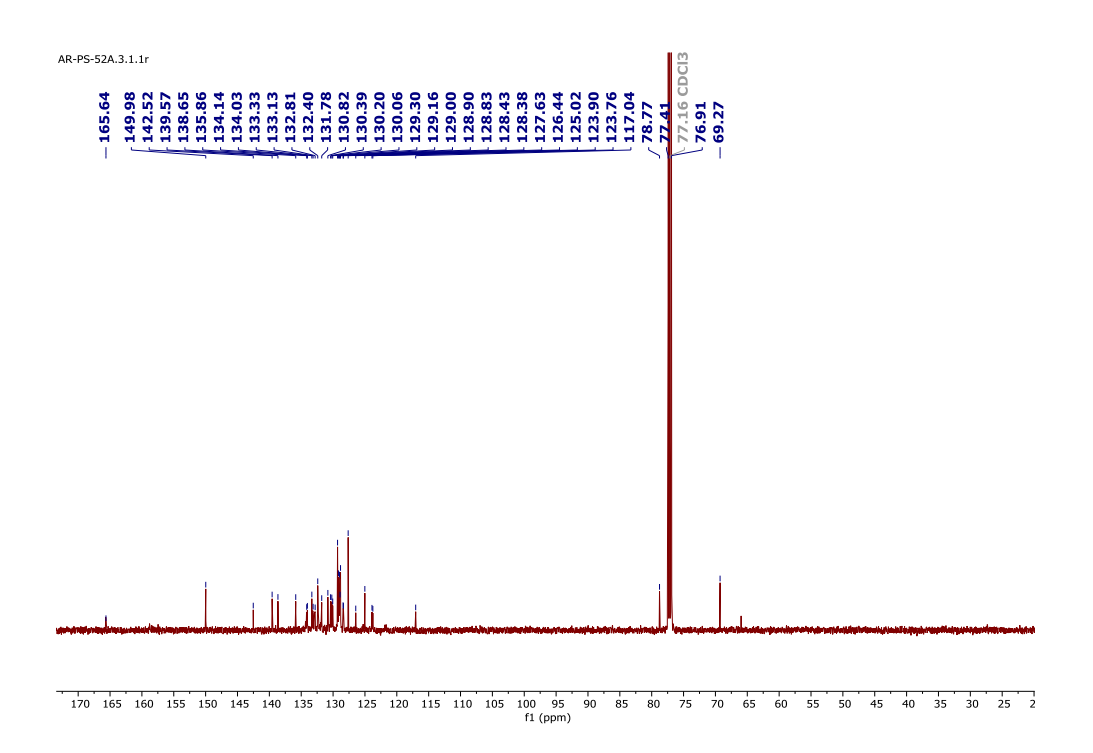


Figure 21: ¹³C{¹H} NMR spectra of C2

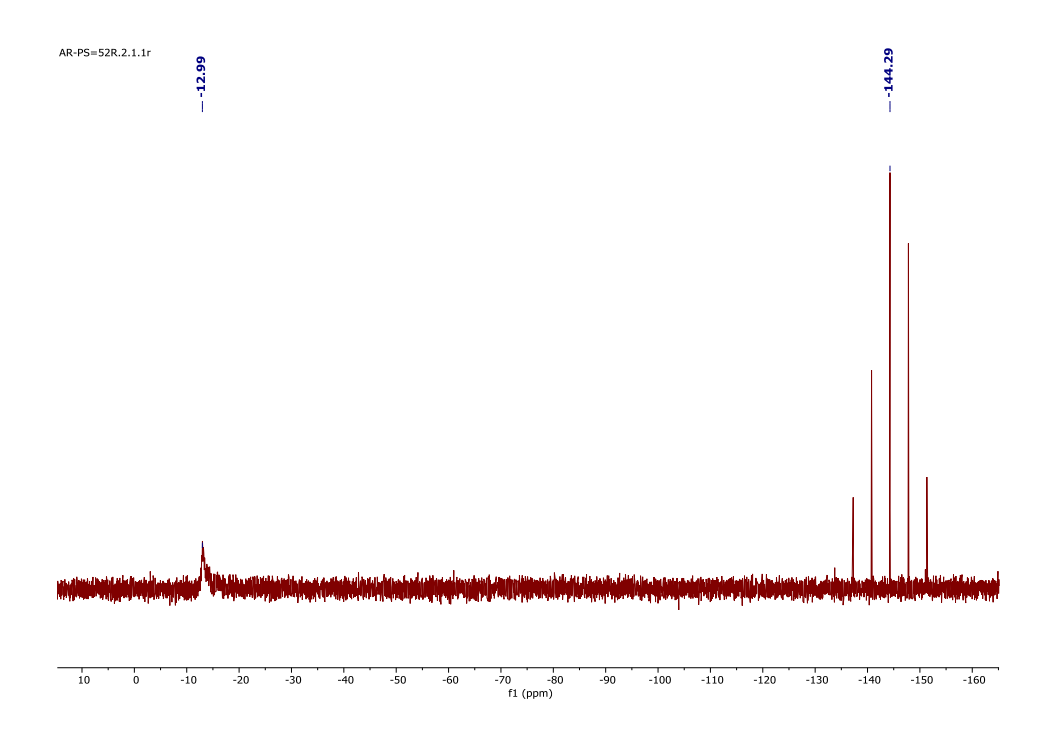


Figure 22: ³¹P{¹H} NMR spectra of C2

3.1.2.3 Characterization of C3

The complex formation of **C3** was confirmed by LCMS (Figure. 23). The complex was yellow in colour when synthesised in the solid state with an yield of 83%. **C3** had good solubility in most of the solvents. It was further characterized by different nuclei NMR ¹H (Figure 24), ¹³C{¹H} (Figure 25), ³¹P{¹H} (Figure 26). The molecular structure of the complex **C3** is confirmed using the single-crystal X-ray diffraction technique (Figure. 27). The crystal structure has a distorted tetrahedral geometry with a P2 space group around the copper center with coordination to two P atoms of Xantphos ligand and two N atoms of chiral ligand occupying the total four coordinate sites of Cu center. The structure has a monoclinic crystal system.

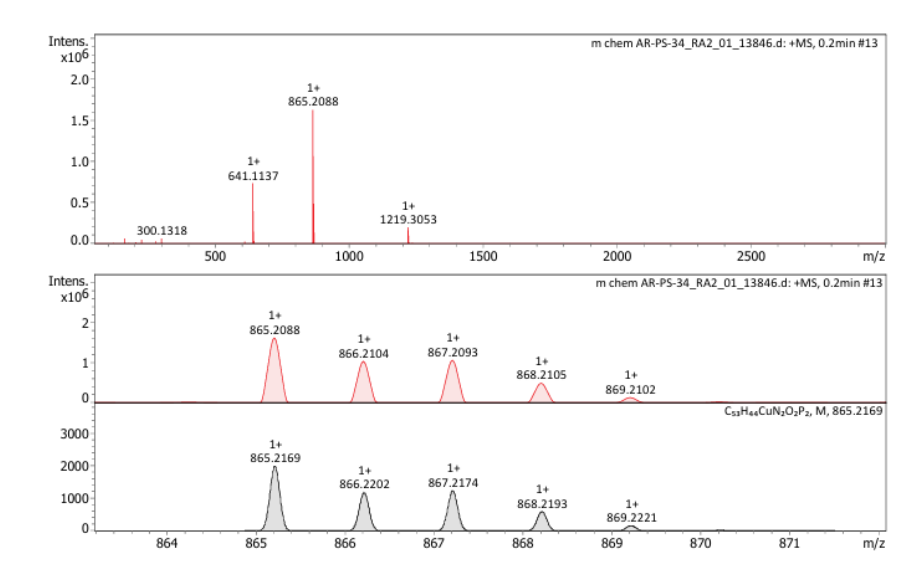


Figure 23: Mass spectrogram of C3

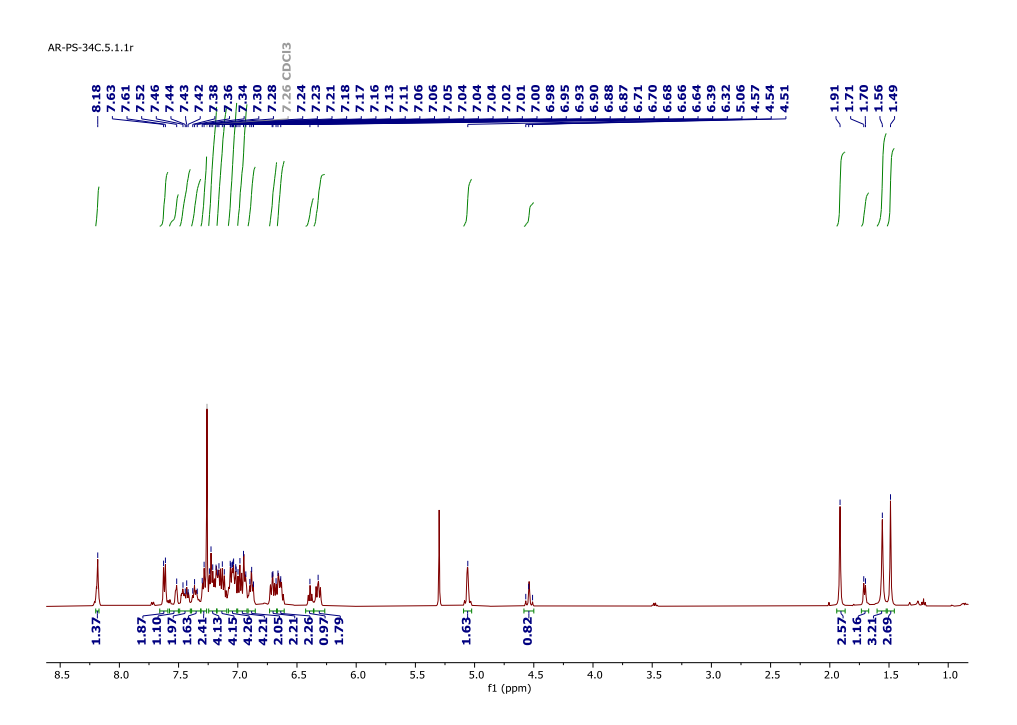


Figure 24: ¹H NMR spectra of C3

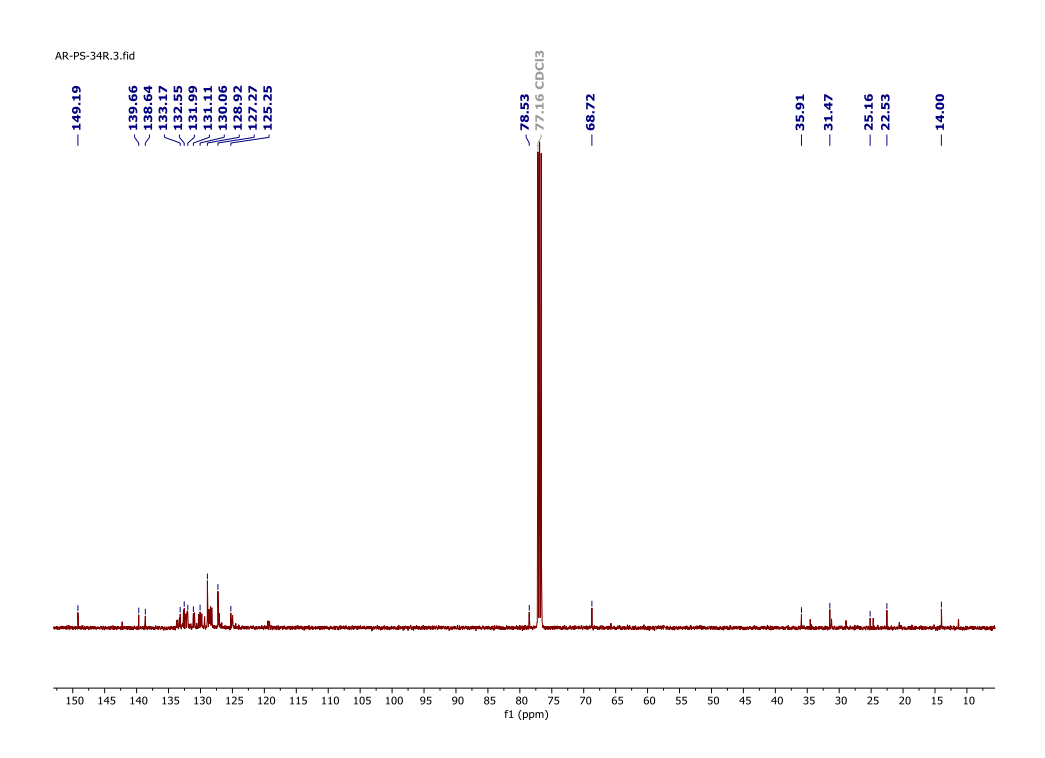


Figure 35: ¹³C{¹H} NMR spectra of C3

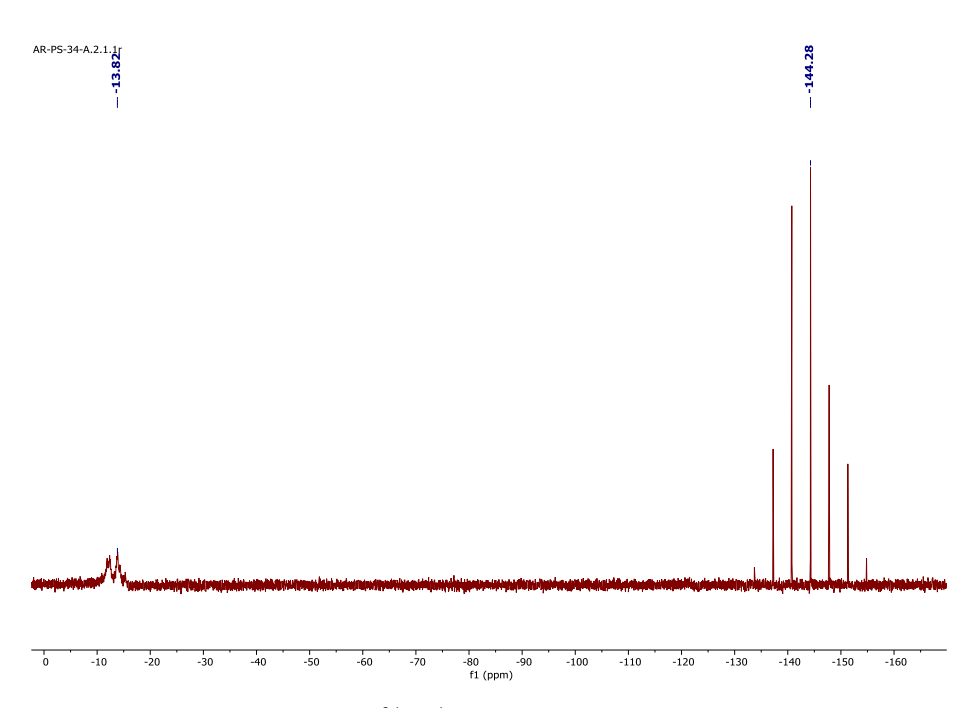


Figure 46: $^{31}P\{^{1}H\}$ NMR spectra of C3

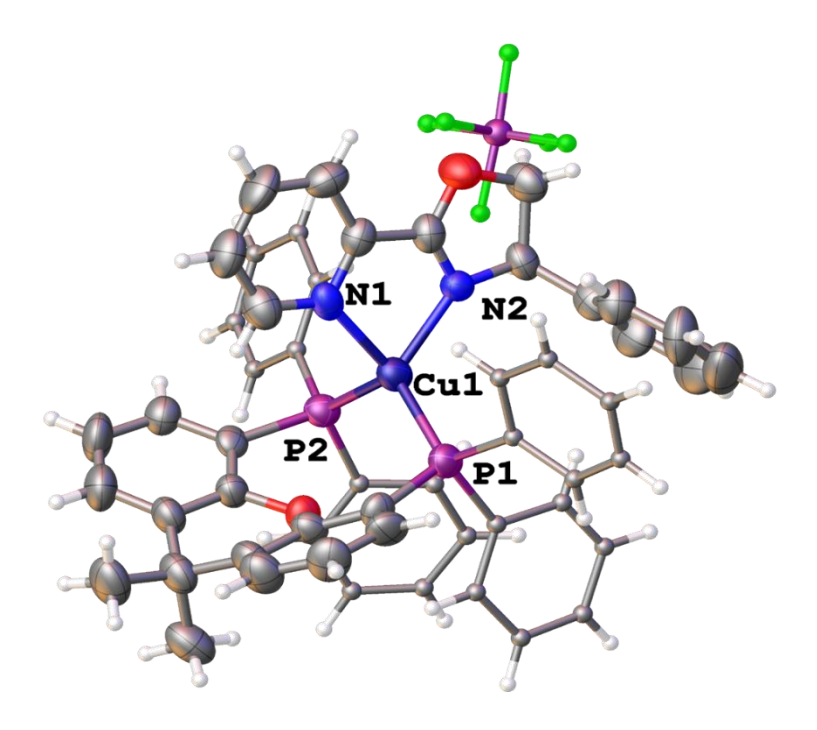


Figure 27: Single crystal diffracted structure of complex C**3**. Selected bond lengths (Å) and angles (°): Cu1-P1; 2.276(2), Cu1-P2; 2.279(2), Cu1-N1; 2.130(8), Cu1-N2; 2.066(7), P1-Cu1-P2; 114.65(9), N1-Cu1-P1; 116.4(2), N1-Cu1-P2; 105.14(19), N2-Cu1-P1; 118.05(19), N2-Cu1-P2; 117.01(19), N2-Cu1-N1; 80.0(3).

3.1.2.4 Characterization of C4

The complex formation of **C4** was confirmed by LCMS (Figure. 28). The complex was yellow in colour when synthesised in the solid state with an yield of 64%. **C4** had good solubility in most of the solvents. It was further characterized by different nuclei NMR ¹H (Figure 29), ¹³C{¹H} (Figure 30), ³¹P{¹H} (Figure 31). The molecular structure of the complex **C3** is confirmed using the single-crystal X-ray diffraction technique (Figure. 32). The crystal structure has a distorted tetrahedral geometry with a P2₁ space group around the copper center with coordination to two P atoms of Xantphos ligand and two N atoms of chiral ligand occupying the total four coordinate sites of Cu center. The structure has a monoclinic crystal system.

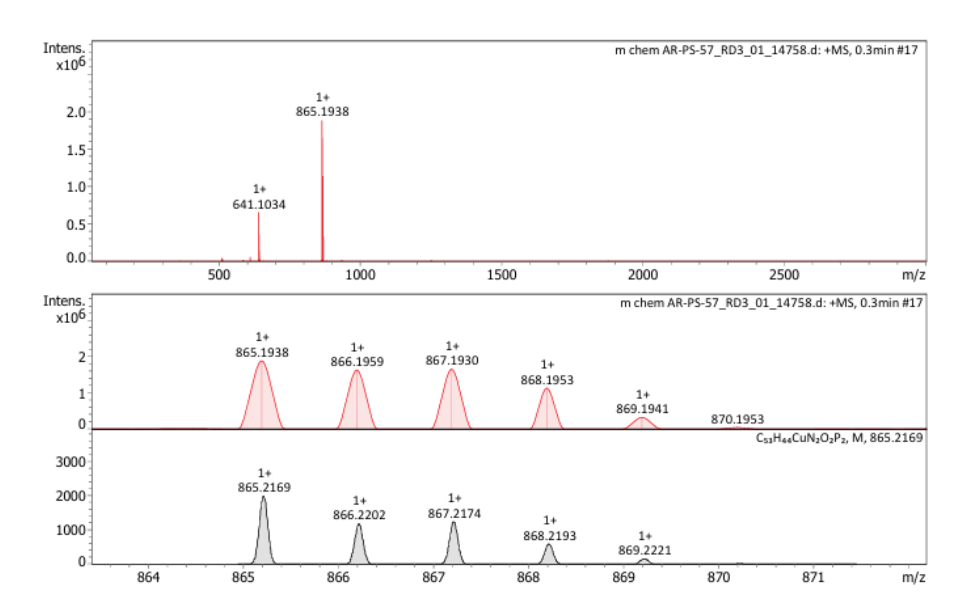
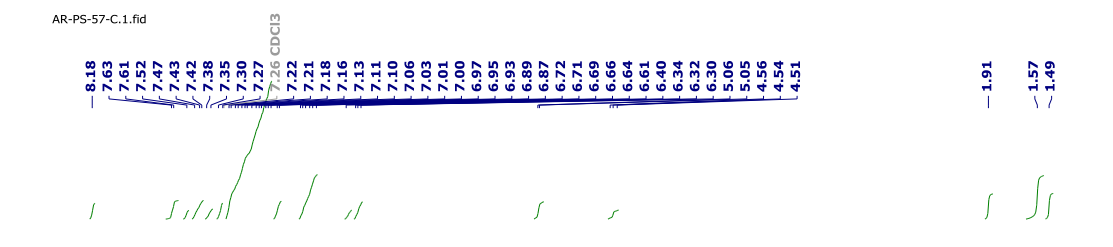


Figure 58: Mass spectrogram of C4



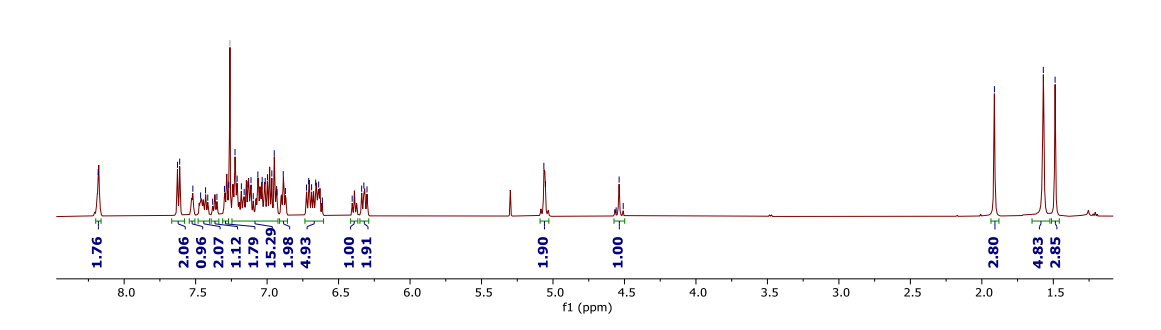


Figure 69: ¹H NMR spectra of C4

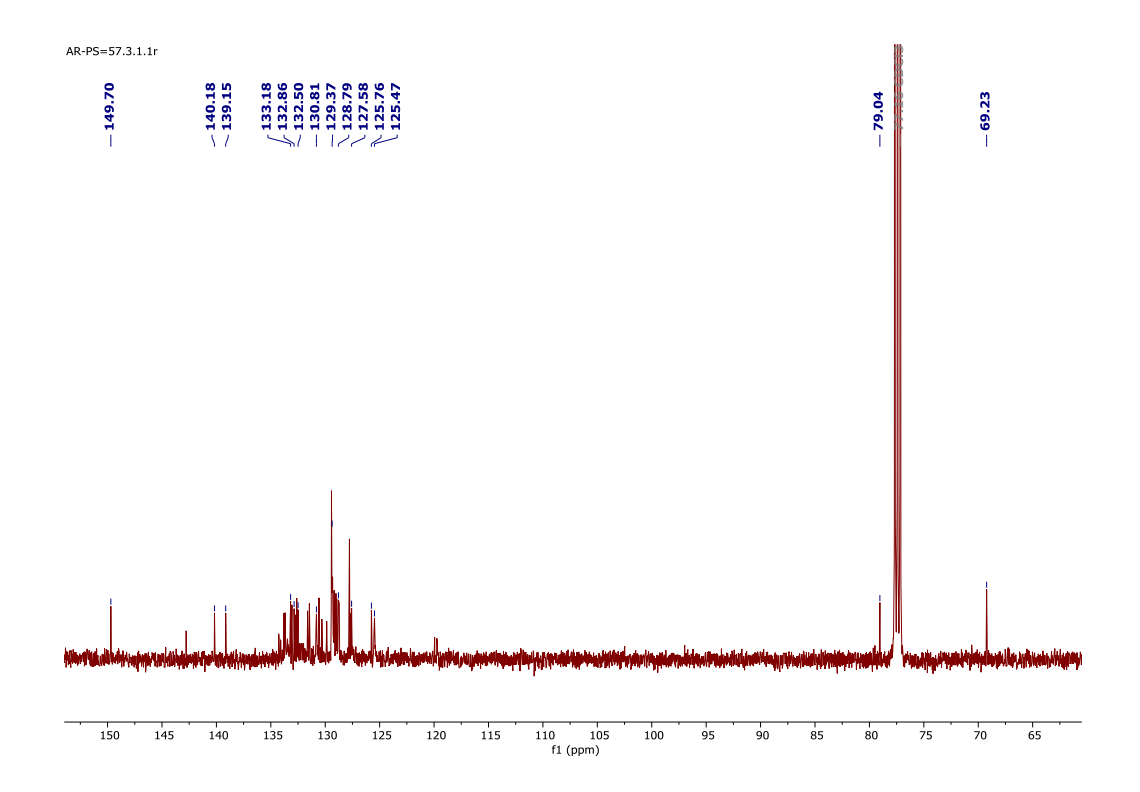


Figure 30: ¹³C{¹H} NMR spectra of C4

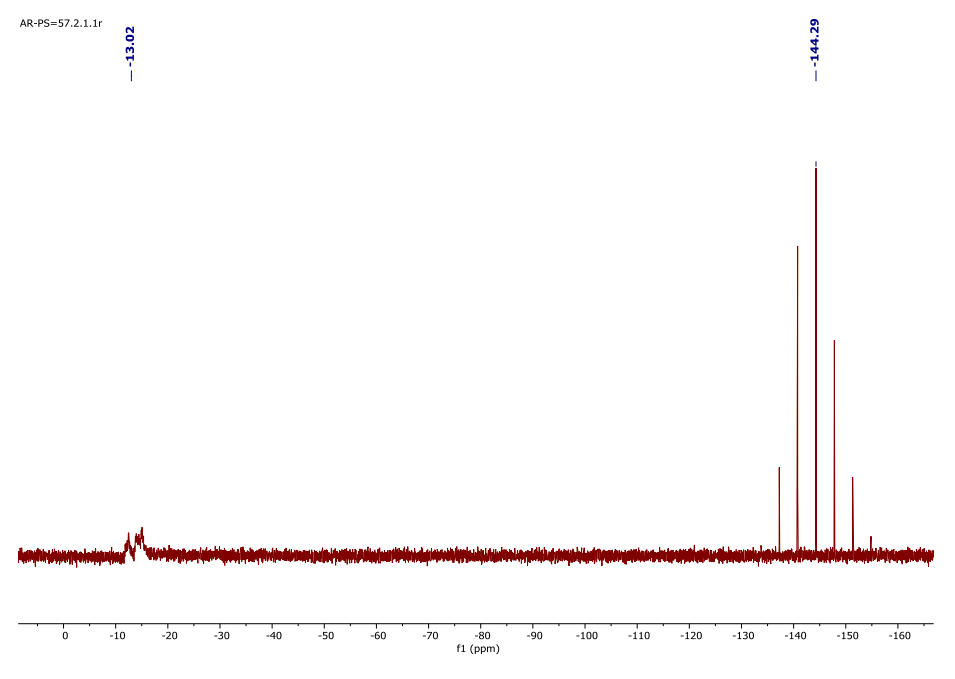


Figure 31: $^{31}P\{^{1}H\}$ NMR spectra of C4

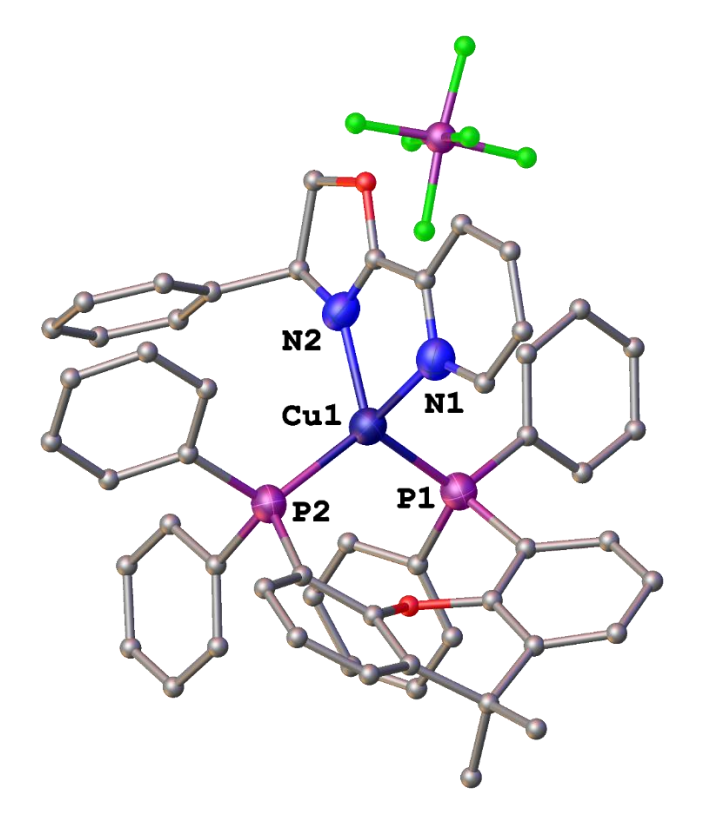


Figure 32: Single crystal diffracted structure of complex C4. Selected bond lengths (Å) and angles (°): Cu1-P1; 2.273(19), Cu1-P2; 2.278(17), Cu1-N1; 2.161(6), Cu1-N2; 2.067(5), P1-Cu1-P2; 115.20(7), N1-Cu1-P1; 106.03(16), N1-Cu1-P2; 115.74(16), N2-Cu1-P1; 116.18(16), N2-Cu1-P2; 118.64(16), N2-Cu1-N1; 78.9(2)

3.1.2.5 Characterization of C5

The complex formation of **C5** was confirmed by LCMS (Figure. 33). The complex was green yellow in colour when synthesised in the solid state with an yield of 75%. **C5** had good solubility in most of the solvents. It was further characterized by different nuclei NMR ¹H (Figure 34), ¹³C{¹H} (Figure 35), ³¹P{¹H} (Figure 36).

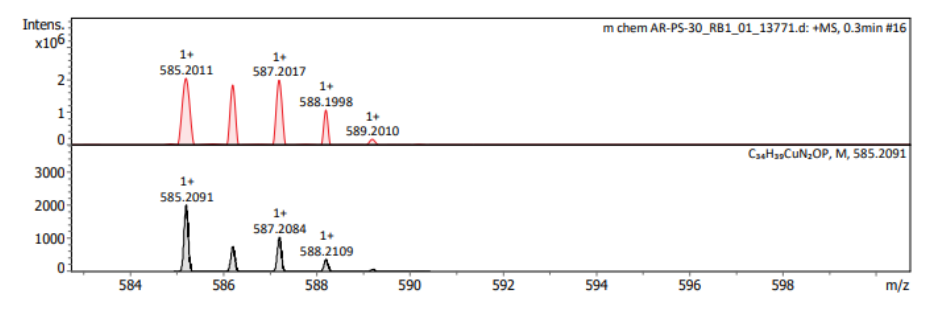


Figure 33: Mass spectrogram of C5

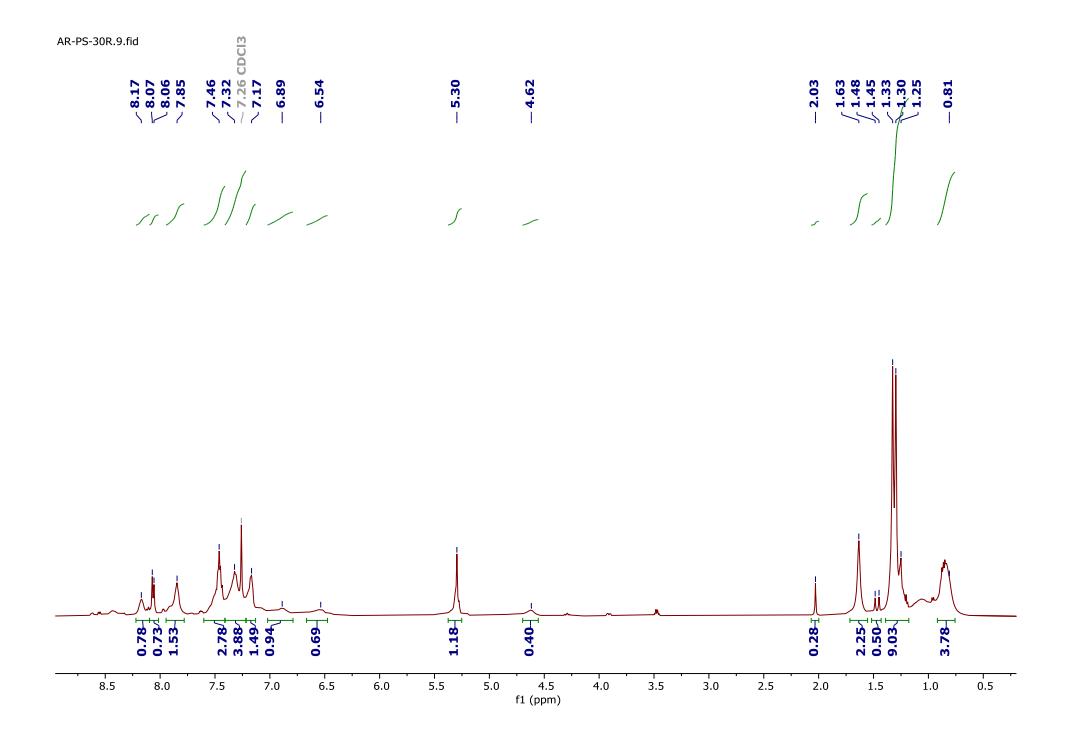


Figure 34: ¹H NMR spectra of C5

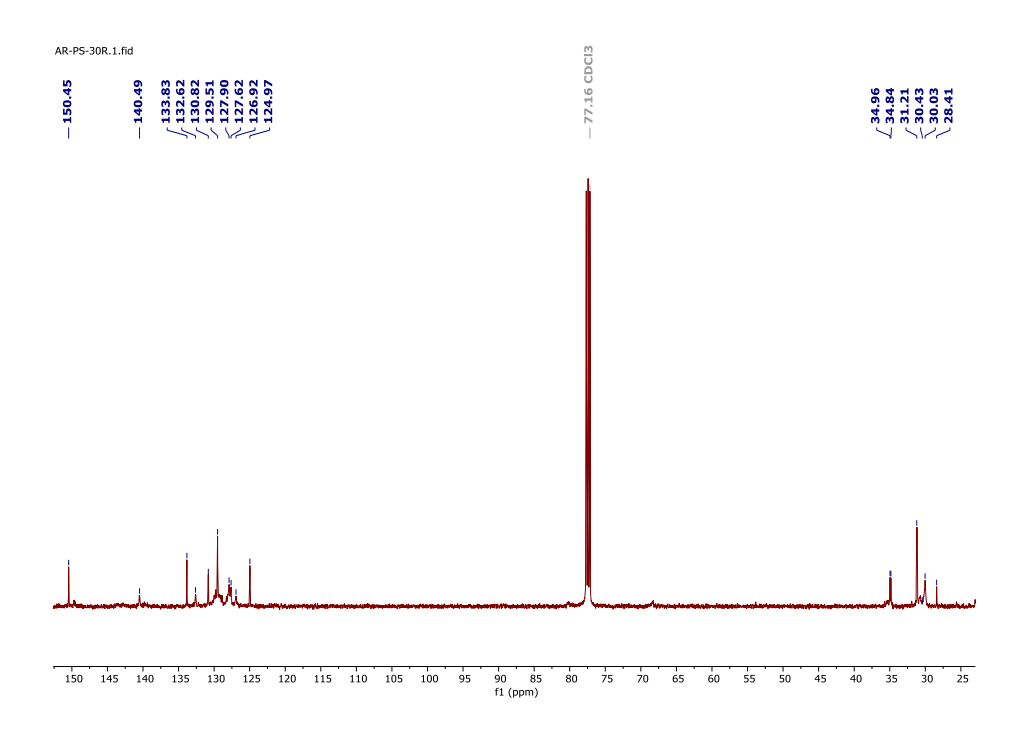


Figure 35: ¹³C{¹H} NMR spectra of C5

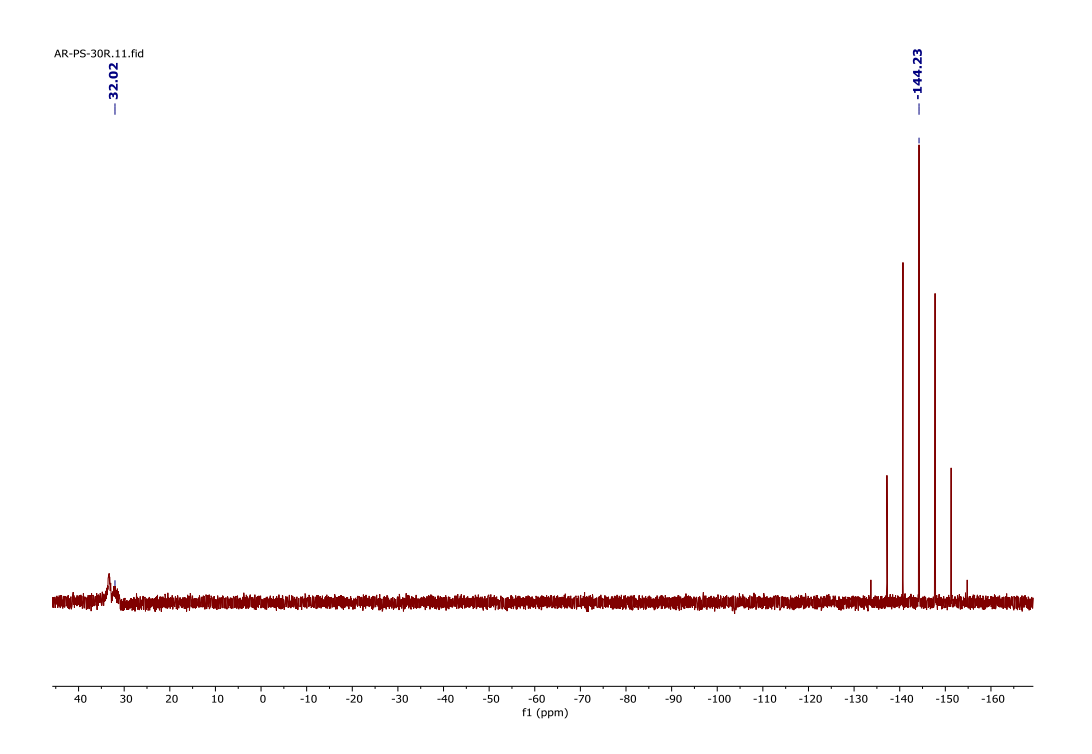


Figure 36: ³¹P{¹H} NMR spectra of C5

3.1.2.6 Characterization of C6

The complex formation of **C6** was confirmed by LCMS (Figure. 37). The complex was green yellow in colour when synthesised in the solid state with an yield of 73%. **C6** had good solubility in most of the solvents. It was further characterized by different nuclei NMR ¹H (Figure 38), ³¹P{¹H} (Figure 39).

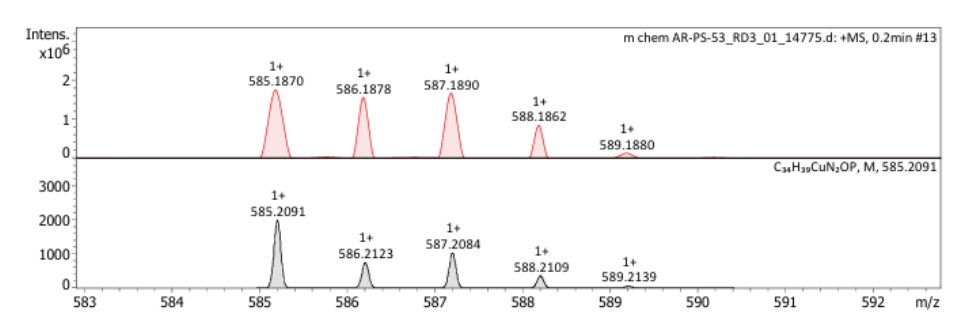


Figure 37: Mass spectrogram of C6

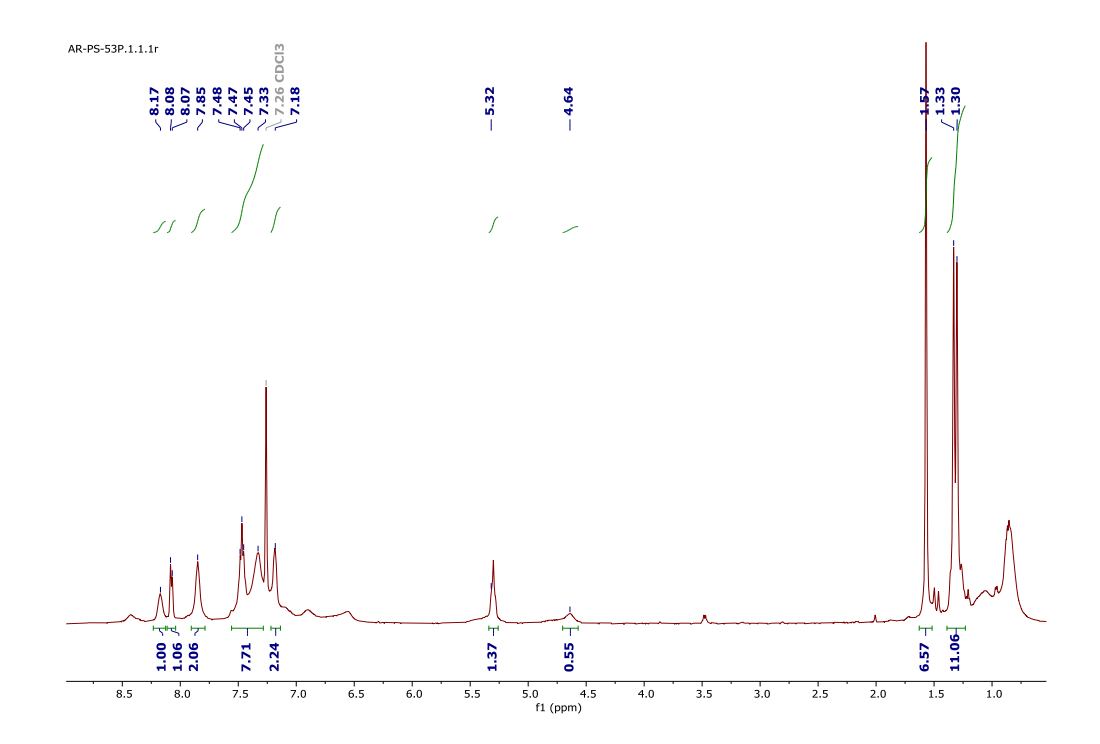


Figure 38: ¹H NMR spectra of C6

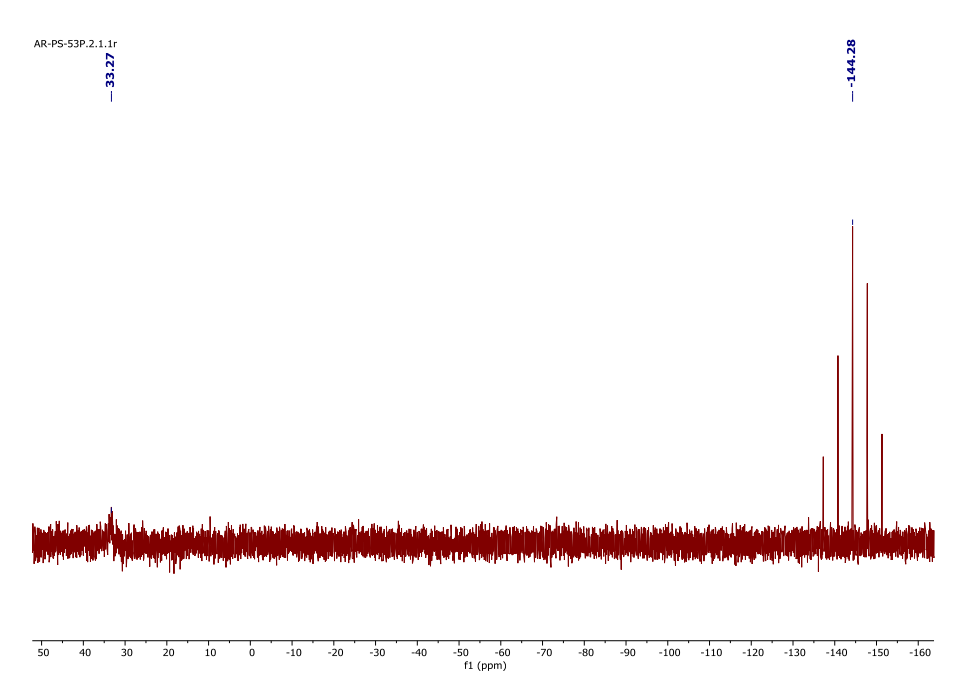


Figure 39: $^{31}P\{^{1}H\}$ NMR spectra of C6

3.1.2.7 Characterization of C7

The complex formation of **C7** was confirmed by LCMS (Figure. 40). The complex was red in colour when synthesised in the solid state with an yield of 58%. **C7** had good solubility in most of the solvents. It was further characterized by different nuclei NMR ¹H (Figure 41), ¹³C{¹H}

(Figure 42). The molecular structure of the complex **C7** is confirmed using the single-crystal X-ray diffraction technique (Figure. 43). The crystal structure has a distorted tetrahedral geometry with P2₁2₁2₁ space group around the copper center with coordination to two N atoms of chiral ligand, one P atom of triphenylphosphine ligand and I occupying the forth coordinate site of Cu center. The structure has an orthorhombic crystal system.

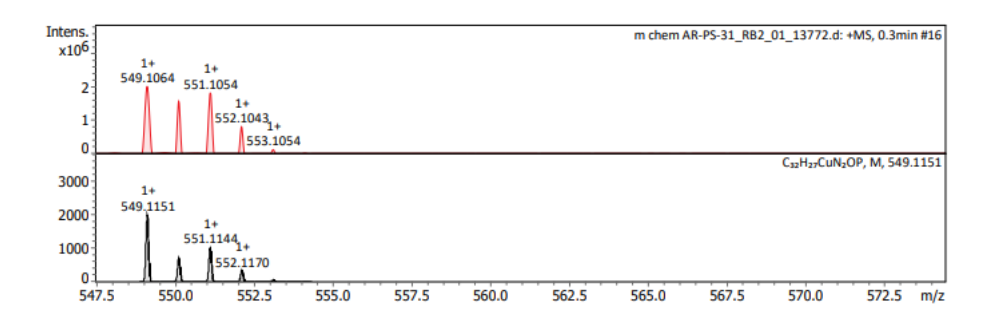


Figure 40: Mass spectrogram of C7

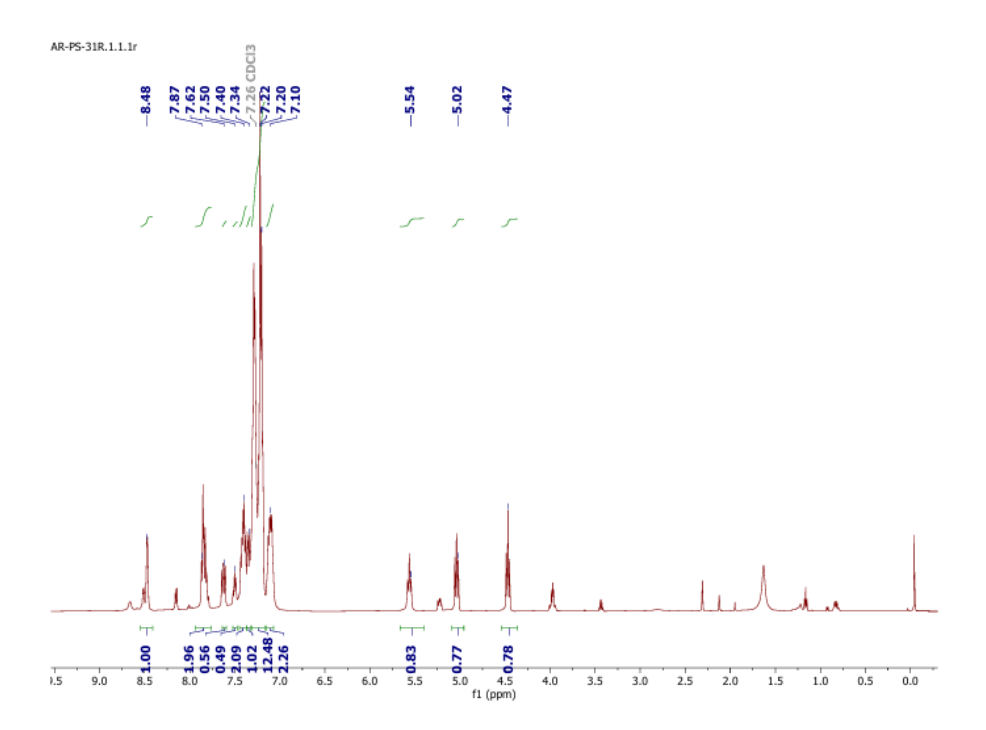


Figure 41: ¹H NMR spectra of C7

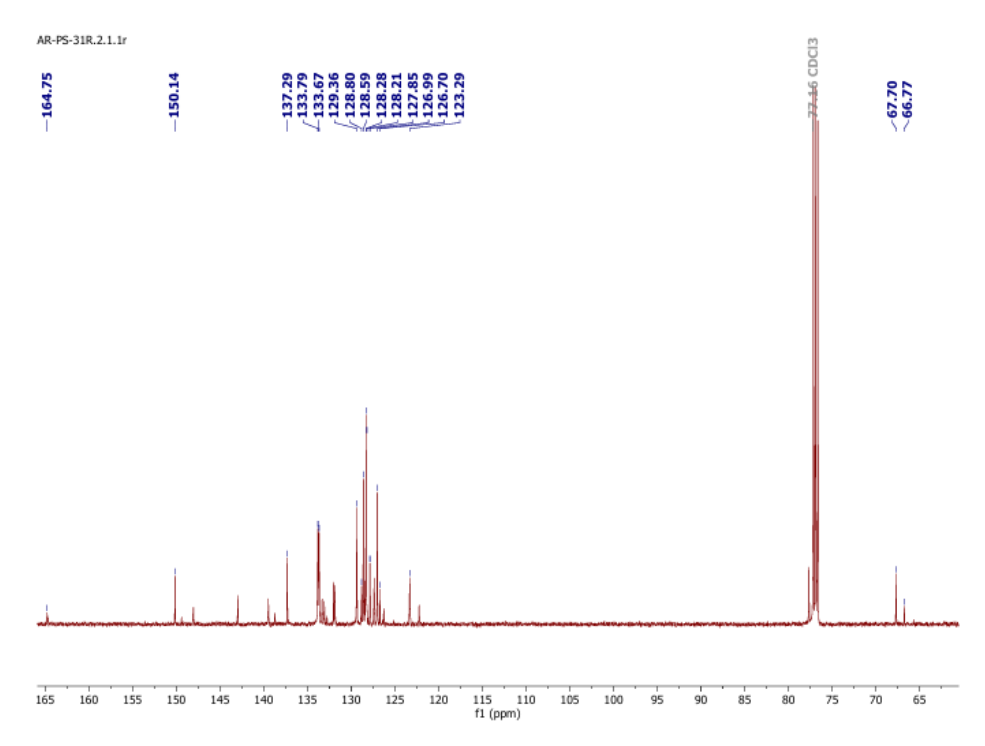


Figure 42: ${}^{13}C\{{}^{1}H\}$ NMR spectra of C7

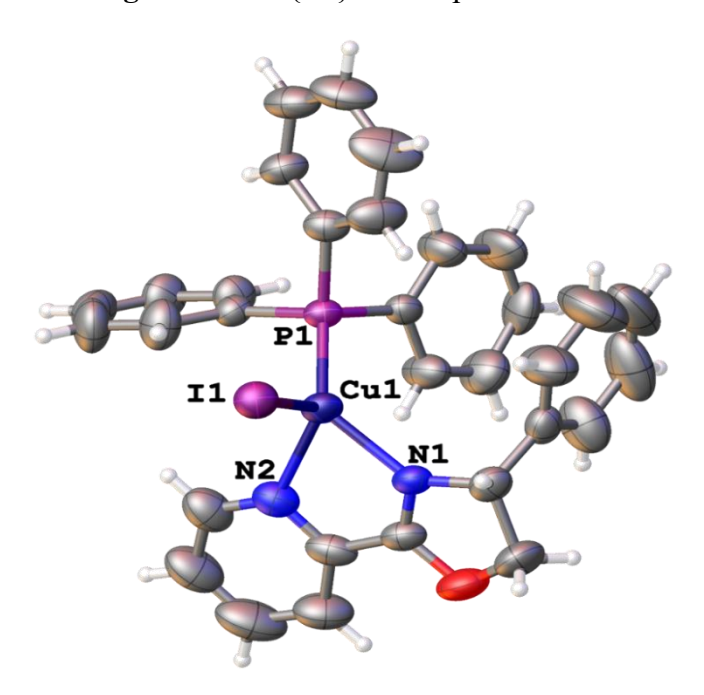


Figure 43: Single crystal diffracted structure of complex C7. Selected bond lengths (Å) and angles (°): I1-Cu1; 2.5921(9), Cu1-P1; 2.2190(16), Cu1-N1; 2.057(5), Cu1-N2; 2.297(6), P1-Cu1-I1; 118.83(5), P1-Cu1-N2; 107.12(15), N1-Cu1-I1; 108.40(15), N1-Cu1-P1; 124.36(15), N1-Cu1-N2; 76.7(2), N2-Cu1-I1; 113.52(15).

3.1.2.8 Characterization of C8

The complex formation of **C8** was confirmed by LCMS (Figure. 44). The complex was red in colour when synthesised in the solid state with an yield of 88% .**C8** had good solubility in most of the solvents. It was further characterized by different nuclei NMR ¹H (Figure 45), ¹³C{¹H} (Figure 46).

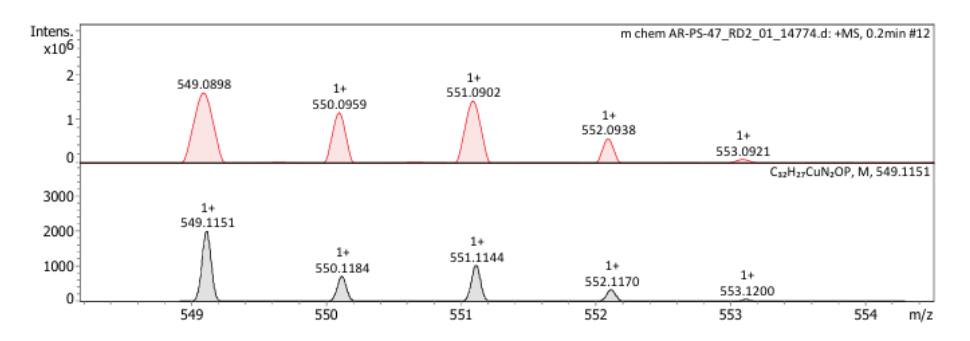


Figure 44: Mass spectrogram of C8

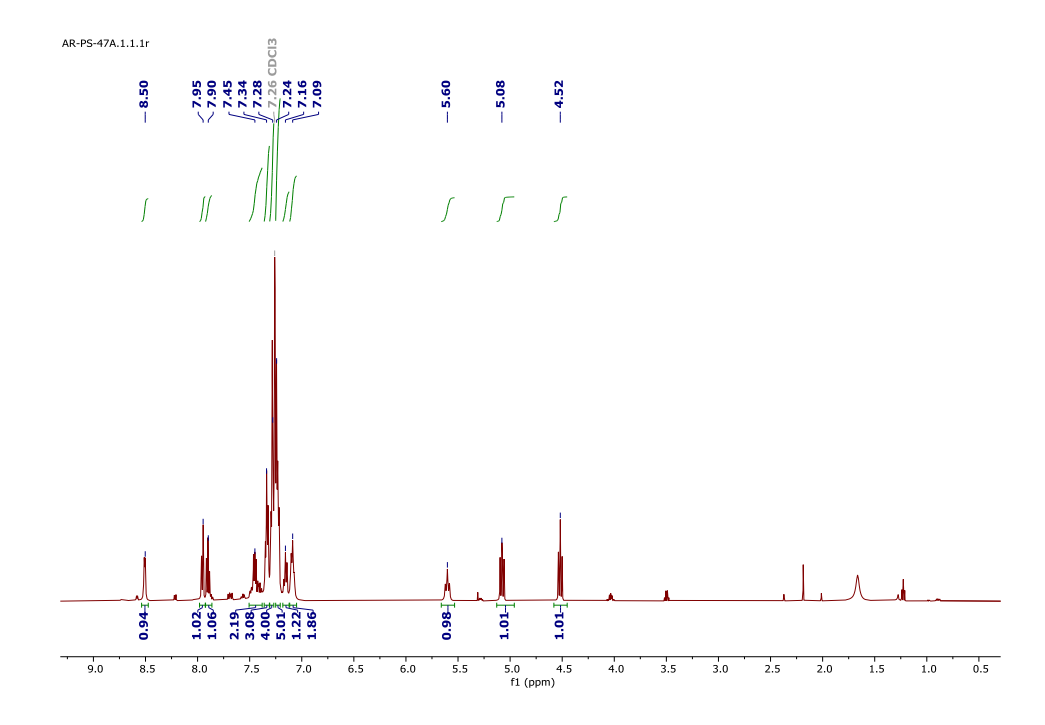


Figure 45: ¹H NMR spectra of C8

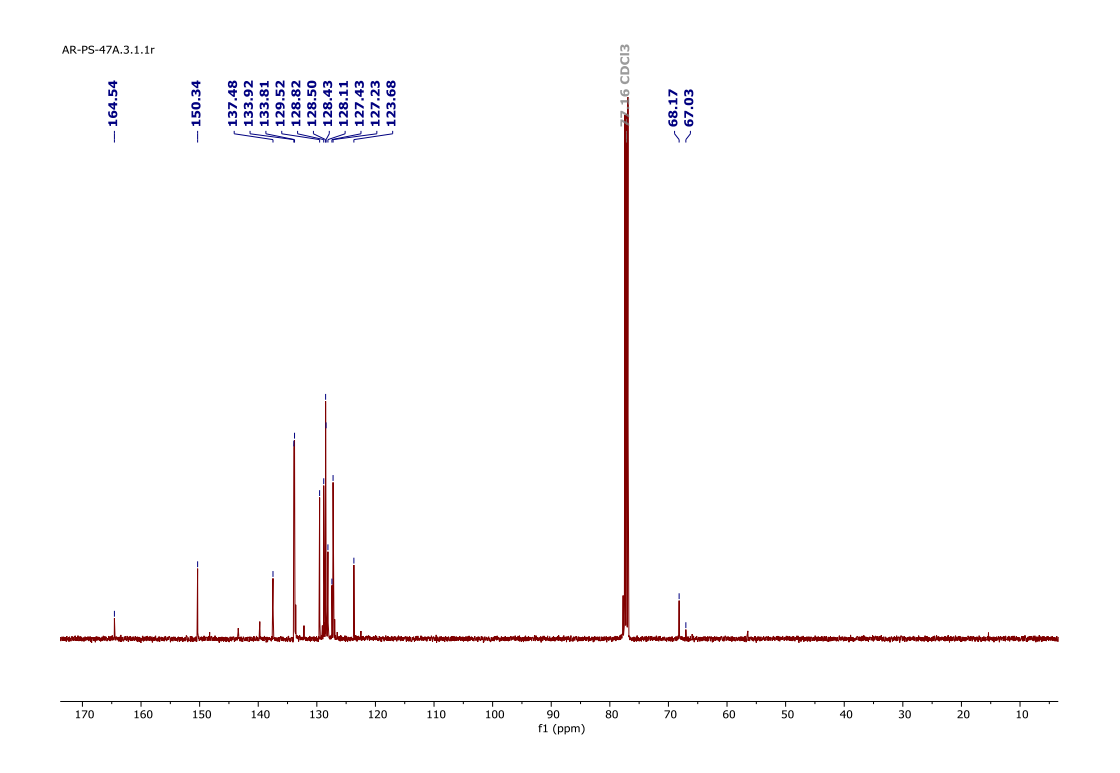


Figure 46: ¹³C{¹H} NMR spectra of C8

3.1.2.9 Characterization of C9

The complex formation of **C9** was confirmed by different nuclei NMR ¹H (Figure 47), ¹³C{¹H} (Figure 48), ³¹P{¹H} (Figure 49). The complex was yellow in colour when synthesised in the solid state with an yield of 83%. **C9** had good solubility in most of the solvents.

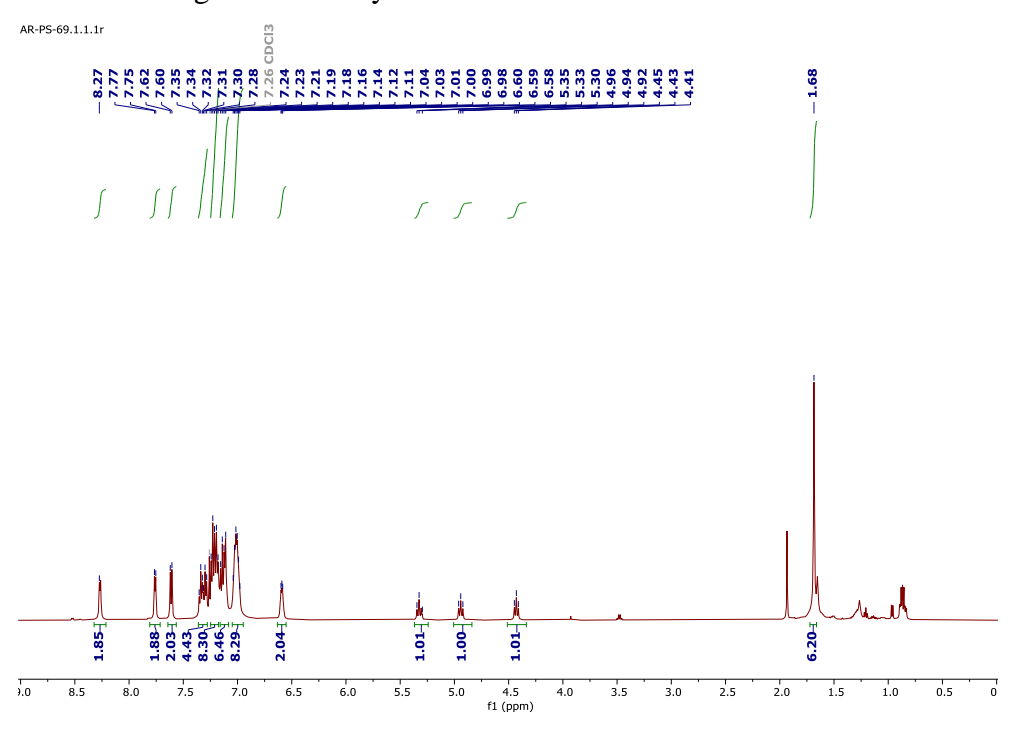


Figure 47: ¹H NMR spectra of C9

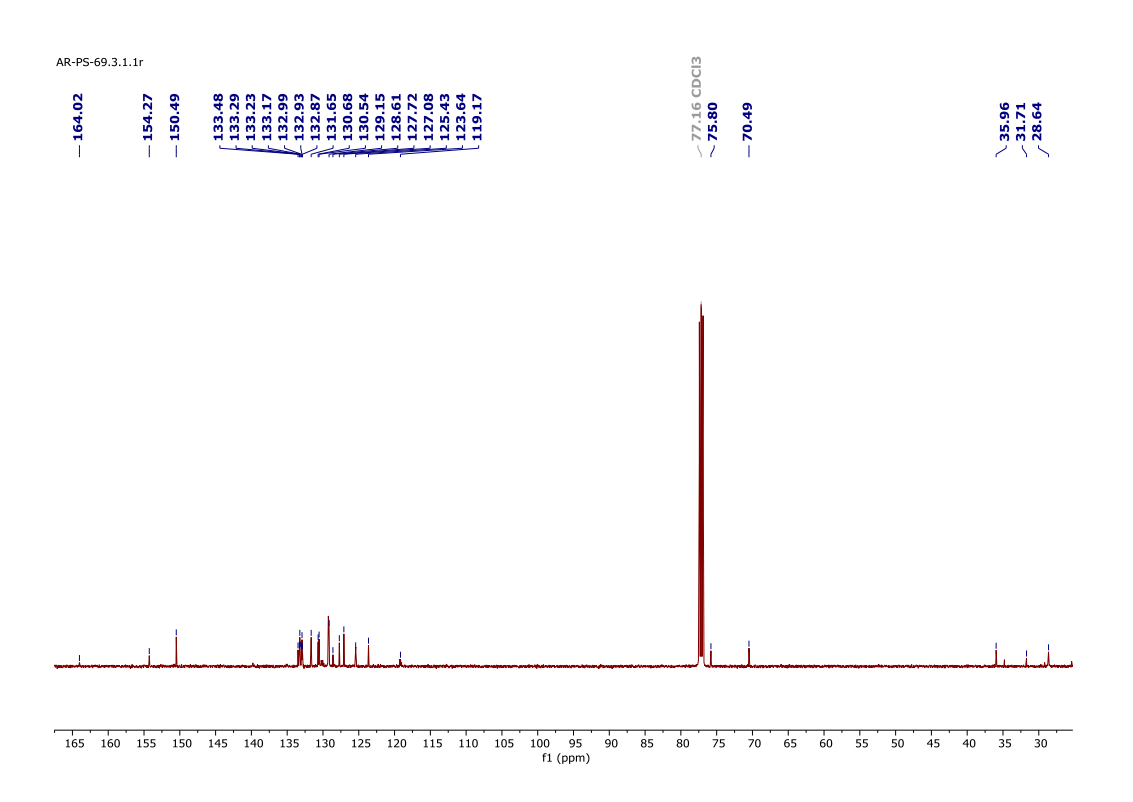


Figure 48: ${}^{13}C{}^{1}H}$ NMR spectra of C9

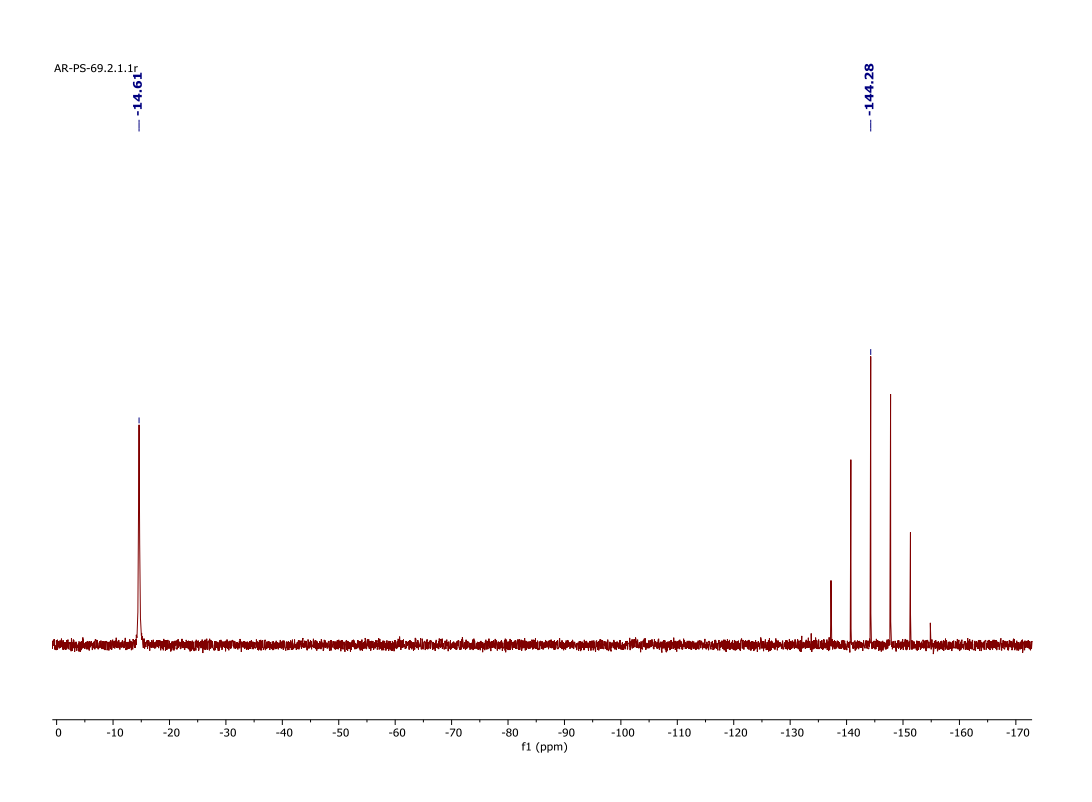


Figure 49: $^{31}P\{^{1}H\}$ NMR spectra of C9

3.1.2.10 Characterization of C10

The complex formation of **C10** was confirmed by different nuclei NMR ¹H (Figure 50), ¹³C{¹H} (Figure 51), ³¹P{¹H} (Figure 52). The complex was yellow in colour when synthesised in the solid state with an yield of 89%. **C10** had good solubility in most of the solvents.

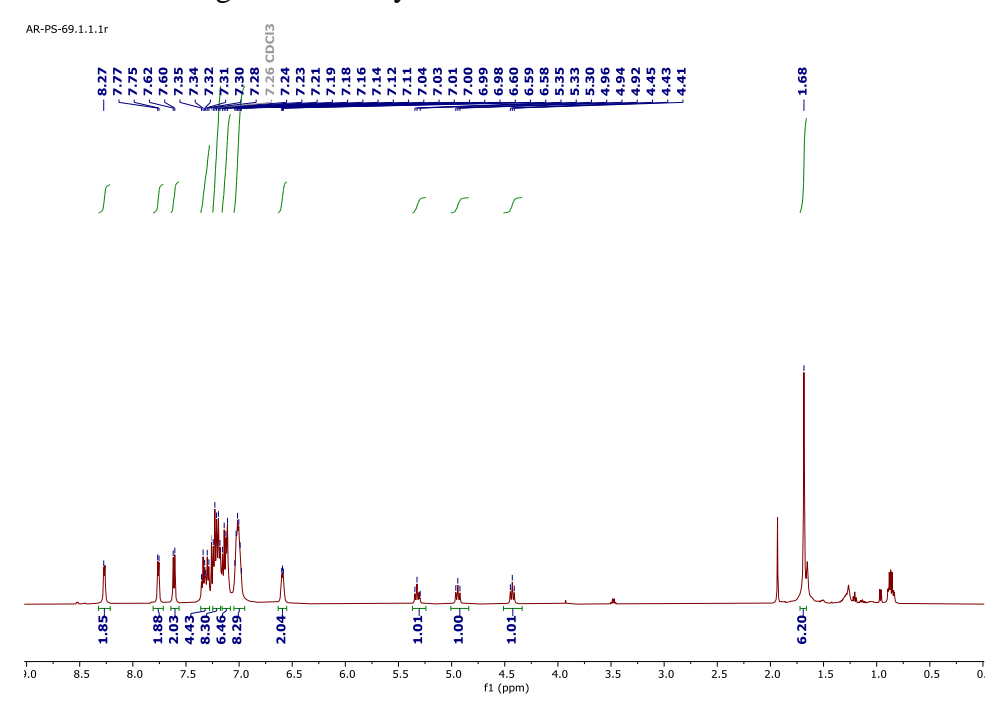


Figure 50: ¹H NMR spectra of C10

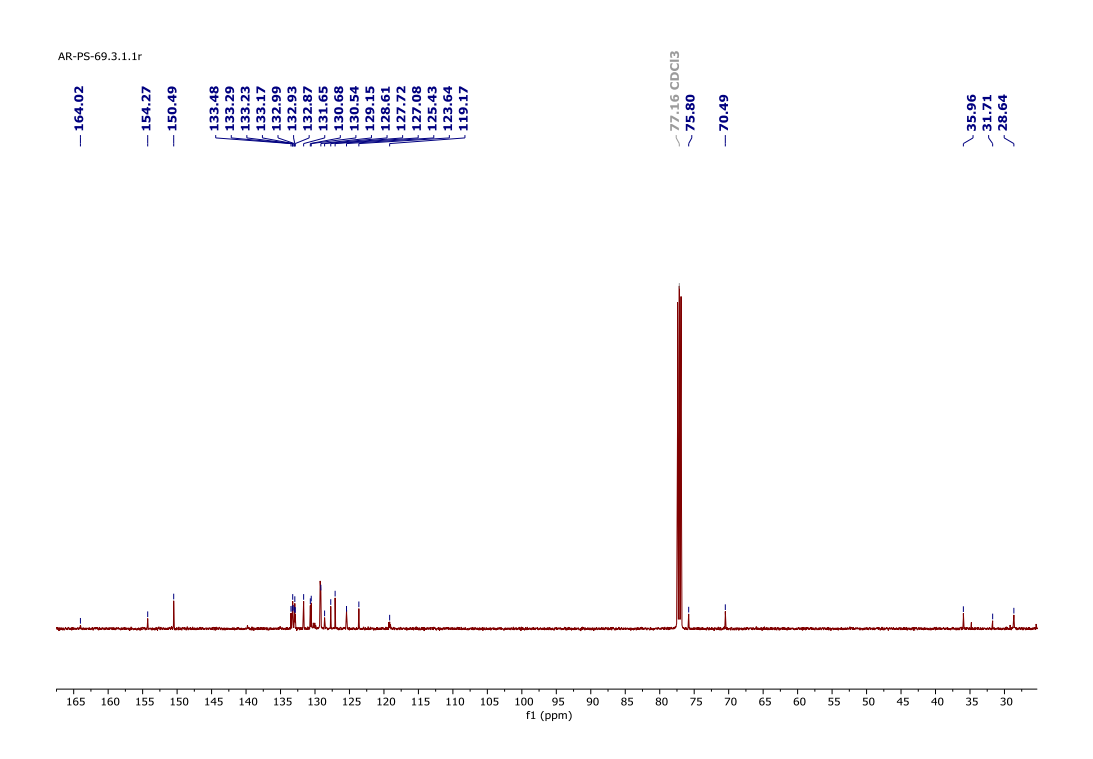


Figure 51: ${}^{13}C\{{}^{1}H\}$ NMR spectra of C10

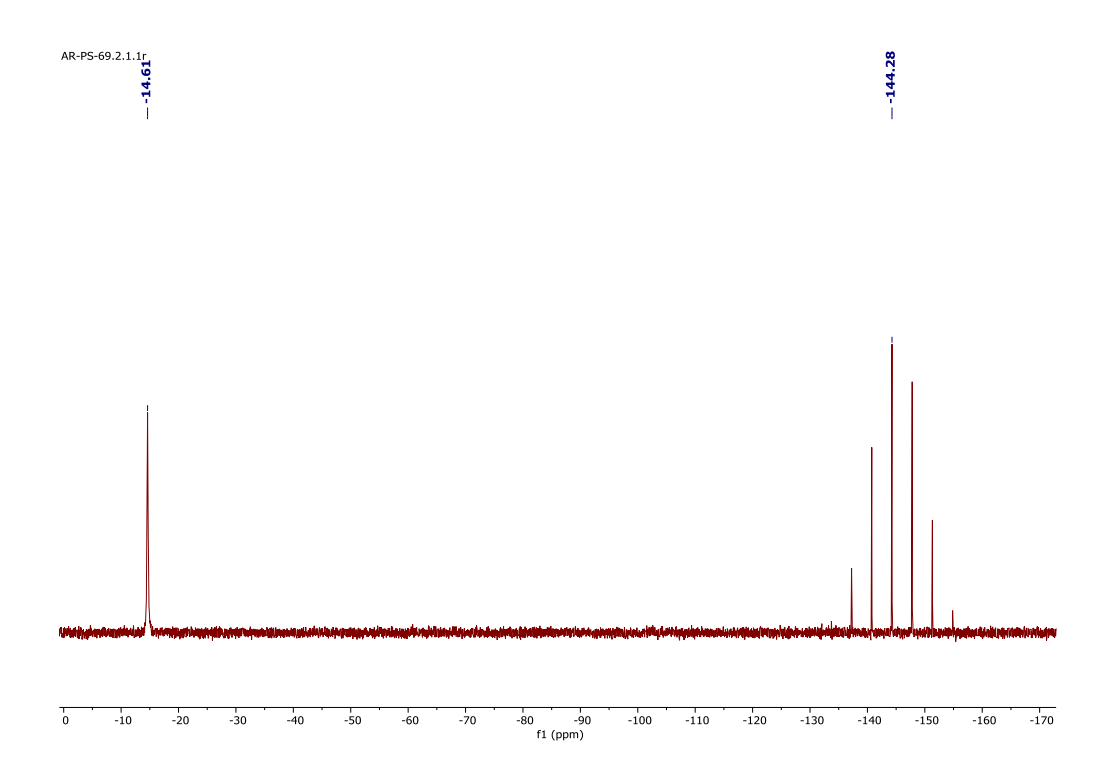


Figure 52: ³¹P{¹H} NMR spectra of **C10**

3.1.2.11 Characterization of C11

The complex formation of **C11** was confirmed by different nuclei NMR ¹H (Figure 53), ¹³C{¹H} (Figure 54), ³¹P{¹H} (Figure 55). The complex was yellow in colour when synthesised in the solid state with an yield of 76%. **C11** had good solubility in most of the solvents.

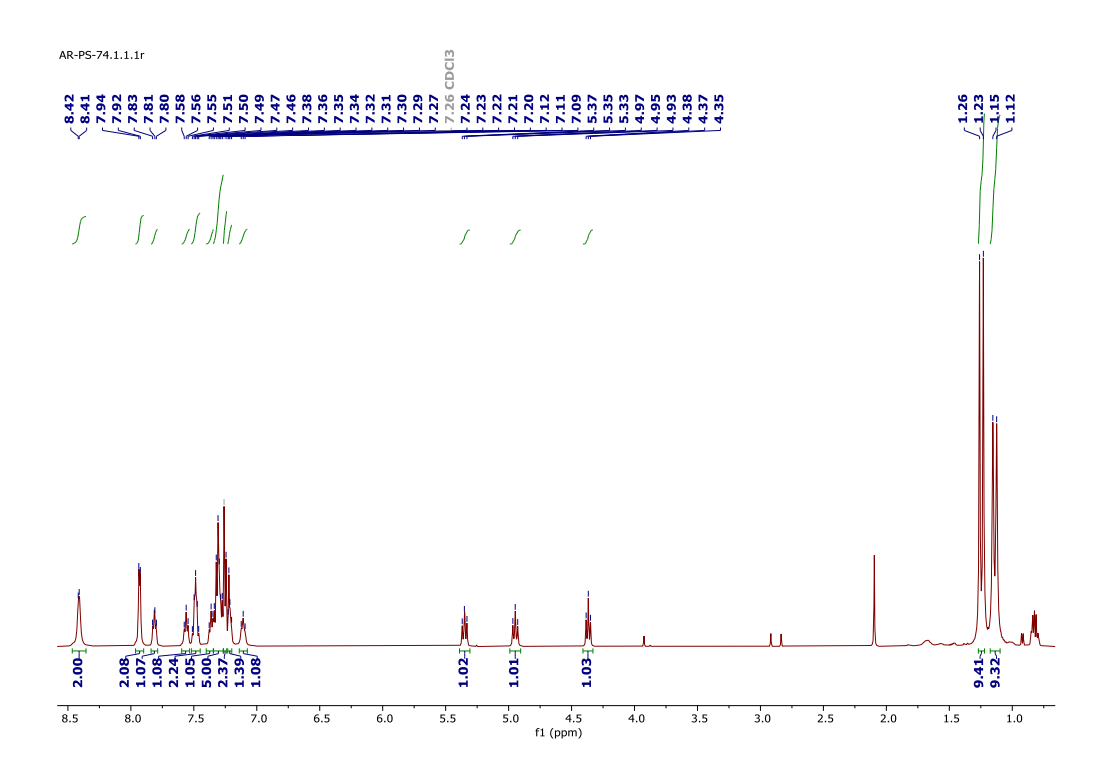


Figure 53: ¹H NMR spectra of C11

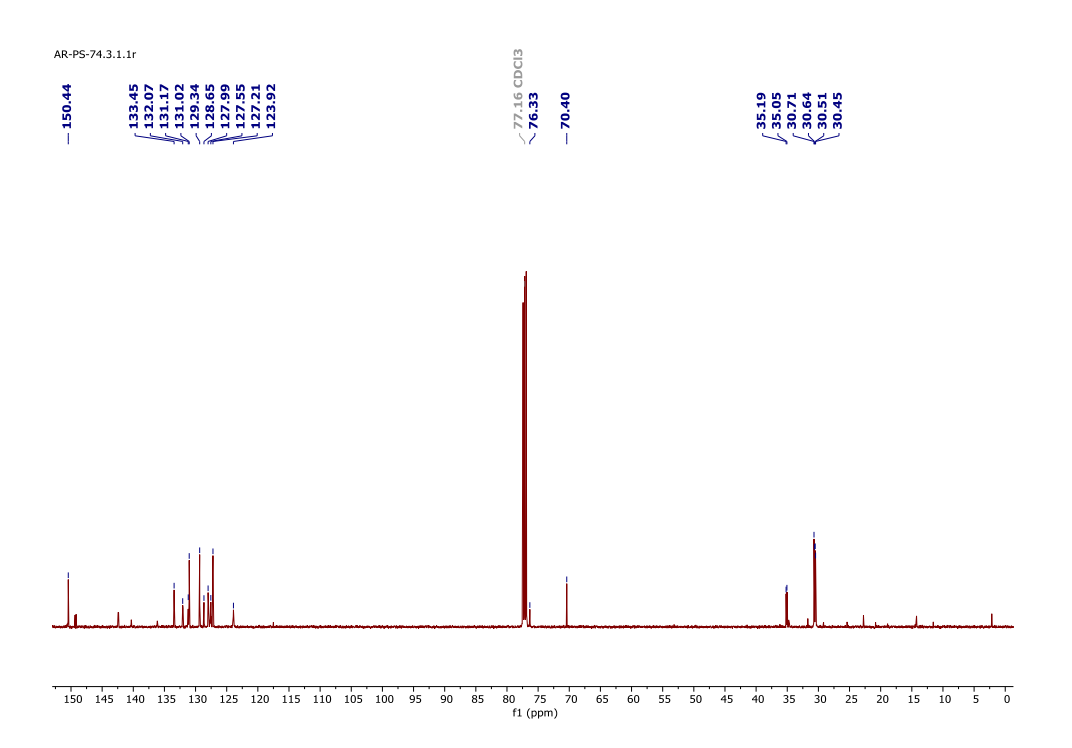


Figure 54: ¹³C{¹H} NMR spectra of C11

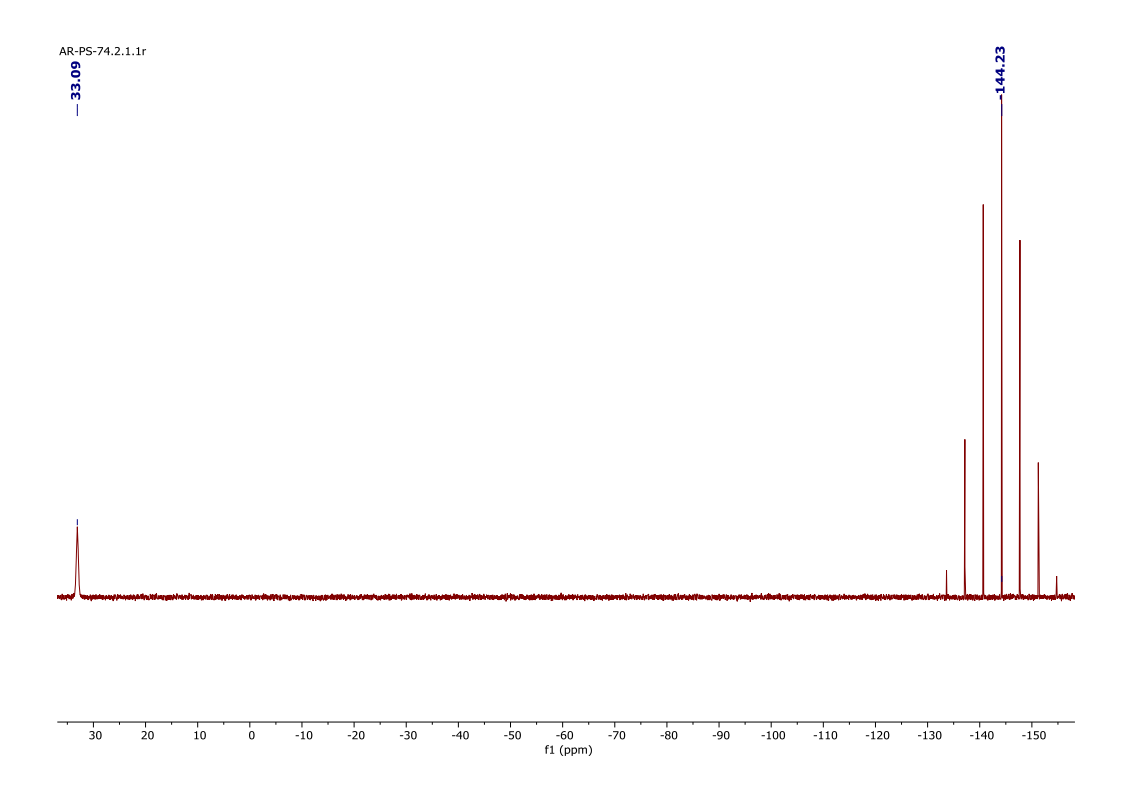


Figure 55: ³¹P{¹H} NMR spectra of C11

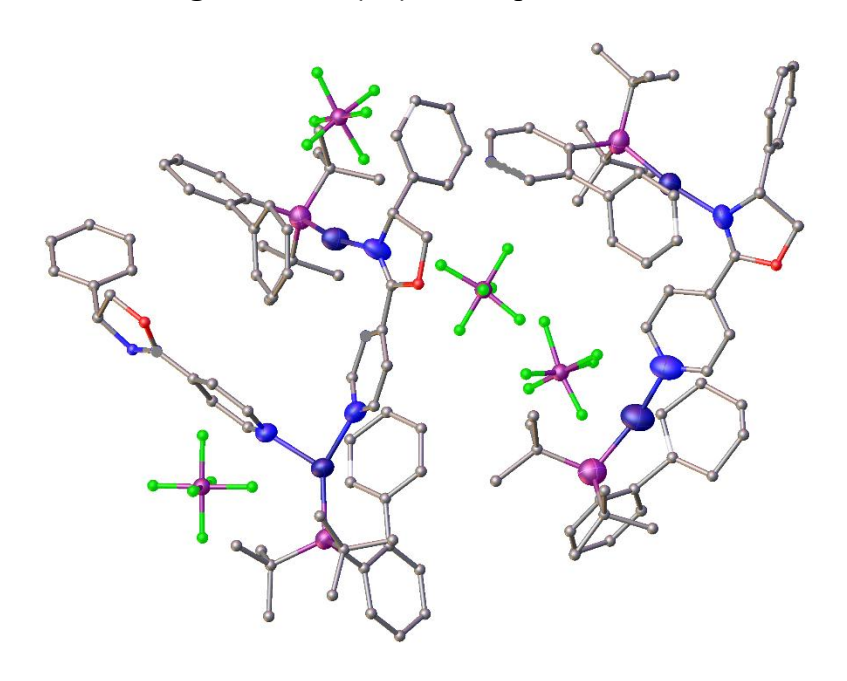


Figure 56: SCXRD of C11

3.1.2.12 Characterization of C12

The complex formation of **C12** was confirmed by different nuclei NMR 1 H (Figure 57), 13 C{ 1 H} (Figure 58), 31 P{ 1 H} (Figure 59). The

complex was yellow in colour when synthesised in the solid state with an yield of 70%. **C12** had good solubility in most of the solvents.

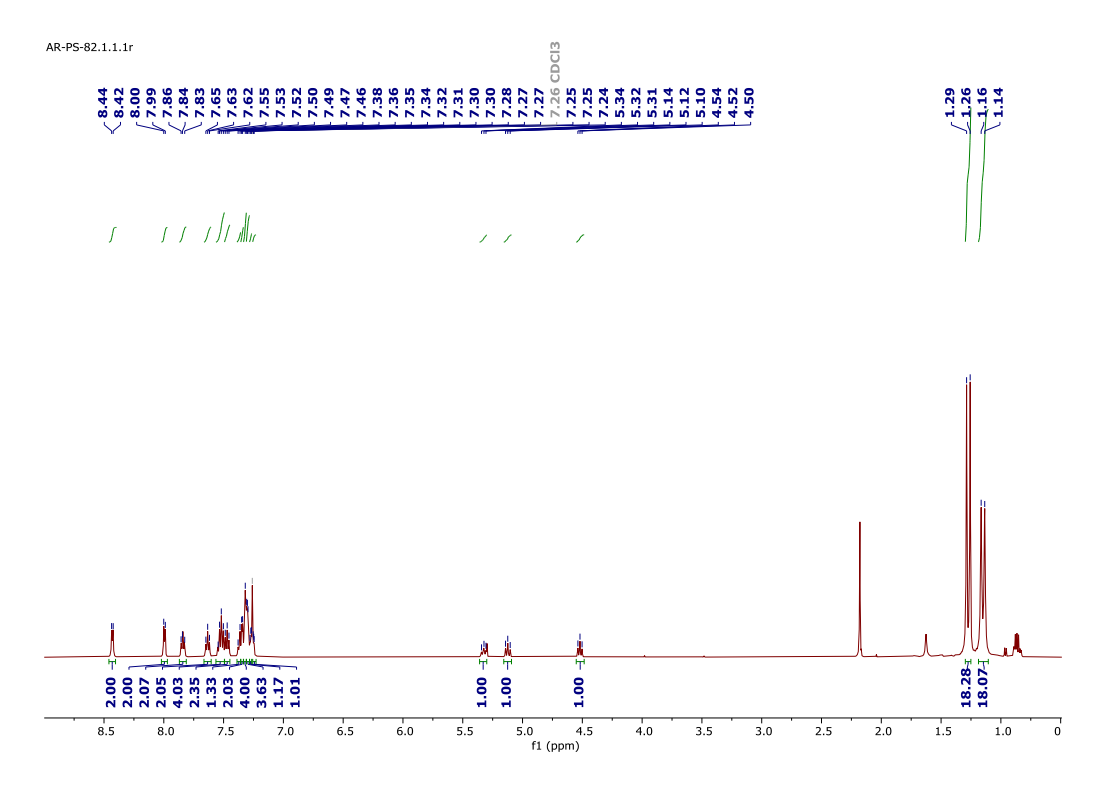


Figure 57: ¹H NMR spectra of C12

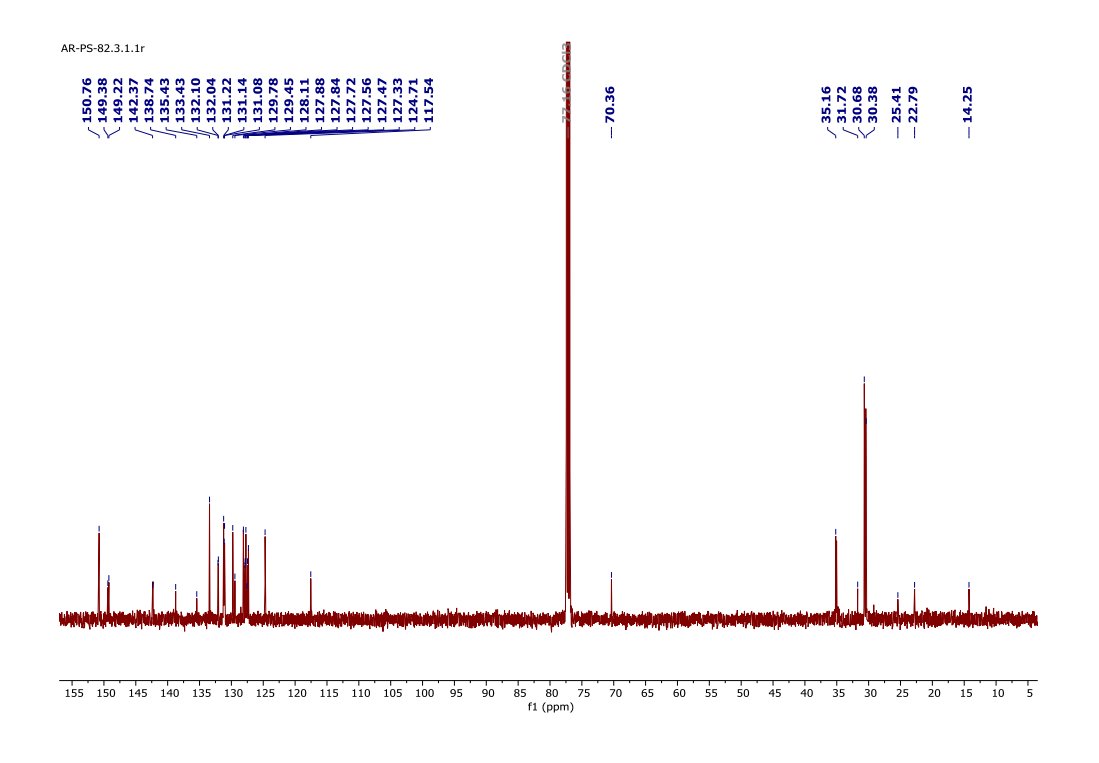


Figure 58: ${}^{13}C\{{}^{1}H\}$ NMR spectra of C12

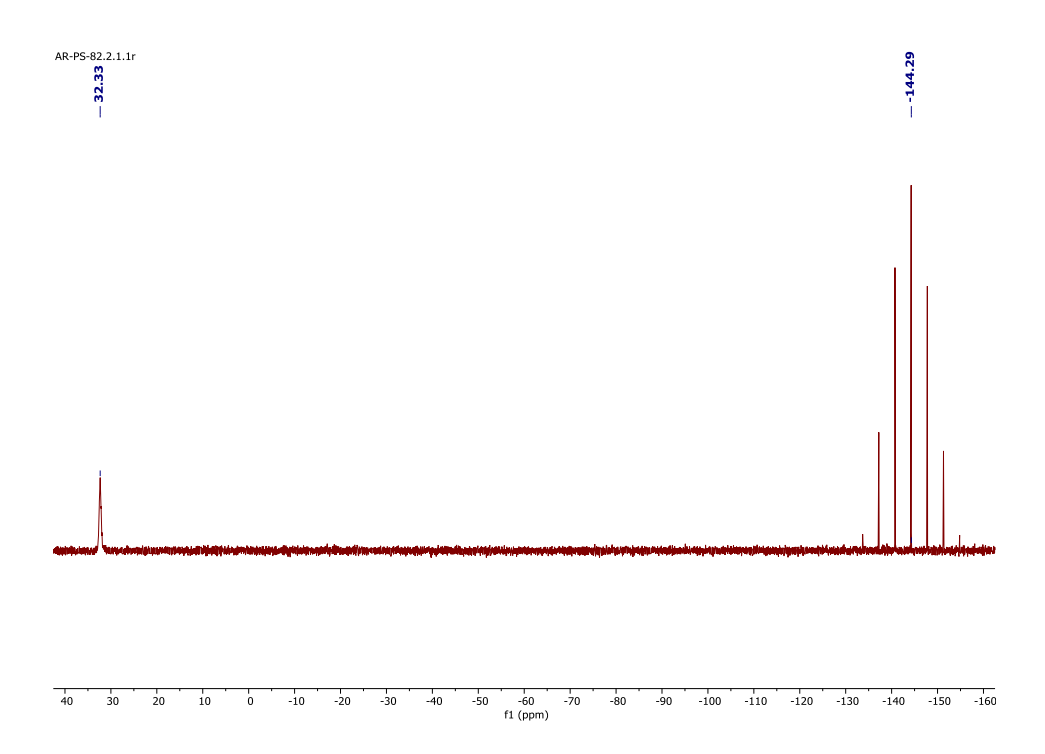


Figure 59: ³¹P{¹H} NMR spectra of C12

3.1.2.13 Characterization of C13

The complex formation of **C13** was confirmed by different nuclei NMR ¹H (Figure 60), ¹³C{¹H} (Figure 61), ³¹P{¹H} (Figure 62). The complex was yellow in colour when synthesised in the solid state with an yield of 68%. **C13** had good solubility in most of the solvents.

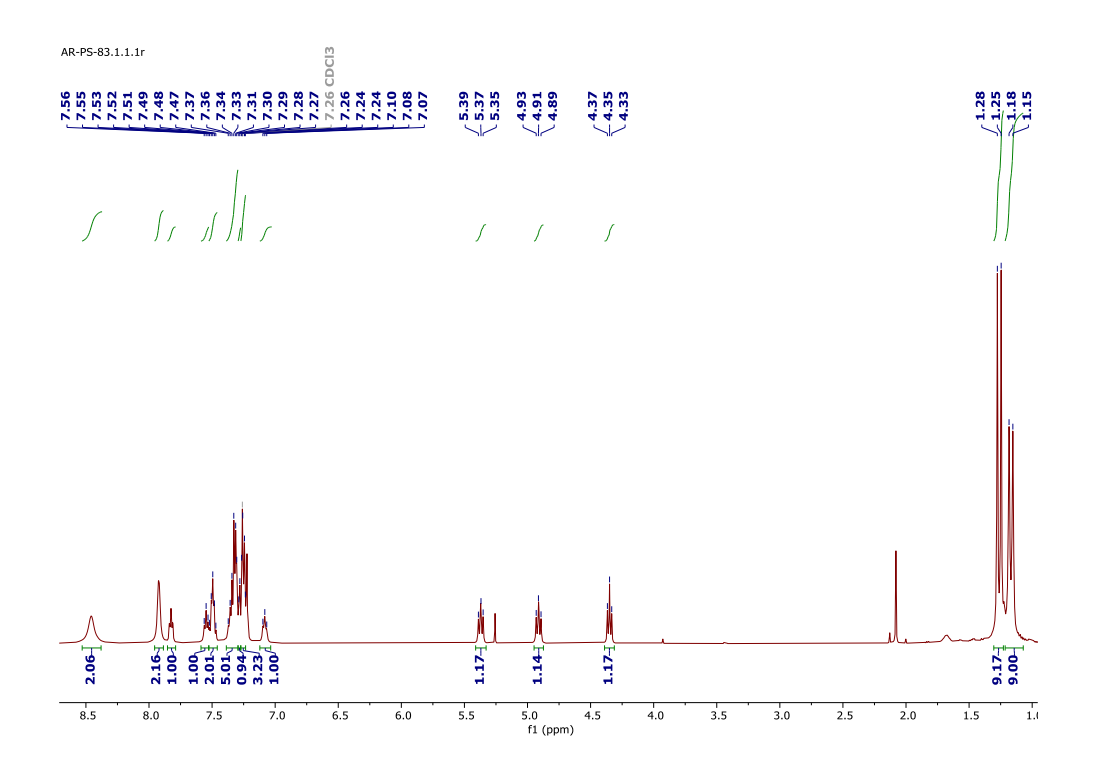


Figure 60: ¹H NMR spectra of C13

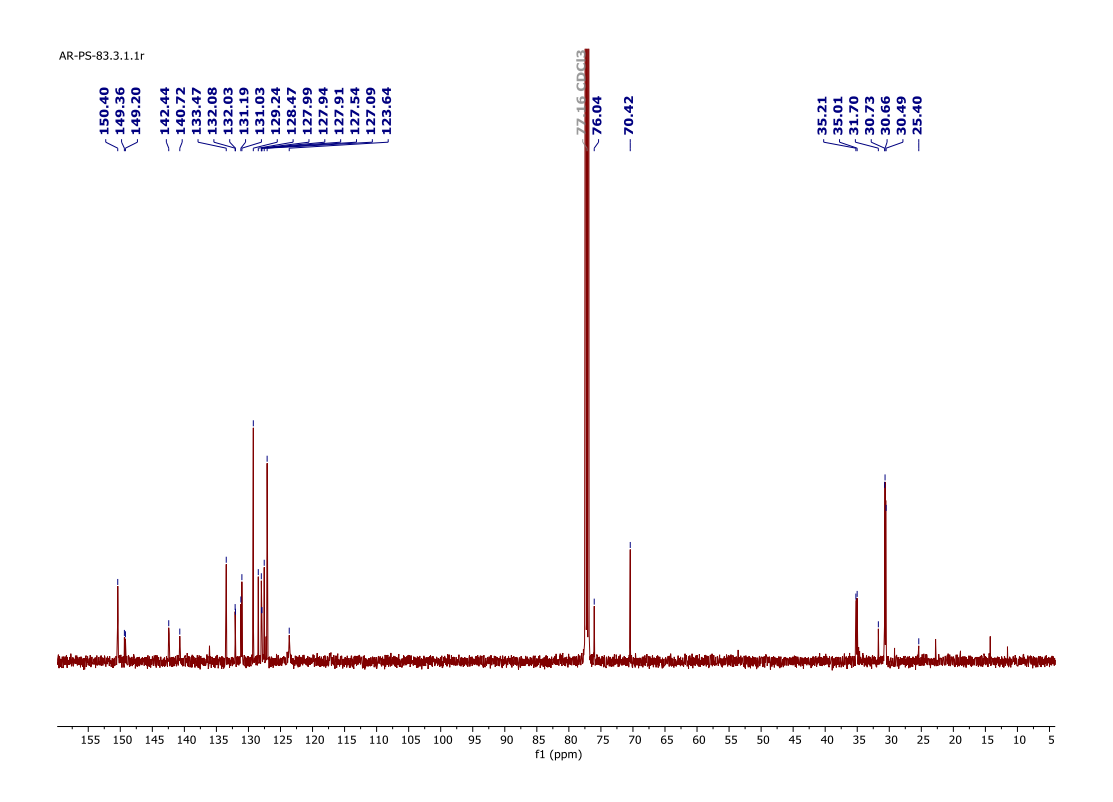


Figure 61: ¹³C{¹H} NMR spectra of C13

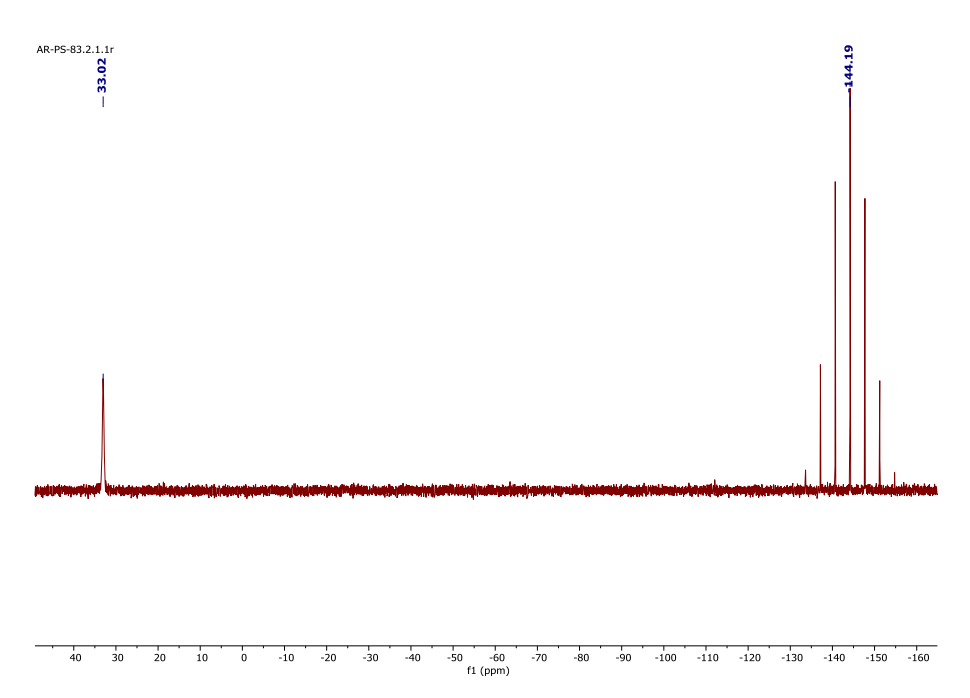


Figure 62: ³¹P{¹H} NMR spectra of C13

3.1.2.14 Characterization of C14

The complex formation of **C14** was confirmed by different nuclei NMR ¹H (Figure 63), ¹³C{¹H} (Figure 64), ³¹P{¹H} (Figure 65). The complex was yellow in colour when synthesised in the solid state with an yield of 77%. **C14** had good solubility in most of the solvents.

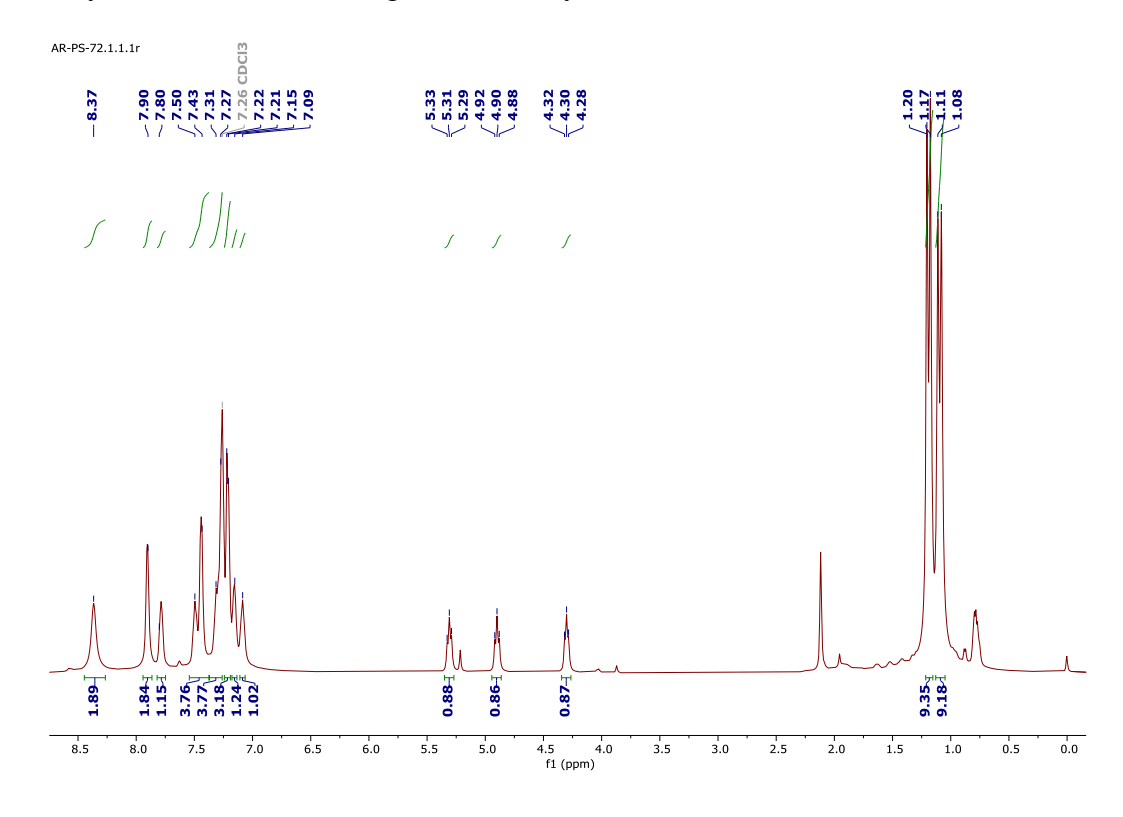


Figure 63: ¹H NMR spectra of C14

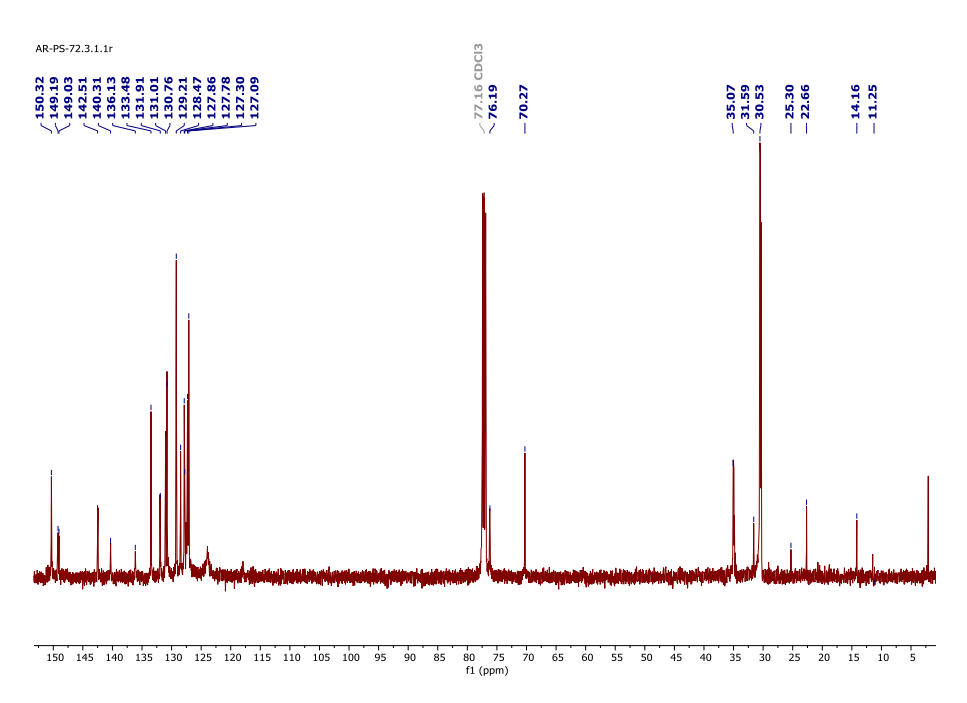


Figure 64: ¹³C{¹H} NMR spectra of C14

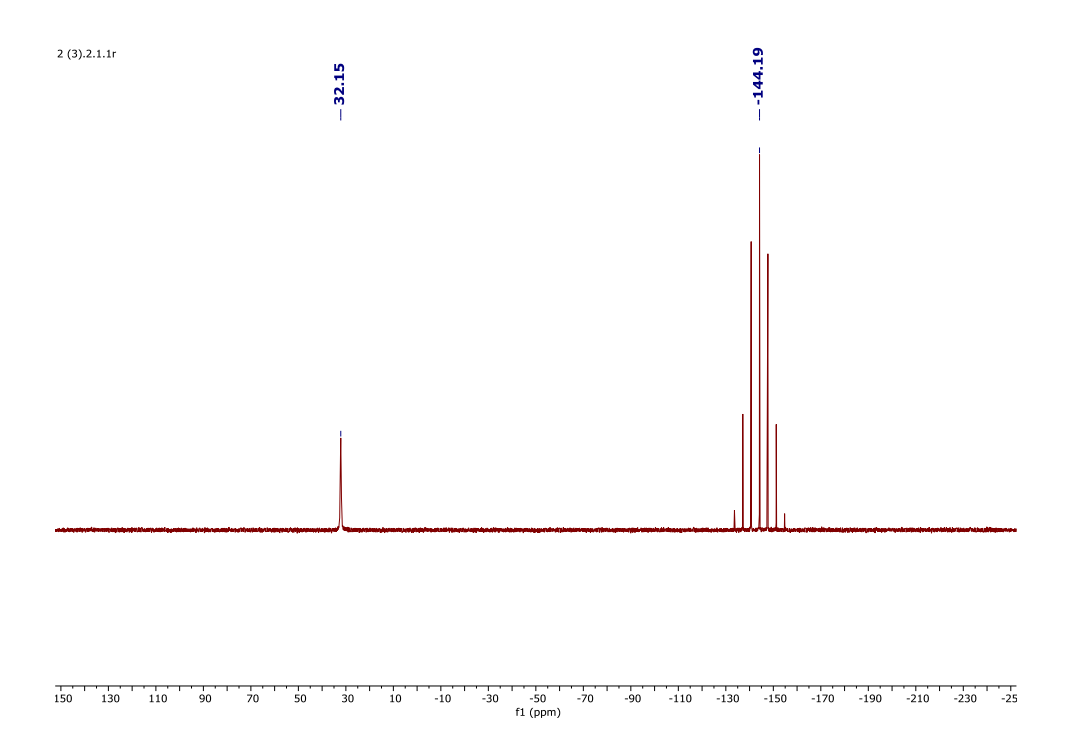


Figure 65: ³¹P{¹H} NMR spectra of C14

3.2 Photoluminescent Studies

3.2.1 Photoluminescence properties of Cu(I) Complexes

3.2.1.1 UV-Vis and PL spectra of C1

UV-Vis and excitation-emission spectra have been recorded to study the photophysical properties of complex C1 (Figure. 66). The PL spectra were recorded in both solid as well as solution state for better understanding of the complex. In UV-Vis spectra two peaks observed (i) 280 nm due to $\pi \rightarrow \pi^*$ transition (ii) 400 nm due to MLCT transition.

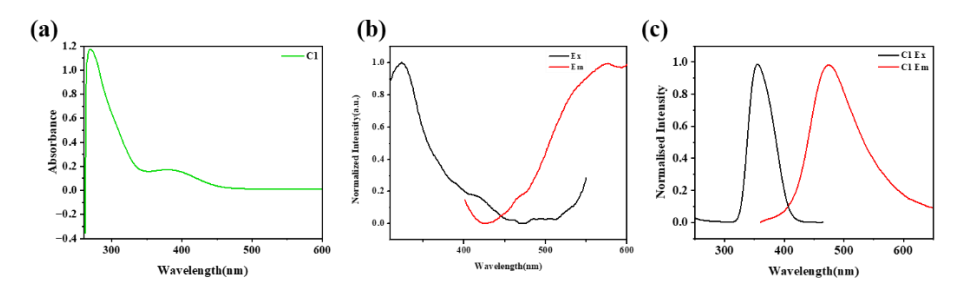


Figure 66: (a) UV-Vis spectra of **C1**, PL spectra of **C1** (b) solid state (c) solution state

3.2.1.2 UV-Vis and PL spectra of C2

UV-Vis and excitation-emission spectra have been recorded to study the photophysical properties of complex C2 (Figure. 67). The PL spectra were recorded in both solid as well as solution state for better understanding of the complex. In UV-Vis spectra two peaks observed (i) 280 nm due to $\pi \rightarrow \pi^*$ transition (ii) 390 nm due to MLCT transition.

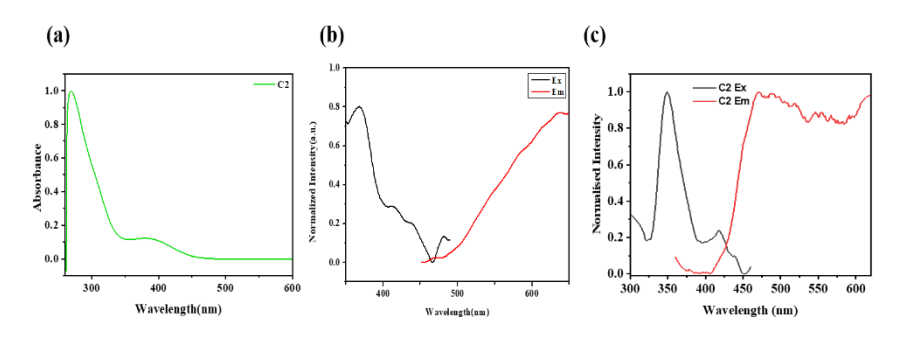


Figure 67: (a) UV-Vis spectra of C2, PL spectra of C2 (b) solid state (c) solution state

3.2.1.3 UV-Vis and PL spectra of C3

UV-Vis and excitation-emission spectra have been recorded to study the photophysical properties of complex C3 (Figure. 68). The PL spectra were recorded in both solid as well as solution state for better understanding of the complex. In UV-Vis spectra two peaks observed (i) 280 nm due to $\pi \rightarrow \pi^*$ transition (ii) 385 nm due to MLCT transition. The lifetime of the complex has been observed 6.71 μ s and quantum yield around 09%.

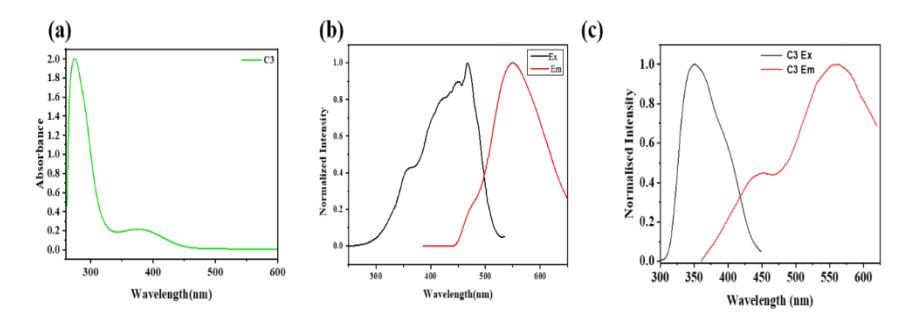


Figure 68: (a) UV-Vis spectra of **C3**, PL spectra of **C3** (b) solid state (c) solution state

3.2.1.4 UV-Vis and PL spectra of C4

UV-Vis and excitation-emission spectra have been recorded to study the photophysical properties of complex C4 (Figure. 69). The PL spectra were recorded in both solid as well as solution state for better understanding of the complex. In UV-Vis spectra two peaks observed (i) 280 nm due to $\pi \rightarrow \pi^*$ transition (ii) 400 nm due to MLCT transition.

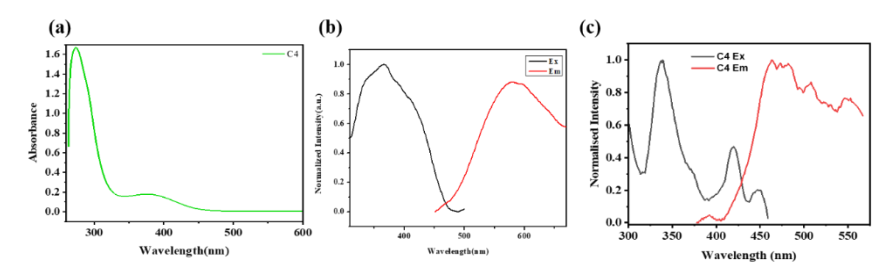


Figure 69: (a) UV-Vis spectra of **C4**, PL spectra of **C4** (b) solid state (c) solution state

3.2.1.5 UV-Vis and PL spectra of C5

UV-Vis and excitation-emission spectra have been recorded to study the photophysical properties of complex C5 (Figure. 70). The PL spectra were recorded in both solid as well as solution state for better

understanding of the complex. In UV-Vis spectra two peaks observed (i) 300 nm due to $\pi \rightarrow \pi^*$ transition (ii) 400 nm due to MLCT transition. The lifetime of the complex has been observed 5.07 μ s and quantum yield around 13%.

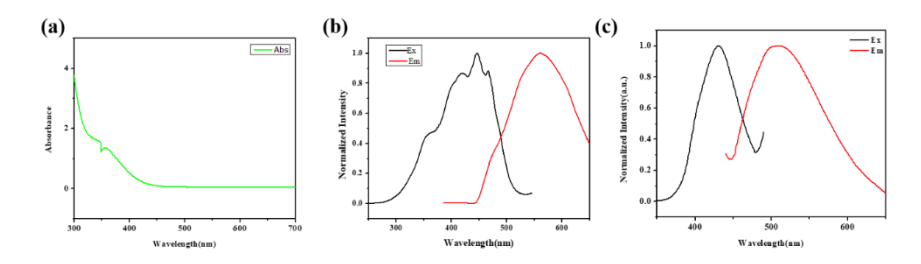


Figure 70: (a) UV-Vis spectra of **C5**, PL spectra of **C5** (b) solid state (c) solution state

3.2.1.6 UV-Vis and PL spectra of C6

UV-Vis and excitation-emission spectra have been recorded to study the photophysical properties of complex C6 (Figure. 71). The PL spectra were recorded in both solid as well as solution state for better understanding of the complex. In UV-Vis spectra two peaks observed (i) 300 nm due to $\pi \rightarrow \pi^*$ transition (ii) 405 nm due to MLCT transition.

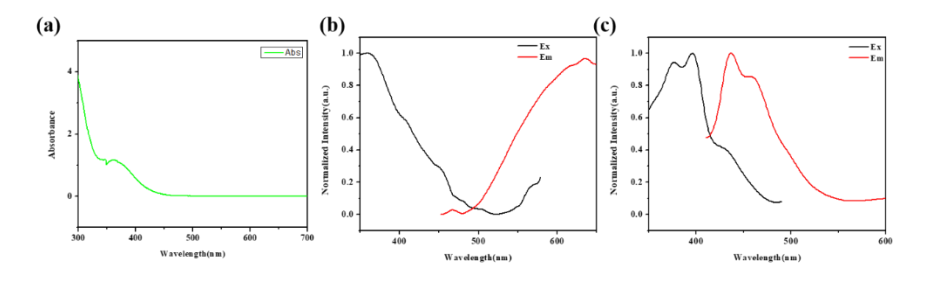


Figure 71: (a) UV-Vis spectra of **C6**, PL spectra of **C6** (b) solid state (c) solution state

3.2.1.7 UV-Vis and PL spectra of C7

UV-Vis and excitation-emission spectra have been recorded to study the photophysical properties of complex C7 (Figure. 72). The PL spectra were recorded in both solid as well as solution state for better understanding of the complex. In UV-Vis spectra two peaks observed (i) 280 nm due to $\pi \rightarrow \pi^*$ transition (ii) 400 nm due to MLCT transition. The lifetime of the complex has been observed 2.69 μ s and quantum yield around 38%.

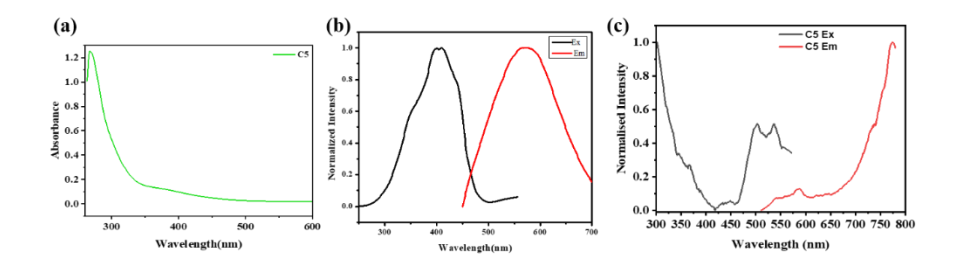


Figure 72: (a) UV-Vis spectra of C7, PL spectra of C7 (b) solid state (c) solution state

3.2.1.8 UV-Vis and PL spectra of C8

UV-Vis and excitation-emission spectra have been recorded to study the photophysical properties of complex C8 (Figure. 73). The PL spectra were recorded in both solid as well as solution state for better understanding of the complex. In UV-Vis spectra two peaks observed (i) 280 nm due to $\pi\rightarrow\pi^*$ transition (ii) 390 nm due to MLCT transition. The lifetime of the complex has been observed 3.03 μ s and quantum yield around 36%.

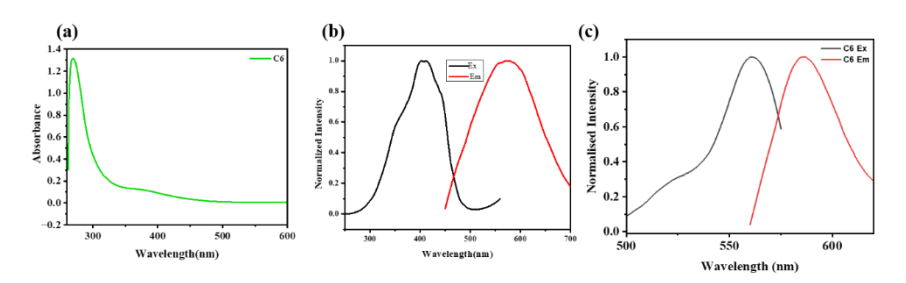


Figure 73: (a) UV-Vis spectra of **C8**, PL spectra of **C8** (b) solid state (c) solution state

3.2.1.9 UV-Vis and PL spectra of C9

UV-Vis and excitation-emission spectra have been recorded to study the photophysical properties of complex C9 (Figure. 74). The PL spectra were recorded in both solid as well as solution state for better understanding of the complex. In UV-Vis spectra two peaks observed (i) 305 nm due to $\pi \rightarrow \pi^*$ transition (ii) 385 nm due to MLCT transition. The emission lifetime of the complex has been observed 4.34 μ s and quantum yield around 08% at room temperature.

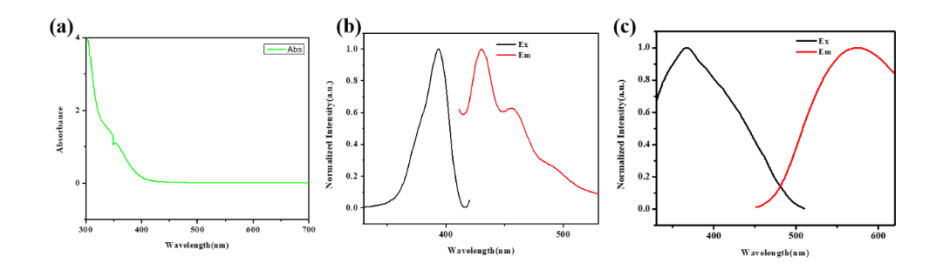


Figure 74: (a) UV-Vis spectra of **C9**, PL spectra of **C9** (b) solid state (c) solution state

3.2.1.10 UV-Vis and PL spectra of C10

UV-Vis and excitation-emission spectra have been recorded to study the photophysical properties of complex C10 (Figure. 75). The PL spectra were recorded in both solid as well as solution state for better understanding of the complex. In UV-Vis spectra two peaks observed (i) 290 nm due to $\pi \rightarrow \pi^*$ transition (ii) 395 nm due to MLCT transition.

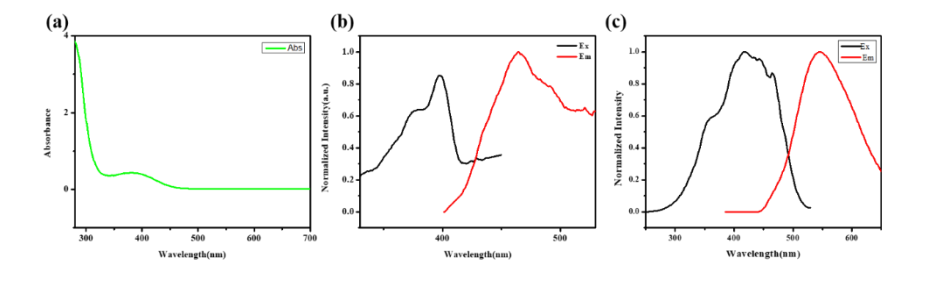


Figure 75: (a) UV-Vis spectra of **C10**, PL spectra of **C10** (b) solid state (c) solution state

3.2.1.11 UV-Vis and PL spectra of C13

UV-Vis and excitation-emission spectra have been recorded to study the photophysical properties of complex C13 (Figure. 76). The PL spectra were recorded in both solid as well as solution state for better understanding of the complex. In UV-Vis spectra two peaks observed (i) 300 nm due to $\pi \rightarrow \pi^*$ transition (ii) 385 nm due to MLCT transition. The lifetime of the complex has been observed 2.82 μ s and quantum yield around 06%.

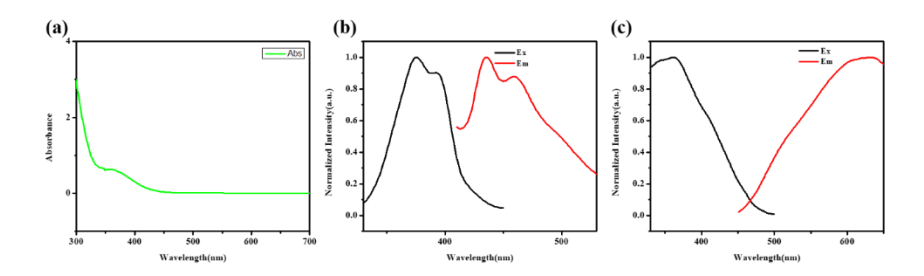


Figure 76: (a) UV-Vis spectra of **C13**, PL spectra of **C13** (b) solid state (c) solution state

3.2.1.12 UV-Vis and PL spectra of C14

UV-Vis and excitation-emission spectra have been recorded to study the photophysical properties of complex C14 (Figure. 77). The PL spectra were recorded in both solid as well as solution state for better understanding of the complex. In UV-Vis spectra two peaks observed (i) 310 nm due to $\pi \rightarrow \pi^*$ transition (ii) 400 nm due to MLCT transition.

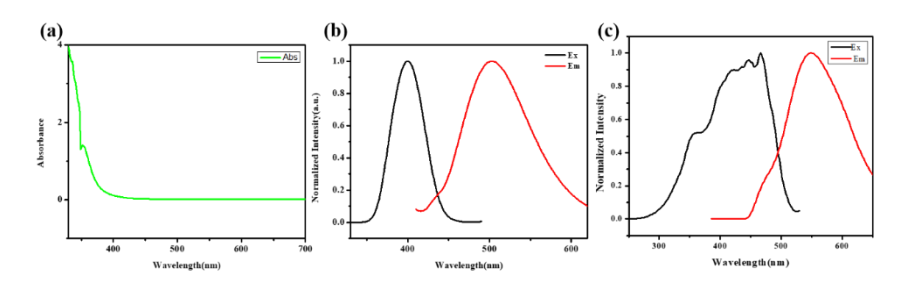


Figure 77: (a) UV-Vis spectra of C14, PL spectra of C14 (b) solid state (c) solution state

3.3 Chiroptical Studies

3.3.1 Chiroptical properties of Cu(I) Complexes

3.3.1.1 CD spectra of C1-C2

Circular Dichroism spectra has been recorded of complex C1 and C2 in DCM solvent. The (Figure. 78) shows a mirror image relationship between two enantiomer complexes at different absorption regions.

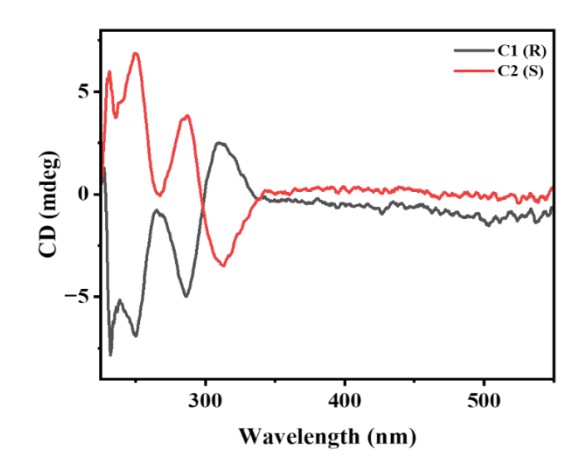


Figure 78: CD spectra of C1 and C2

3.3.1.2 CD spectra of C3-C4

Circular Dichroism spectra has been recorded of complex C3 and C4 in DCM solvent. The (Figure. 79) shows a mirror image relationship between two enantiomer complexes at different absorption regions.

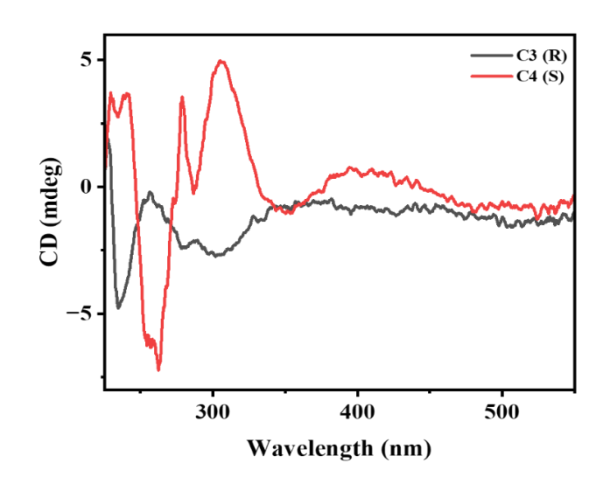


Figure 79: CD spectra of C3 and C4

3.3.1.3 CD spectra of C7-C8

Circular Dichroism spectra has been recorded of complex C7 and C8 in DCM solvent. The (Figure. 80) shows a mirror image relationship between two enantiomer complexes at different absorption regions.

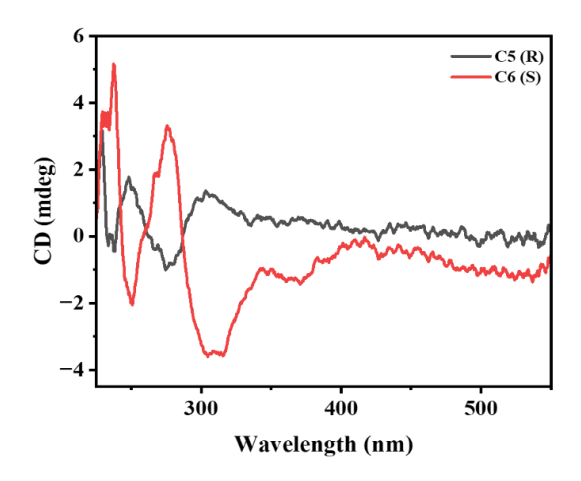


Figure 80: CD spectra of C7 and C8

Chapter 4: CONCLUSION

4.1 CONCLUSION

Herein, we have successfully synthesized and characterized four chiral (R and S) oxazoline based ligands (L1-L4). Furthermore, we have further synthesized fourteen (C1-C14) Cu(I) chiral complexes. Most of the complexes were characterized by LCMS and multi-nuclear (¹H, ¹³C{¹H}, ³¹P{¹H}) NMR spectroscopy. The molecular structures of some complexes were also authenticated by SCXRD analysis. Further photophysical and chiroptical properties of these complexes were studied. Preliminary analysis suggests that the use of bulky phosphine in the synthesis of three-coordinate complexes and complexes with copper iodide gives better quantum yield and could be suitable for further applications.

References

- (1) El Sayed Moussa, M.; Evariste, S.; Wong, H.-L.; Le Bras, L.; Roiland, C.; Le Polles, L.; Le Guennic, B.; Costuas, K.; Yam, V. W.-W.; Lescop, C. A Solid State Highly Emissive Cu(I) Metallacycle: Promotion of Cuprophilic Interactions at the Excited States. *Chem. Commun.* 2016, 52 (76), 11370–11373. https://doi.org/10.1039/C6CC06613E.
- (2) Yang, H.; Zheng, J.; Xie, M.; Luo, D.; Tang, W.-J.; Peng, S.-K.; Cheng, G.; Zhang, X.; Zhou, X.-P.; Che, C.-M.; Li, D. Aggregation-Enhanced Emission in a Red Cu(I) Emitter with Quantum Yield >99%. *ACS Mater. Lett.* **2022**, *4* (10), 1921–1928. https://doi.org/10.1021/acsmaterialslett.2c00661.
- (3) Ying, A.; Huang, Y.-H.; Lu, C.-H.; Chen, Z.; Lee, W.-K.; Zeng, X.; Chen, T.; Cao, X.; Wu, C.-C.; Gong, S.; Yang, C. High-Efficiency Red Electroluminescence Based on a Carbene–Cu(I)–Acridine Complex. *ACS Appl. Mater. Interfaces* **2021**, *13* (11), 13478–13486. https://doi.org/10.1021/acsami.0c22109.
- (4) Kharabe, L. S.; Sahu, B.; Mishra, S.; Kumar, R.; Raghuvanshi, A. Redox Dependent Color Modulating Copper(I) Complex for Flexible Electrochromic Device. *ChemPhotoChem* 2025, e202400354. https://doi.org/10.1002/cptc.202400354.
- (5) Zhou, Y.-H.; Zhang, A.-W.; Huang, R.-J.; Sun, Y.-H.; Chen, Z.-J.; Zhu, B.-S.; Zheng, Y.-X. Circularly Polarised Photoluminescence and Electroluminescence of Chiral Copper(I) Dimers Based on R / S -2,2'-Bis(Diphenylphosphino)-1,1'-Binaphthalene Ligands. J. Mater. Chem. C 2023, 11 (4), 1329–1335. https://doi.org/10.1039/D2TC04895G.
- (6) Longhi, G.; Castiglioni, E.; Koshoubu, J.; Mazzeo, G.; Abbate, S. Circularly Polarized Luminescence: A Review of Experimental

- and Theoretical Aspects. *Chirality* **2016**, 28 (10), 696–707. https://doi.org/10.1002/chir.22647.
- (7) Petyuk, M. Yu.; Meng, L.; Ma, Z.; Agafontsev, A. M.; Bagryanskaya, I. Yu.; Berezin, A. S.; Zhang, J.; Chu, A.; Rakhmanova, M. I.; Meng, H.; Tkachev, A. V.; Yam, V. W.; Artem'ev, A. V. Outstanding Circularly Polarized TADF in Chiral Cu(I) Emitters: From Design to Application in CP-TADF OLEDs. Angew. Chem. Int. Ed. 2024, 63 (52), e202412437. https://doi.org/10.1002/anie.202412437.
- (8) Tao, Y.; Yuan, K.; Chen, T.; Xu, P.; Li, H.; Chen, R.; Zheng, C.; Zhang, L.; Huang, W. Thermally Activated Delayed Fluorescence Materials Towards the Breakthrough of Organoelectronics. *Adv. Mater.* 2014, 26 (47), 7931–7958. https://doi.org/10.1002/adma.201402532.
- (9) Mockrin, S. C.; Byers, L. D.; Koshland, D. E. Subunit Interactions in Yeast Glyceraldehyde-3-Phosphate Dehydrogenase. *Biochemistry* 1975, 14 (25), 5428–5437. https://doi.org/10.1021/bi00696a008.
- (10) Hayashi, T. Chiral Monodentate Phosphine Ligand MOP for Transition-Metal-Catalyzed Asymmetric Reactions. *Acc. Chem. Res.* **2000**, *33* (6), 354–362. https://doi.org/10.1021/ar990080f.
- (11) Nagata, Y.; Mori, T. Irreverent Nature of Dissymmetry Factor and Quantum Yield in Circularly Polarized Luminescence of Small Organic Molecules. *Front. Chem.* 2020, 8, 448. https://doi.org/10.3389/fchem.2020.00448.
- (12) Housecroft, C. E.; Constable, E. C. TADF: Enabling Luminescent Copper(I) Coordination Compounds for Light-Emitting Electrochemical Cells. *J. Mater. Chem. C* **2022**, *10* (12), 4456–4482. https://doi.org/10.1039/D1TC04028F.
- (13) Muthig, A. M. T.; Mrózek, O.; Ferschke, T.; Rödel, M.; Ewald, B.; Kuhnt, J.; Lenczyk, C.; Pflaum, J.; Steffen, A. Mechano-Stimulus and Environment-Dependent Circularly Polarized TADF in Chiral Copper(I) Complexes and Their Application in

- OLEDs. *J. Am. Chem. Soc.* **2023**, *145* (8), 4438–4449. https://doi.org/10.1021/jacs.2c09458.
- (14) Trippe, S. POLARIZATION AND POLARIMETRY: A REVIEW. *J. Korean Astron. Soc.* **2014**, *47* (1), 15–39. https://doi.org/10.5303/JKAS.2014.47.1.15.
- (15) Garg, P.; Chaudhary, S.; Milton, M. D. Synthesis of 2-Aryl/Heteroaryloxazolines from Nitriles under Metal- and Catalyst-Free Conditions and Evaluation of Their Antioxidant Activities. *J. Org. Chem.* **2014**, 79 (18), 8668–8677. https://doi.org/10.1021/jo501430p.